Structural and functional analysis of YopR and identification of an additional key component of the SPβ phage lysis-lysogeny management system

Katharina Kohm[1,2,6], Ekaterina Jalomo-Khayrova[3,6], Syamantak Basu[1], Wieland Steinchen[3], Gert Bange[3,4], Robert Hertel[1,5,*], Fabian M. Commichau[1,2,*], Laura Czech[3,*]

[1]FG Synthetic Microbiology, Institute for Biotechnology, BTU Cottbus-Senftenberg, Senftenberg, Germany
[2]FG Molecular Microbiology, Institute for Biology, University of Hohenheim, Stuttgart, Germany
[3]Center for Synthetic Microbiology (SYNMIKRO) and Department of Chemistry, Phillips-University Marburg, Marburg, Germany
[4]Max-Planck Institute for Terrestrial Microbiology, Marburg, Germany
[5]Department of Genomic and Applied Microbiology, Institute of Microbiology and Genetics, Georg-August-University of Göttingen, Göttingen, Germany
[6]Equally contributing

*Corresponding authors:
czechla@staff.uni-marburg.de; fabian.commichau@uni-hohenheim.de; rhertel@gwdg.de

Universität Göttingen
37077 Göttingen
Phone: +49-175-7916901
Mail: rhertel@gwdg.de

Universität Hohenheim
70699 Stuttgart
Phone: +49-711459-22222
Mail: fabian.commichau@uni-hohenheim.de

Phillips-Universität Marburg
35043 Marburg
Phone: +49-177-7555527
Mail: czechla@staff.uni-marburg.de

RUNNING TITLE: Control of the SPβ phage lysogeny management system

KEYWORDS: prophage, regulation, repressor, recombinase, suppressor mutant

ABSTRACT

Prophages need to tightly control their lifestyle to either be maintained within the host genome or enter the lytic cycle. The SPβ prophage present in the genome of *Bacillus subtilis* 168 was recently shown to possess an *arbitrium* system defining its replication stage. Using an historic *B. subtilis* strain harboring the heat-sensitive SPβ c2 mutant, we analyzed a key component of the lysis-lysogeny decision system called YopR, which is critical for maintenance of lysogeny. Here, we demonstrate that the heat-sensitive SPβ c2 phenotype is due to a single nucleotide exchange in the *yopR* gene, rendering the encoded $YopR^{G136E}$ protein temperature sensitive. Structural characterization of YopR revealed that the protein is a DNA-binding protein with an overall fold like tyrosine recombinases. Biochemical and functional analyses indicate that YopR has lost the recombinase function and the G136E exchange impairs its higher order structure and DNA binding activity. We further show that the heat-inducible SPβ excision of the c2 mutant still depends on the serine recombinase SprA. Finally, an evolution experiment identified the YosL protein of unknown function as a novel component of the lysis-lysogeny management system, as the presence of *yosL* is crucial for the induction of the lytic cycle of SPβ.

INTRODUCTION

Phages are bacterial viruses whose replication strictly depends on the host cell. While most host cells are killed after phage infection during the lytic cycle, some phages may enter the lysogenic or temperate life cycle [Salmond and Fineran, 2015; Dion et al., 2020]. In the latter case, the phage genome integrates into the host chromosome and the bacteria carrying the prophage become lysogens. Prophages multiplying together with the host chromosome may enter the lytic cycle through the action of mutagenic agents [Warner et al., 1977].

We are interested in the biology of the temperate phage SPβ that infects the endospore-forming Gram-positive model bacterium *Bacillus subtilis* and resides as a prophage in the genome of the *B. subtilis* laboratory strain 168 [Zeigler et al., 2008]. SPβ resembles the *Siphoviridae* morphotype and carries a 130 kb long genome [Kohm and Hertel, 2021]. It was discovered about 50 years ago in the *B. subtilis* strain CU1050 that was subjected to chemical mutagenesis and cured of the prophage [Georgopoulos, 1969; Warner et al., 1977; Johnson and Grossman, 2016]. Interestingly, cultures of *B. subtilis* that are lysogenic for SPβ release the *S*-linked glycopeptide sublancin, which belongs to the class of antimicrobial natural products named glycocins [Hemphill et al., 1980; Oman et al., 2011]. Sublancin inhibits the growth of SPβ-free *B. subtilis* strains by interfering with essential cellular processes such as DNA replication and transcription [Hemphill et al., 1980; Wu et al., 2019]. *B. subtilis* strains carrying the SPβ prophage in their genomes can therefore be identified based on their antimicrobial properties [Hemphill et al., 1980]. Like other temperate phages, SPβ may enter either the lytic or the lysogenic cycle. The lytic cycle of SPβ can be induced by treating *B. subtilis* with either *N*-methyl-*N'*-nitro-*N*-nitroso-guanidine or mitomycin C [Warner et al., 1977]. A study focusing on sporulation revealed that the SPβ genome is excised from the mother cell genome during the formation of the spore (Figure 1) [Abe et al., 2014]. The excision process depends on the serine recombinase SprA (SPβ site-specific recombination factor A), whose activity is controlled by the accessory factor SprB [Abe et al., 2014, 2017, 2020]. Remarkably, the excision of the SPβ genome from the host cell genome causes the reconstitution of the *spsM* gene in the mother cell, which encodes an enzyme involved in sugar decoration of the spore and is thus crucial for spore maturation [Abe et al., 2014, 2017, 2020]. While the *sprA* gene is actively transcribed during vegetative growth, the expression of the *sprB* gene depends on the sporulation-specific sigma factors SigE and SigK [Abe et al., 2014]. The temporal synthesis of SprB prevents excision of the SPβ genome during vegetative growth of *B. subtilis*. Interestingly, while SPβ resides as a prophage in the spore genome, it is only excised in the mother cell to form the functional *spsM* gene. Moreover, this excision does not result in the formation of infectious phage particles [Abe et al., 2014].

Recently, it has been demonstrated that the phages of the SPβ group use a small-molecule communication system (termed the "arbitrium" system) to coordinate lysis-lysogeny decisions (Figure 1) [Erez et al., 2017; Trinh & Zeng, 2019]. The core of the arbitrium system consists of the *aimP*, *aimR* and *aimX* genes encoding the AimP peptide, the transcriptional activator AimR and the non-coding (nc) RNA AimX, respectively [Erez et al., 2017]. In the early stage of infection, the number of phages and the concentration of AimP is low. Apo-AimR binds as a homodimer *via* its helix-turn-helix domain to the operator in the P_{aimX} promoter and activates transcription of the AimX ncRNA that promotes the lytic cycle (Figure 1) [Erez et al., 2017; Gallego Del Sol et al., 2019, 2022; Guan et al., 2019; Pei et al., 2021]. During the lytic cycle, accumulating AimP is secreted *via* the Sec pathway and processed by extracellular proteases. The resulting hexapeptide is transported into the cell by the Opp oligopeptide transport system [Lazzazera et al., 1997]. The formation of an AimP-hexapeptide/AimR complex inhibits the DNA-binding activity of AimR and promotes the switch to the lysogenic

cycle [Erez et al., 2017]. While the molecular details of the AimP-hexapeptide/AimR complex have been elucidated [Wang et al., 2018; Dou et al., 2018; Zhen et al., 2019; Gallego Del Sol et al., 2019, 2022; Guan et al., 2019; Pei et al., 2021], the components that act downstream of the AimX ncRNA remain to be identified (Figure 1). However, the AimP-hexapeptide-dependent control of AimR is crucial to prevent the killing of the entire bacterial population by SPβ, thereby ensuring long-term prophage replication.

Two recent studies uncovered several novel players of the SPβ lysis-lysogeny decision system [Brady et al., 2021; Kohm et al., 2022]. For instance, a suppressor analysis with a SPβ *aimR* mutant, which generates more lysogenic cells, revealed that the spontaneous inactivation of the *yopN* gene, encoding a protein of unknown function, partially restores the control of lysis-lysogeny [Brady et al., 2021]. The same studies identified YopR as the master repressor of the lytic cycle of SPβ [Brady et al., 2021; Kohm et al., 2022]. Although it is unclear how AimR, YopN and YopR interact with each other, it has been proposed that YopN stimulates the repressor activity of YopR [Brady et al., 2021]. Furthermore, a recent comparative genome analysis identified the core genes of SPβ-like phages. These genes are *yopR*, *yopQ*, *yopP*, *aimR* and *yokI*, which are most likely transcriptionally active during the lysogenic cycle [Kohm et al., 2022]. The inactivation of the *yokI* gene indeed verified its role in the lysis-lysogeny decision system of SPβ because the *yokI* mutant released about four times more virions into the supernatant as compared to the parental strain [Kohm et al., 2022]. It has been hypothesized that YokI could act as an RNase that prevents the accumulation of the AimX ncRNA, thereby hindering the entry into the lytic cycle (Figure 1) [Kohm et al., 2022].

The above-mentioned prophage-free *B. subtilis* strain CU1050 also served as a host to isolate the "historic" SPβ mutant variants c1 and c2 that likely acquired mutations in genes of the lysis-lysogeny decision system [Zahler et al., 1977; Rosenthal et al., 1979]. The c1 mutant had an apparent plaque phenotype and did not lysogenize *B. subtilis*. By contrast, the c2 mutant proved to be temperature sensitive and entered the lytic cycle when the temperature was shifted to 50 °C for a few minutes. It has been suggested that c1 and c2 are alleles of the same gene encoding a repressor of SPβ like other temperate phages [Rosenthal et al., 1979]. However, the mutations in the SPβ c1 and c2 mutants and their impact on the lysogeny management system have not been identified and studied to date [McLaughlin et al., 1986]. Previous searches for regulator binding sites identified the SPbeta repeated element (SPBRE) [Lazarevic et al., 1999]. Yet, the protein capable of binding to SPBRE has not been discovered.

Here, we demonstrate that the heat-sensitive SPβ c2 phenotype is due to a single nucleotide exchange in the *yopR* gene, rendering the encoded $YopR^{G136E}$ protein temperature sensitive. Genetic complementation studies revealed that the wild type YopR protein is dominant over the $YopR^{G136E}$ mutant. Thermal shift assays and biochemical analyses uncovered that the G136E exchange renders YopR less stable and reduces its affinity to bind DNA *in vitro*. Structural and functional characterization of YopR revealed that the protein is a DNA-binding protein that has an overall fold like tyrosine recombinases but lacks crucial amino acid residues to function as a recombinase enzyme. Moreover, cell lysis occurred after heat shock in strains lacking either serine recombinase SprA or its accessory factor SprB. Finally, a genetic suppressor analysis with a *B. subtilis* strain carrying the SPβ c2 *yopR* G407A allele identified the YosL protein as a novel player in the lysis-lysogeny management system. Further analysis showed that the presence of *yosL* seems to be crucial for the lytic cycle of SPβ. The current model of the SPβ lysis-lysogeny management system is discussed.

MATERIALS AND METHODS

Reagents

Primers used in this study were purchased from Sigma-Aldrich and are listed in Table S1. Chromosomal DNA was isolated from *B. subtilis* using the peqGOLD Bacterial DNA Kit (VWR). Plasmid DNA was isolated using the Nucleospin Extract Kit (Macherey-Nagel), Gene Jet Mini Prep Kit (Thermo Scientific), or Monarch® Plasmid Miniprep (NEB). DNA fragments that were generated by the polymerase chain reaction (PCR) were purified using the PCR Purification Kit (Qiagen), Monarch® PCR & DNA Cleanup Kit (NEB), or Gene Jet gel extraction kit (Thermo Scientific). Phusion DNA polymerase, restriction enzymes and T4 DNA ligase were purchased from Thermo Scientific, NEB, or Promega and used according to the manufacturer's instructions [Sambrook et al., 1989]. Miscellaneous chemicals and media were purchased from Sigma-Aldrich, Carl Roth, and Becton-Dickinson. Plasmids were sequenced by the SeqLab Sequence Laboratories (Microsynth).

Bacterial strains, media and growth conditions

Bacterial strains are listed in Table S2. *Escherichia coli* strains were grown in lysogeny broth (LB) at 37 °C with constant shaking at 200 rpm or on LB agar plates. Unless otherwise stated, *B. subtilis* was grown in LB or sporulation (SP) medium at 37 °C [Commichau et al., 2007]. For phage induction, fresh LB was inoculated to an OD_{600} of 0.1 and the culture was incubated for 2.5 h at 37 °C. A heat shock was then applied in a water bath for 10 min at 50 °C. To allow phage replication, the culture was further incubated for 2 h at 37 °C.

DNA manipulation, transformation, strain construction and phenotypic analysis

The *E. coli* strains XL1-Blue (Stratagene) and DH10B [Grant et al., 1990] were used for cloning and transformants were selected on LB agar plates supplemented with ampicillin (100 µg/ml) (Sigma-Aldrich or Carl Roth). *B. subtilis* was transformed with plasmid or chromosomal DNA according to the two-step protocol described previously [Kunst and Rapoport, 1995]. Transformants were selected on LB plates containing chloramphenicol (5 µg ml^{-1}), kanamycin (25 µg ml^{-1}), or erythromycin (5 µg ml^{-1}). The plasmids constructed in this study are listed in Table S2. The plasmid pRH005 was constructed for the deletion of the *cat* gene in the strain TS01 using the CRISPR-Cas9 system [Altenbuchner et al., 2016]. The gRNA was introduced into the plasmid pJOE8999 using the primer pair RH080/RH081 resulting in plasmid pRH004. Next, DNA fragments flanking the *cat* gene were introduced into the plasmid pRH004 using the primer pairs RH082/RH083 and RH084/RH085. The deletion of the *cat* gene in the strain TS01 was performed as described previously [Schilling et al., 2018]. To enable the deletion of the genes of interest with the *ermC* deletion cassette [Koo et al., 2017], we had to remove the *ermD* resistance cassette in the *B. subtilis* strains KK001 and KK137, giving the strains KK002 (SPβ c2) and KK009 (SPβ), respectively. The plasmid pRH29 was generated for this purpose. The gRNA targeting the *ermD* gene was made by hybridizing the primers RH075 and RH076. The dsDNA fragment was ligated to pJOE8999 [Schilling et al. 2018; Otte et al. 2020] generating pRH001. The *ermD* deletion cassette was made with the primer pairs RH070/RH112 (flank A) and RH113/RH114 (flank B) and introduced into pRH001, resulting in pRH029. To express the *yopR*^{G407A} (YopR^{G136E}), *yopR*^{A911T} (YopR^{Y304F}) and *yopR*$^{TAT910-912GCG}$ (YopR^{Y304A}) mutant alleles from the *amyE* locus in *B. subtilis*, the plasmids pRH166, pRH180 and pRH181, respectively, were constructed. The *yopR*^{G407A}, *yopR*^{A911T} and *yopR*$^{TAT910-912GCG}$ alleles were amplified by PCR using the primer pair PP375/PP376, digested with *Eco*RI and *Bam*HI and ligated to pAC7 that was cut with the same enzymes. SPβ c2 DNA (*yopR*^{G407A}) as well as the plasmids pEJK27 (*yopR*^{A911T}) and the plasmid pEJK29 (*yopR*$^{TAT910-912GCG}$) served as

templates. The isogenic plasmid pRH167 carrying the wild- type *yopR* allele was constructed previously [Kohm et al., 2022]. The plasmid pRH182 carrying the *yopR*$^{AAG505-507GCG}$ allele (YopR ^{K169A}) was constructed as follows. Two halves of the plasmid pRH167 were amplified with the primer pairs PP396/HLHR4 and PP397/HLHR16 and purified. The fragments were combined and digested with the enzyme *Bsa*I. The remaining plasmid pRH167 was removed by digesting the sample with *Dpn*I. The purified fragments were then ligated and used to transform *E. coli* XL1-Blue. The integrity of the resulting plasmid pRH182 was verified by control digestion and Sanger sequencing. The expression of the *yopR* alleles from the plasmids pRH166, pRH167, pRH180, pRH181 and pRH182 is driven by the artificial P_{alf4} promoter and the ribosome-binding site of the *B. subtilis gapA* that were attached by PCR [Gundlach et al., 2017]. To express the wild type *yopR* and the *yopR*^{G407A} alleles from the *ganA* locus in *B. subtilis*, we constructed the plasmid pRH174 and pKK005, respectively. The *yopR* alleles were amplified by PCR using the primer pair PP375/PP376 and introduced into the plasmid pGP888 via the enzymes *Eco*RI and *Bam*HI. The artificial P_{alf4} promoter for constitutive expression was attached by PCR. To study the role of YopR on the activity of the P_{aimR} promoter, we constructed the plasmid pRH173 (P_{aimR} *cat*). For this purpose, we amplified the intergenic region upstream of the *aimR* gene with the primer pair and PP390/PP391 and introduced the fragment into the plasmid pAC5 using the restriction sites of *Eco*RI and *Bam*HI. Plasmid pRH168 was constructed for the xylose-dependent *yosL* gene from the *ganA* locus. For this purpose, the *yosL* gene was amplified by PCR with the primer pair PP366/PP367, digested with *Eco*RI and *Bam*HI and ligated to pGP888 that was cut with the same enzymes. The SPβ and SPβ c2 phages were isolated from overnight cultures of the *B. subtilis* strains 168 and CU1147, respectively, by centrifuging 2 ml of the cultures for 1 min at 10,000 x g. Bacterial cells were removed by filtration and the sterile supernatants were used to infect the *B. subtilis* strain TS01 resulting in the lysogens KK001 (SPβ) and KK137 (SPβ c2). The isolation of lysogens from plaques and the sublancin assay to verify the presence of the prophages were described previously [Otte et al., 2020; Kohm et al., 2022]. For the purification of the YopR, YopR^{G136E} and YosL proteins, the underlying gene fragments were amplified by PCR using the primer pairs LC195/LC196 for both versions of YopR and LC192/193 for YosL and introduced into a pET24d (Novagen) derivative modified for modular cloning via BsaI restriction sites. This resulted in the plasmids pEJK11 (YopR), pEJK13 (YopR^{G136E}) and pEJK9 (YosL) (Table S2). All expression constructs contained a C-terminal hexa-histidine (His_6) tag fused to the target protein. Proteins derived from *B. subtilis* were produced in *E. coli* BL21 (DE3) (NEB). Deletion of the *sprA* and *sprB* in the strain KK002 was achieved by transformation using PCR products that were generated with the primer pairs PPKK001/PPKK002 and PPKK003/PPKK004, respectively, and chromosomal DNAs of the strains BKK21660 and BKK19820 as the template.

Site-directed mutagenesis

For the overproduction of YopR variants with amino acid substitutions, we constructed the plasmids pEJK25 (YopR^{K169A}), pEJK27 (YopR^{Y304F}), and pEJK29 (YopR^{Y304A}) using the Q5 Site-Directed Mutagenesis Kit (New England Biolabs; Ipswich, USA) according to the manufacturer's protocol. The primers for mutagenesis were designed with the NEBaseChanger online tool and are listed in Table S1.

Genome sequencing

Genomic DNA was prepared from 500 µl overnight cultures using the peqGold bacterial DNA mini kit following the instruction of the manufacturer with the modification of physically opening cells with the TissueLyser II (Qiagen). Purified genomic DNA was paired end

sequenced (2 x 150 bp) (GENEWIZ). Sequence libraries were prepared with the NEBNext Ultra II FS DNA Library Prep 136 kit (New England Biolabs GmbH, Frankfurt, Germany) and sequenced with the NovaSeq6000 (Illumina, San Diego, CA, USA). The sequencing reads were mapped onto the genome of the *B. subtilis* strain SP1 and mutations were identified using the applications bowtie2 and breseq [Langmead and Salzberg, 2012; Deatherage and Barrick, 2014]. SP1 is prototrophic for tryptophan and a derivative of the laboratory strain 168 [Richts et al., 2020]. All identified mutations were verified by PCR and Sanger sequencing.

Electrophoretic mobility shift assays

EMSAs were carried out to analyze the DNA-binding activity of wild type YopR and its variants. Regions containing the P_{aimR}, P_{yosX} and *attR* sites were amplified from *B. subtilis* WT168 chromosomal DNA using the primer pairs LC226/LC252, LC230/LC254 and LC255/LC256, respectively (Table S1). In a binding reaction, 1 pmol of the DNA fragment was mixed with the indicated protein concentrations in EMSA buffer containing 20 mM HEPES-Na (pH 7.5), 200 mM NaCl, 20 mM KCl, 50 µg ml^{-1} herring sperm DNA in a final volume of 20 µl. After incubation of the reaction mixture at RT for 15 min, samples were loaded onto a 2% (w/v) agarose gel (in 1 × TBE containing 90 mM Tris, 90 mM boric acid, and 2 mM EDTA). Samples were separated at 100 V for 90 min, stained in 1 x TBE buffer containing ethidium bromide and subsequently imaged using a UV detector system.

***In vitro* recombination assays**

The *in vitro* recombination assays were performed as described previously [Abe et al., 2017] with minor modifications. Fluorescently labeled DNA substrates were amplified from *B. subtilis* wild type strain 168 chromosomal DNA using the primer pairs LC255*(Cy3 modification at 5')/LC256 (610 bp) for *attR* site and EJK54/EJK55*(Cy5 modification at 5') (242 bp) for *attL* site (Table S1). In the assayed reaction, 20 nM of the DNA substrates were mixed with 20 µM YopR or the indicated YopR variant in a buffer containing 20 mM HEPES-Na (pH 7.5), 200 mM NaCl and 20 mM KCl, in a final volume of 10 µl. The mixture was incubated at 37 °C for 60 minutes. The recombination reaction was stopped by the addition of 0.1% (w/v) SDS and by heat treatment at 85 °C for 3 min. Samples were loaded onto a native 6% (w/v) polyacrylamide gel (in 0.5 × TBE containing 45 mM Tris, 45 mM boric acid and 1 mM EDTA). Samples were separated at 100 V for 90 min and subsequently imaged with the 600 and 700 nm channels of an Odyssey FC Imager (LI-COR Biosciences, Lincoln, US).

β-galactosidase activity assay

Quantitative studies of *lacZ* expression in *B. subtilis* were performed as described previously [Kunst and Rapoport, 1995]. Cells were grown at 37 °C and 220 rpm in 30 ml of LB medium. The medium was supplemented in 300 ml shake flasks and the cells were grown without additional aeration. Cells were harvested before heat shock and at, 30 min, 60 min, 90 min, 120 min and 150 min incubation at 50 °C. Specific β-galactosidase activities were determined with cell extracts obtained by lysozyme treatment. One unit of β-galactosidase is defined as the amount of enzyme which produces 1 nmol of *o*-nitrophenol per min at 28 °C. The BioRad dye-binding assay was used to determine the protein concentrations.

Overexpression and protein purification

For recombinant overexpression of YopR-His_6 (pEJK11), the YopR-His_6 variants G136E (pEJK13), K169A (pEJK25), Y304F (pEJK27) and Y304A (pEJK29) and YosL-His_6 (pEJK9), 2 l of LB medium containing kanamycin (50 µg ml^{-1}) and 1% (w/v) lactose for autoinduction of the P_{lac}

promoter driving the expression of the T7 polymerase required for recombinant gene expression were incubated in an aerial shaker for 18 h at 30 °C. After harvesting, cells were lysed by a microfluidizer (M110-L, Microfluidics). The lysis buffer contained 20 mM HEPES-Na (pH 8.0), 250 mM NaCl, 20 mM KCl and 40 mM imidazole. Cell debris was then removed by high-speed centrifugation for 20 min at 48,000 × g. All proteins were initially purified by nickel ion affinity chromatography and eluted with lysis buffer containing 250 mM imidazole. Further purification using HiTrap Heparin HP columns (Cytiva, Marlborough, USA) was performed according to the manufactures protocol. The eluted proteins were concentrated by centrifugation (3 kDa or 10 kDa MWCO) and further polished by size-exclusion chromatography on a S200 XK16 column (for YopR and variants) or S75 XK16 column (for YosL) (Cytiva, Marlborough, USA) with size-exclusion chromatography (SEC) buffer consisting of 20 mM HEPES-Na (pH 7.5), 200 mM NaCl and 20 mM KCl. Purified proteins were analyzed for the presence of bound nucleotides by agarose gel electrophoresis and analytical size-exclusion chromatography.

Analytical size-exclusion chromatography

For the analytical SEC, purified YopR and YopR variants were diluted in a buffer containing 20 mM HEPES-Na (pH 6.37), 200 mM NaCl and 20mM KCl to a final concentration of 100 µM. 100 µl were then injected at 4 °C on to a pre-equilibrated S200 300/10 GL analytical size-exclusion column (Cytiva, Marlborough, USA) on an ÄKTA system (UNICORN 7.6; Cytiva). For size calibration, a mixture of standard proteins [thyroglobulin (660 kDa), ferritin (474 kDa), aldolase (160 kDa), conalbumin (76 kDa), ovalbumin (43 kDa) and ribonuclease A (13.7 kDa)] was used according to the manufacturer's protocol (Cytiva, Marlborough, USA). Data were plotted using GraphPad Prism (GraphPad Prism Corp. San Diego, USA).

Thermal shift assays using nanoDSF

To assess the protein folding and thermal stability of YopR and its variants, thermal shift assays were performed with nanoDSF integrated in the Prometheus NT.48 (NanoTemper Technologies GmbH, Germany). Protein solutions of 75-100 µM of YopR WT, YopR^{G136E}, YopR^{K169A}, YopR^{Y304A} and YopR^{Y304F} were soaked into a Prometheus NT.48 Series nanoDSF Grade Standard Capillaries and analyzed using PR. ThermControl software. Data were evaluated and plotted using GraphPad Prism (GraphPad Prism Corp., San Diego, USA). The normalized data were fitted to Boltzmann sigmoidal equation. The T_m values correspond to the inflection point of the sigmoidal curve [Boltzmann, 1970; Niesen et al., 2007].

Isothermal titration calorimetry

Ligands and proteins (purified wild type protein YopR and YopR^{G136E} and YopR^{Y304F} variants) were diluted with a buffer containing 20 mM HEPES-Na (pH 7.5), 200 mM NaCl and 20 mM KCl. The DNA ligand (*aimR* promotor) was obtained by the hybridization of LC292/LC293 primers at 95 °C for 2 minutes. The sample cell was filled with DNA (*aimR* promotor) at a nominal concentration of 20 µM. The YopR proteins were placed in the syringe and their concentrations were predetermined by absorbance at 280 nm to saturate the DNA sample during the titrations. All the measurements were performed at 25 °C with the instrument MicroCal PEAQ-ITC (©Malvern Panalytical) with a method consisting of 13 injections (first 0.4 µl, and the rest 3 µl each) and 150 s of spacing. The raw data were processed with the MicroCal PEAQ-ITC Analysis Software (Malvern Panalytical) using the "one set of sites" models.

Crystallization and structure determination

Crystallization was performed by the sitting drop vapor diffusion method at 20 °C in 250 nl drops consisting of equal parts of protein and precipitation solutions. Protein solutions of 480 µM YopR-His_6 were used for crystallization. A total of 384 different conditions were included in the screen (JCSG Core Suite I-IV, Qiagen) and crystals obtained in 0.2 M disodium tartrate supplemented with 20% (w/v) PEG3350. Prior to data collection, crystals were flash-frozen in liquid nitrogen using a cryo-solution that consisted of mother liquor supplemented with 20% (v/v) glycerol. Data were collected under cryogenic conditions at the European Synchrotron Radiation Facility (Grenoble, France) [Theveneau et al., 2013]. MxCube3 was used for data collection (https://github.com/mxcube). Data were processed with XDS (version January 31, 2020) and scaled with XSCALE [Kabsch, 2010]. The structure was determined by molecular replacement with PHASER [McCoy, 2006], manually built in COOT (Coot Version 0.9.4.1) [Emsley and Cowtan, 2004], and refined with PHENIX [Liebschner et al., 2019] (Phenix Version 1.17.1-3660 and 1.19). The search model for the YopR structure was the N-terminal domain (residues 1-105) of the Alphafold2 model [Jumper et al., 2021]. Figures were prepared with Pymol (www.pymol.org). Crystallization data collection and refinement statistics are given in Table 2. Structure coordinates and structure factors of YopR have been deposited under the PDB-ID: 8a0a (https://doi.org/10.2210/pdb8A0A/pdb).

Hydrogen/deuterium exchange mass spectrometry

Preparation of samples for HDX-MS was aided by a two-arm robotic autosampler (LEAP Technologies) as described previously with minor modifications [Osorio-Valeriano et al., 2019]. YopR protein variants and DNA (where indicated) were employed at concentrations of 25 µM each. Hydrogen/deuterium exchange (HDX) was initiated by 10-fold dilution of YopR, $YopR^{G136E}$ or $YopR^{Y304F}$ in buffer (20 mM HEPES-Na pH 7.5, 20 mM KCl, 200 mM NaCl) prepared in D_2O. After incubation at 25 °C for 10, 30, 100, 1,000 or 10,000 s, the HDX was stopped by mixing the reaction with an equal volume of quench buffer (400 mM KH_2PO_4/H_3PO_4, 2 M guanidine-HCl; pH 2.2) temperated at 1 °C, and 100 µl of the resulting mixture injected (loop volume 50 µl) into an ACQUITY UPLC M-Class System with HDX Technology [Wales et al., 2008]. Non-deuterated samples were generated similarly by 10-fold dilution in buffer prepared with H_2O. The injected HDX samples were washed out of the injection loop with H_2O + 0.1% (v/v) formic acid at 100 µl min^{-1} flow rate and guided over a column (2 mm x 2 cm) filled with immobilized protease facilitating proteolytic digestion at 12 °C. The resulting peptides were collected on a trap column (2 mm x 2 cm), that was filled with POROS 20 R2 material (Thermo Scientific) kept at 0.5 °C. After three minutes of digestion and trapping, the trap column was placed in line with an ACQUITY UPLC BEH C18 1.7 µm 1.0 x 100 mm column (Waters) and peptides eluted through a gradient of H_2O + 0.1% (v/v) formic acid (eluent A) and acetonitrile + 0.1% (v/v) formic acid (eluent B) at 60 µl min^{-1} flow rate as follows: 0-7 min/95-65% A, 7-8 min/65-15% A, 8-10 min/15% A. Eluting peptides were guided to a Synapt G2-Si mass spectrometer (Waters) and ionized with by electrospray ionization (250 °C capillary temperature, 3.0 kV spray voltage). Mass spectra were acquired from 50 to 2,000 *m/z* in enhanced high-definition MS ($HDMS^E$) [Geromanos et al., 2009; Li et al., 2009] or high-definition MS (HDMS) mode for non-deuterated and deuterated samples, respectively. Continuous lock mass correction was implemented with [Glu1]-Fibrinopeptide B standard (Waters). During separation of the peptides on the ACQUITY UPLC BEH C18 column, the pepsin column was washed three times by injecting 80 µl of 0.5 M guanidine hydrochloride in 4% (v/v) acetonitrile. Blank runs (injection of H_2O instead of protein) were performed between each sample. The experiment was conducted twice in triplicates (individual HDX reactions) whereby either immobilized porcine pepsin or a mixture of immobilized protease type XVIII

from *Rhizopus* sp. and protease type XIII from *Aspergillus saitoi* were employed for proteolytic digestion. Peptides were identified and evaluated for their deuterium incorporation with the softwares ProteinLynx Global SERVER 3.0.1 (PLGS) and DynamX 3.0 (both Waters) as described [Osorio-Valeriano et al., 2019]. Peptides were identified with PLGS from the non-deuterated samples acquired with $HDMS^E$ employing low energy, elevated energy and intensity thresholds of 300, 100 and 1,000 counts, respectively and matched using a database containing the amino acid sequence of YopR, porcine pepsin and their reversed sequences with search parameters as follows: Peptide tolerance = automatic; fragment tolerance = automatic; min fragment ion matches per peptide = 1; min fragment ion matches per protein = 7; min peptide matches per protein = 3; maximum hits to return = 20; maximum protein mass = 250,000; primary digest reagent = non-specific; missed cleavages = 0; false discovery rate = 100. For quantification of deuterium incorporation with DynamX, the data obtained from pepsin or fungal protease digestion were combined, and peptides had to fulfil the following criteria: Identification in at least 2 of 3 non-deuterated samples for either protease digestion protocol; the minimum intensity of 10,000 counts; maximum length of 30 amino acids; minimum number of products of two; maximum mass error of 25 ppm; retention time tolerance of 0.5 minutes. All spectra were manually inspected and omitted, if necessary, e.g. in case of low signal-to-noise ratio or the presence of overlapping peptides disallowing the correct assignment of the isotopic clusters. Residue-specific deuterium uptake from peptides identified in the HDX-MS experiments was calculated with the software DynamX 3.0 (Waters). In the case that any residue is covered by a single peptide, the residue-specific deuterium uptake is equal to that of the whole peptide. In the case of overlapping peptides for any given residue, the residue-specific deuterium uptake is determined by the shortest peptide covering that residue. Where multiple peptides are of the shortest length, the peptide with the residue closest to the peptide C-terminus is utilized. Raw data of deuterium uptake by the identified peptides and residue specific HDX are provided in Supplemental Dataset.

Western blot analysis

Heterologously produced and purified YopR-His_6 and YosL-His_6 proteins were used to generate rabbit polyclonal antibodies (Dr. Benli, Göttingen). For Western blot analyses, the cells were grown as described for the β-galactosidase activity assay. Proteins were separated by 15% SDS-PAA gels. After electrophoresis, the proteins were transferred to a polyvinylidene difluoride membrane (PVDF, BioRad) by electroblotting. YopR and YosL were detected with polyclonal antibodies [Commichau et al., 2007]. Antibodies were visualized by using anti-rabbit immunoglobulin G-alkaline phosphatase secondary antibodies (Promega) and the CDP-star detection system (Roche Diagnostics) as described previously [Commichau et al., 2007].

RESULTS

Verification of the SPβ c2 phenotype and generation of lysogens in a prophage-free strain

To verify the heat-sensitive phenotype of the historical *B. subtilis* strain CU1147 carrying the SPβ c2 prophage, we performed a heat shock experiment [Zahler et al., 1977; Rosenthal et al., 1979]. For this purpose, cultures containing exponentially growing cells of CU1147 were shifted from 37 °C to 50 °C for 5 minutes as described previously [Rosenthal et al., 1979]. As shown in Figure 2A, only the cells of CU1147 started to lyse 1 hour after heat treatment, confirming the presence of the SPβ c2 in the genome of CU1147 and the heat-sensitive phenotype of the prophage. To explore the underlying genotype of the SPβ c2 phage mutant and to prevent a potential crosstalk between SPβ c2 and other prophages and prophage-like

elements, we established the *B. subtilis* strain TS01 as the new host. The TS01 strain is a descendant of 168, lacking the prophages SPβ and PBSX, the prophage-like elements prophage 1, prophage 3, and *skin*, as well as the *pks* polyketide synthesis operon [Westers et al., 2003; Reuss et al., 2016; Schilling et al., 2018]. New lysogens carrying SPβ and SPβ c2 designated as KK009 and KK002, respectively, were isolated from plaques of TS01-infected cells (Figure 2B, upper panel). Further experiments revealed that a cultivation temperature of 37 °C and a 10 min-long heat shock are best suited to induce the lytic cycle of SPβ c2. The sublancin assay indicated the presence of the prophages and the subsequent heat shock experiment confirmed that the heat-induced cell lysis was caused by SPβ c2 (Figure 2B, lower panel; Figure 2C).

The YopR^{G136E} variant confers heat induction of the SPβ c2 prophage

Previously, it has been suggested that the c2 allele encodes a repressor of SPβ [Rosenthal et al., 1979]. However, the mutation causing the c2 phenotype remained unknown. To identify the mutation(s) conferring heat inducibility of SPβ c2, we re-sequenced the SPβ c2 genome. Sequence variations were identified through a direct alignment with the SPβ genome of the *B. subtilis* laboratory strain SP1 [Richts et al., 2020]. We identified four sequence variations in the *yorN-yorM* intergenic region and in the *yoqA*, *yopR* and *yokI* genes. The mutation in the *yorN-yorM* intergenic region could also affect either the transcription of the *yorN* gene of unknown function or the translation of the *yorN* mRNA. The sequence deviations in the remaining three genes cause amino acid exchanges in the encoded proteins (Table 1). While YoqA shares no similarity to any known protein domains, YokI and YopR share sequence similarities with ribonucleases and DNA breaking-rejoining proteins, respectively. Since it was recently shown that YopR is the master repressor of the lytic cycle of SPβ [Brady et al., 2021; Kohm et al., 2022], we speculated that the base exchange G407A in the coding region of *yopR* is responsible for the heat-sensitivity of SPβ c2. To test this idea, we fused the constitutively active synthetic P_{alf4} promoter [Gundlach et al., 2017] and the ribosome binding site of the *B. subtilis gapA* gene to the *yopR* wild type and the *yopR*^{G407A} alleles and integrated the constructs into the *amyE* locus of the strains KK002 (SPβ c2 [*yopR*^{G407A}]) and KK009 (SPβ [*yopR*]), respectively. The resulting strains were designated as KK011 (SPβ c2 [*yopR*^{G407A}] P_{alf4}-*yopR*) and KK014 (SPβ [*yopR*] P_{alf4}-*yopR*^{G407A}). Next, we constructed the strain KK015 (SPβ [*yopR::ermC*] P_{alf4}-*yopR*^{G407A}) lacking the native SPβ *yopR* allele. The following heat shock experiment confirmed that the heat-induced cell lysis of *B. subtilis* was due to the mutation in *yopR* because all strains carrying SPβ and the *yopR*^{G407A} allele (KK002 and KK015) lysed after the heat shock (Figure 2C). Furthermore, no cell lysis was observed with the strains KK011 (SPβ c2 [*yopR*^{G407A}*::ermC*] P_{alf4}-*yopR*) and KK014 (SPβ [*yopR*] P_{alf4}-*yopR*^{G407A}) that carried both *yopR* alleles (Figure 2C). Thus, the wild type YopR protein is dominant over the YopR^{G136E} variant. To conclude, the G407A mutation in *yopR* causes the heat sensitivity of YopR^{G136E}.

Characterization of YopR and YopR^{G136E}

To assess whether the heat shock affects the cellular concentration of the YopR^{G136E} variant, we performed a Western blot experiment with crude extracts from the strains TS01 (no phage) and KK002 (SPβ c2) that were grown over night at 37 °C. We also analyzed samples from a culture of the strain KK002 that was grown for 2.5 h at 37 °C and for 10 min at 50 °C. As expected, the strain TS01 did not synthesize YopR (Figure 3A). By contrast, the strain KK002 produced a protein corresponding to the molecular weight of YopR. Moreover, the bacteria produced comparable amounts of YopR^{G136E} variant before and after the heat shock. Thus, the G136E exchange in YopR probably does not affect the *in vivo* stability of the protein.

Next, we assessed the effect of the temperature on the folding of the YopR wild-type protein and the YopR^{G136E} variant *in vitro*. For this purpose, the affinity-purified proteins were assessed for their unfolding behavior in response to increasing temperature by nanoDSF. While the YopR wild-type protein exhibited an unfolding temperature of 47.8 °C, the heat-sensitive YopR^{G136E} variant unfolded approximately 10 °C earlier, at a temperature of 38.4 °C (Figure 3B). To assess the correct folding of YopR^{G136E}, the variant was also analyzed by analytical size-exclusion chromatography (SEC). The wild-type protein as well as the YopR^{G136E} variant showed a single symmetrical peak corresponding to the size of a YopR monomer (calculated size: 36 kDa, experimentally determined size: 43.06 kDa for YopR-WT and 53.8 kDa for YopR^{G136E} (Figure S1A, C). Additionally, examination of the proteins through SDS-PAGE revealed signs of degradation for YopR^{G136E} (Figure S1G). Hence, mutation of G136E in YopR renders the protein less stable and temperature sensitive *in vitro*.

YopR is a DNA binding protein

To further analyze the role of the G136E amino acid exchange in YopR, we aimed to study the protein biochemically. Hence, the YopR wild type protein and the YopR^{G136E} variant carrying a C-terminal His$_6$-tag were produced in *E. coli* and purified by Ni-NTA affinity purification. During initial purification of YopR, co-purification of substantial amounts of DNA was observed, indicating that YopR is a DNA-binding protein (Figure S2). To obtain a DNA-free YopR protein sample an additional purification step using a Heparin column and a salt-gradient elution was performed after Ni-NTA purification (Figure S1A, B). Absence of DNA was assessed by analyzing the molecular weight of purified YopR by analytical size-exclusion chromatography (Figure S1A-C and G). We further wanted to test if YopR specifically binds to sequences found in the genome/intergenic regions of SPβ. Hence, electrophoretic mobility shift assays (EMSAs) using purified DNA-free YopR and YopR^{G136E} were performed with the fragments upstream of *aimR* and *yosX* harboring the previously described SPBRE (SPβ repeated element) [Lazarevic et al., 1999]. While the YopR wild type protein only required the presence of 5-fold protein excess to result in a shift of the DNA fragments, the YopR^{G136E} variant showed a decrease in binding affinity (approx. 10 to 20-fold excess of YopR^{G136E} required for a similar DNA shift) (Figure 4A-D). To further assess the reduced binding affinity, we performed binding studies using isothermal titration calorimetry (ITC). We employed the region upstream of the *aimR* promoter and added increasing amounts of the YopR wild type protein or the YopR^{G136E} variant. While the wild type protein had a DNA binding affinity of 0.238 ± 0.08 µM (Figure S3A, C), the binding affinity of the YopR^{G136E} variant was increased by approximately 7-fold to 1.69 ± 0.69 µM (Figure S3B, D). To conclude, the EMSAs and ITC analysis indicate that YopR is a DNA-binding protein and that the G136E exchange reduces its affinity for DNA. Since it was unclear if the tested DNA fragments containing the previously described SPBRE (SPβ repeated element) are the correct DNA binding targets of YopR, we also analyzed DNA binding of the *attR* region at the corner of the SPβ genome and an unrelated gene from *B. subtilis* (*yaaA*) (Figure 4E, F and Figure S4). EMSAs of both regions indicate a DNA binding behavior of the wild-type YopR protein like that observed for the SPBRE-containing regions upstream of the SPβ *aimR* and *yosX* genes (Figure 4E and Figure S4A). In contrast, the EMSA assessing the binding of YopR^{G136E} to the unrelated gene from *B. subtilis* (*yaaA*) indicates even less binding affinity as compared to the other tested regions. While for YopR^{G136E} a shift of the DNA-protein complex using the *attR* region, and the regions upstream of the SPβ *aimR* and *yosX* genes was observed upon addition of approximately 20-fold protein excess, a shift of the *yaaA* genetic region was only observed in a DNA:protein-ratio of 1:100 (Figure S4B). Therefore, the factors that establish the specificity of YopR DNA binding are still unclear.

***In vivo* DNA binding activity of YopR**

To assess the effect of the environmental temperature on the *in vivo* DNA-binding activity of YopR and YopR^{G136E}, we monitored the activity of a translational P_{aimR}-*lacZ* fusion. For this purpose, the *yopJ-aimR* (219 bp) intergenic region containing the predicted SPBRE site and the promoter region [Lazarevic et al., 1999] was fused to a promoter-less *lacZ* gene. The P_{aimR} fragment consists of SPBRE site, which is followed by the promoter (Figure 4G). The construct was integrated into the *amyE* locus of the strains TS03 (no *yopR*) and KK101 (*yopR*^{G407A}), resulting in the strains KK100 (P_{aimR}-*lacZ*) and KK098 (P_{aimR}-*lacZ yopR*^{G407A}), respectively. The strain KK139 (P_{aimR}-*lacZ yopR*) was generated by transformation of KK100 with the plasmid pKK005. Next, we cultivated the bacteria for 2.5 h at 37 °C, shifted the cultures for to 50 °C and continued the cultivation for 2.5 h. The activity of the β-galactosidase was measured every half hour (Figure 4G). As expected, the P_{aimX} promoter was active over a period of 2.5 h in the strain KK100 lacking *yopR*. The decrease in β-galactosidase activity is probably due to the thermosensitivity of the enzyme. Similarly, the P_{aimX} promoter in the strain KK098 synthesizing the thermosensitive YopR^{G136E} protein also stayed active within 2.5 h of cultivation. By contrast, β-galactosidase activity in the strain KK139 carrying the wild type *yopR* allele was already greatly reduced after 30 min of incubation. To conclude, β-galactosidase activity assays revealed that YopR is a DNA-binding protein that binds to the *yopJ-aimR* intergenic region of the SPβ genome. We could also confirm that YopR^{G136E} does indeed respond to the ambient temperature *in vivo.* However, the fact that the P_{aimR} promoter was active at 37 °C when either YopR or YopR^{G136E} was present suggests that other factors exist to inactivate the P_{aimX} promoter and to prevent entry into the lytic cycle.

Structural analysis of YopR reveals protein fold typical for tyrosine recombinases

In accordance with our observation that YopR is a DNA binding protein, bioinformatical analysis using the amino acid sequence of YopR identified a potential DNA breaking-re-joining catalytic domain (InterProScan5), and BLAST analysis showed weak similarities to potential integrases and recombinases. Hence, to gain molecular insight into the mode of action of YopR, we performed a crystallographic analysis. After overproduction of YopR fused to a C-terminal His_6-tag in *E. coli*, the protein was purified using Ni-NTA-affinity and size-exclusion chromatography, concentrated, and used for crystallization screens. Crystals formed within one week of incubation, and we determined the structure of YopR at a resolution of 2.8 Å by molecular replacement using the N-terminal domain (residues 1-105) of the YopR Alphafold model [Jumper et al., 2021] and manually building of the C-terminal part (residues 106-320) (Table 2). Two YopR molecules were present in the crystallographic asymmetric unit (Figure S5). The monomers interact only weakly via residues of mainly two α-helices (helix H' and I) (Figure S5D-F). As YopR elutes as a monomer in analytical SEC experiments (Figure S1A), the formation of a potential YopR dimer appears to be an artifact of crystal packing (Figure 5, and S5). The YopR monomer consists of 15 α-helices and 4 β-strands (Figure 5A, B; PDB-ID: 8a0a). The overall structure of a YopR monomer shows a high similarity to bacterial and phage tyrosine recombinases (Figure 5E-F and Figure S6) [Meinke et al., 2016; Grindley et al., 2006]. As other proteins with a tyrosine recombinase fold, YopR harbors a CB (core-binding) domain (Gly1-Lys84, helix A-D) at the N-terminus, a catalytic (CAT) domain at the C-terminus (Tyr108-Ala320, helix F-M), which are connected by a central unfolded linker (Gly85-Leu107, helix/loop E) (Figure 5). While amino acid sequence alignments of YopR to tyrosine recombinases do not yield a high percentage of sequence identity (below 25 percent), structural comparison using PDBefold identifies the highest similarity to the structurally and functionally characterized

tyrosine recombinases Cre from *E. coli* phage P1 [Duyne, 2001; Ennifar et al., 2003], XerH from *Helicobacter pylori* [Bebel et al., 2016], and the integrase (Int) from *E. coli* phage lambda [Kwon et al., 1997; Biswas et al., 2005; Aihara et al., 2003] (Figure 5E-H and Figure S6). Most of these tyrosine recombinases have been crystallized in complex with DNA to elucidate the recombination mechanisms in detail, while YopR was crystallized in its apo form. When YopR is structurally aligned to these proteins, the RMSD values for the CB (N-terminal domain) and CAT (C-terminal domain) range between 4 and 6 Å (Table 3). Overlay of YopR with structures of Cre (PDB-ID: 1q3u) [Ennifar et al., 2003], XerH (PDB-ID: 5jk0) [Bebel et al., 2016], and lambda Int (PDB-ID: 1p7d) [Aihara et al., 2003] bound to DNA, revealed the requirement of immense structural rearrangements of YopR during potential DNA binding. While the CB domain in the YopR crystal structure (in absence of DNA) is rotated by approximately 180° vertically and 45° horizontally compared to Cre, XerH and Lambda Int, the CAT domain needs to be flipped by 90° horizontally (Figure 5B, E-H and Figure S6). We hypothesize that the observed organization of YopR might be a crystallographic artefact since YopR was not co-crystallize with DNA. The flexibility for the proposed rearrangements is provided by the approximately 22 residue long linker present between the CB and CAT domain (labelled as helix E' located between α-helices E and F), which is also present in Cre, XerH and Lambda Int (Figure 5 and Figure S6). This structural rearrangement would also generate a positively charged groove between the CB and CAT domains of YopR suitable for DNA interaction (Figure 5C, D).

Perturbations in secondary and higher order structure of YopR^{G136E}

The difference in melting temperature suggested to us that YopR^{G136E} may differ in its conformation from YopR causative for the higher instability of the former. We thus employed hydrogen/deuterium exchange mass spectrometry (HDX-MS) to ascertain potential differences in conformation between both YopR variants. HDX-MS probes the rate with which the amide protons contained in the peptide bond exchange for protons from the solvent, the degree of which is an intrinsic characteristic of an amino acid sequence, whether the amide protons establish hydrogen bonding interactions and their solvent accessibility. Incubation of a protein in D_2O-containing solvent visualizes this exchange rate because a successful exchange results in a mass shift that can be quantitated by MS. Hence, HDX-MS may provide insights into a protein's higher order structure and conformational dynamics [Masson, 2019]. The comparison of the HDX of YopR and YopR^{G136E} reveals that the latter incorporates more deuterium in many parts of the protein (Figure 6A and Figure S7). These regions are mainly located in the CAT domain, but less extensive changes are also apparent in the CB domain (e.g., residues 51-63, Figure 6B). While the G136E site of variation cannot be directly compared in this way because different peptides are obtained for either protein, areas in spatial proximity of the site of variation similarly show elevated HDX for YopR^{G136E} (residues 250-258, Figure 6B). Illustration of all the YopR areas in which YopR^{G136E} incorporates more deuterium on its crystal structure highlights that almost the entire CAT domain and the proximal portions of the CB domain (Figure 6C) are affected. As the HDX rate is inversely correlated with the degree of higher order structure, the higher HDX of YopR^{G136E} than native YopR is indicative for a less ordered conformation in most parts of this protein variant coinciding with its lower melting temperature (Figure 3B).

Mutational and functional analysis of YopR

Tyrosine recombinases are site-specific DNA modifying enzymes that bind, cleave, strand exchange, and rejoin DNA at their respective, typically palindromic, recognition target sites. The function of this enzyme family has been best studied in detail for the Cre, Xer and Lambda

Int recombinases. For each of these recombinases, detailed molecular studies have led to the identification of residues that are crucial for DNA recombination activity [Grindley et al., 2006; Ennifar et al., 2003; Aihara et al., 2003; Bebel et al., 2016; Jayaram et al., 2015]. The analyzed residues listed in Table 3 resemble a core active site of tyrosine recombinases, with highly conserved catalytic core: R, D/E, K, H, R, H/W and Y. These residues engage the scissile phosphate and a tyrosine nucleophile that forms a 3' phosphotyrosine linkage with the cleaved DNA. When exemplarily compared to the closest structural homologs Cre, XerH, and Lambda Int, only three of the seven residues crucial for catalysis are present in YopR (Table 3, Figure 5 D-E, Figure 7 and Figure S8). Especially the crucial arginine and histidine residues are substituted by serine, valine and asparagine in YopR (Table 3, Figure 5, Figure 7, Figure S8). The first conserved residue also present in YopR is K169, which is homologous to K201 in Cre, K239 in XerH and K235 in Int (Table 3, Figure 7, Figure S8). In Cre recombinase, K201 contacts a base adjacent to the cleaved phosphate in the minor groove of the DNA and the residue is positioned in a flexible loop. Alanine mutants of this lysine residue in XerD and Cre were defective in recombination [Duyne et al., 2001]. The second conserved residue is a nucleophilic tyrosine (Y304 in YopR, Y324 in Cre, Y344 in XerH, and Y342 in Int; Table 3, Figure 7, Figure S8) that is described to form a phosphor-protein covalent linkage. As shown for Cre and Lambda Int, it attacks the scissile phosphate forming a 3'-phosphotyrosine linkage and resulting in a free 5'-HO during DNA cleavage [Duyne et al., 2001; Biswas et al., 2005]. The third conserved residue also found in YopR is E144. In some tyrosine recombinases such as Lambda Int it is substituted by an aspartate (Table 3). This residue appears to contribute indirectly to transition state stabilization by hydrogen bonding to catalytic residues and promoting the integrity of the active site [van Duyne et al., 2001; Biswas et al., 2005; Meinke et al. 2016]. The other residues (histidines and arginines) required for catalytic activity, synapsis formation and stabilization of the transition state during recombination are not conserved in YopR and are replaced by serine, valine and asparagine residues (Table 3, Figure 7, Figure S8). Hence, it is questionable if YopR also functions as a DNA-cleaving recombinase or rather has lost this enzymatic activity.

It has previously been shown that replacement of the nucleophilic tyrosine in the tyrosine recombinases Cre, XerH and Lambda Int by either a phenylalanine or alanine residue renders the recombinase inactive [Grindley et al., 2006; Ennifar et al., 2003; Aihara et al., 2003; Bebel et al., 2016; Jayaram et al., 2015]. Since this potential nucleophilic tyrosine (Y304 in YopR) is also found in YopR and to further investigate the biological function of YopR, we introduced point mutations in the *yopR* gene leading to a replacement of Y304 by alanine or phenylalanine. We further generated a YopR mutant in which the conserved catalytical residue K169 is exchanged by an alanine. Each of these proteins could be produced heterologously in *E. coli* and purified (Figure S1G). We first characterized these YopR variants biochemically and analyzed their folding and oligomeric state via analytical size exclusion. All tested variants except YopR ^{Y304A} showed a monomeric protein peak in this analysis (Figure S1D-G). YopR ^{Y304A} possessed a peak shoulder, showed bands of degradation in SDS-PAGE analysis and large parts of the protein were insoluble during overproduction indicative for problems in protein folding and stability (Figure S1E, H). We further tested the thermostability of these variants using nanoDSF. While the YopR^{K169A} variant showed the same thermal unfolding behavior as the wild type YopR protein, the thermal stabilities of the YopR^{Y304F} and YopR^{Y304A} variants were reduced by about 6 °C (Figure 3B) comparable to the initially tested heat sensitive YopR^{G136E} variant. This inference is also substantiated by changes in HDX-MS of YopR^{Y304F} compared to native YopR, which are highly reminiscent in quality and quantity to those observed for the heat sensitive YopR^{G136E} variant (Figure 6).

Next, we assessed the YopR^{K169A} and YopR^{Y304F} variants for their *in vitro* DNA binding affinity via ITC using the same regions as described previously. While the YopR^{K169A} variant possessed a DNA binding affinity to the fragment upstream of *aimR* in a similar range as YopR wild type in the ITC analysis (0.238 ± 0.08 µM for YopR wild type and 0.346 ± 0.15 µM for YopR^{K169A}), the Y304F exchange resulted in a phenotype comparable to the heat sensitive G136E mutant (1.69 ± 0.69 µM for YopR^{G136E} and 1.34 ± 0.5 µM for YopR^{Y304F}) (Figure S3). To further consolidate this notion, we performed HDX-MS on YopR, YopR^{G136EF} and YopR^{Y304F} in presence of DNA and compared the HDX rate of those to their respective apo states (Figure 8). The protein regions exhibiting reduced HDX in presence of DNA are similar for all three variants except for the linker region between helices E and F, and the C-terminal YopR portion encompassing helices K to N (Figure 8A). These concur with the areas where YopR^{G136E} and YopR^{Y304F} showed the most pronounced defects in higher-order structure (Figure 6). Collectively, these data suggest that both variants are, in principle, still capable of DNA coordination via the CAT domains' N-terminal portion and that their reduced DNA binding affinity is causally linked to structural defects in the C-terminal part of the CAT domain (Figure 8C).

YopR does not show recombination activity

Since YopR possesses a similar fold as tyrosine recombinases and at least harbors the catalytically important tyrosine and lysine residue, we wondered if YopR can function as a recombinase *in vitro* using the *attL* and *attR* sites of the SPβ phage [Abe et al., 2017]. To assess the activity of YopR WT, and the YopR^{G136E}, YopR^{Y304F} and YopR^{K169A}, we employed an *in vitro* recombination assay previously described by Abe et al. with minor changes as we used fluorescently labeled fragments of the *attL* (242 bp, labelled with Cy5) and *attR* (616 bp, labelled with Cy3). If YopR would be able to cleave, strand exchange, and rejoin the SPβ recombination sites, we would expect the appearance of a hybrid DNA fragment with the size of 426 bp carrying both fluorescence labels (Figure S9A). YopR wild type and the tested YopR^{G136E}, YopR^{Y304F}, and YopR^{K169A} variants were incubated with the labeled *attL* and *attR* sites for 60 min at 37 °C, boiled to release YopR from the DNA and analyzed on a native polyacrylamide gel. Neither YopR wild type, nor any of the tested YopR variants resulted in the formation of a hybrid DNA fragment carrying both fluorescence labels, which would be indicative for a DNA recombination event of the SPβ *att* sites (Figure S9B).

Next, we assessed the *in vivo* activities of the YopR^{K169A}, YopR^{Y304F} and YopR^{Y304A} variants by performing a heat shock experiment. For this purpose, we introduced the *yopR*^{A911T} (Y304F), *yopR*$^{TAT910-912GCG}$ (Y304A) and *yopR*$^{AAG505-507GCG}$ (K169A) alleles into the *amyE* locus of the strain KK002 (SPβ c2). Next, we deleted the native *yopR*^{G407A} copy from the SPβ c2 genome resulting in the strains KK120 (SPβ c2 [*yopR*^{G407A}*::ermC*] P_{alf4}-*yopR*^{A911T}), KK121 (SPβ c2 [*yopR*^{G407A}*::ermC*] P_{alf4}-*yopR*$^{TAT910-912GCG}$) and KK138 (SPβ c2 [*yopR*^{G407A}*::ermC*] P_{alf4}-*yopR*$^{AAG505-507GCG}$). The fact that it was possible to delete the native *yopR*^{G407A} allele indicates that the YopR^{K169A}, YopR^{Y304F} and YopR^{Y304A} variants were functional because they prevented the entry of the SPβ *yopR* mutant to enter the lytic cycle under unstressed conditions (Figure 3C). Consistent with the nanoDSF experiments (Figure 3B), only the YopR^{Y304F} and YopR^{Y304A} variants but not YopR^{K169A} showed increased temperature sensitivities (Figure 3C). Thus, the residues G136 and Y304 are critical for the thermal stability of YopR. Moreover, it is unlikely that YopR functions as a recombinase because the replacement of the tyrosine residue, which is crucial for enzyme catalysis of known recombinases (see above), still allows the phage to enter the lytic cycle.

Heat induction of the lytic cycle of SPβ c2 does not depend on SprB

Previously, it was shown that SprA and SprB are required for SPβ prophage excision during sporulation (Figure 1) [Abe et al., 2014]. We were wondering if the heat-inducible SPβ excision of the c2 mutant also depends on SprA and SprB. To test this idea, we deleted the *sprA* and *sprB* genes in the strain KK002 carrying SPβ c2. Genome sequencing verified the deletion of the *sprA* and *sprB* genes in the strains KK124 (*sprA::aphA3*) and KK125 (*sprB::aphA3*), respectively. Both strains also carried the four mutations that were identified in the SPβ c2 phage (Table 1). Next, we performed a heat shock experiment and assessed cell lysis of the strains KK124 (SPβ c2 [*sprA::aphA3*]) and KK125 (SPβ c2 [*sprB::aphA3*]). As shown in Figure 9, both strains still lysed in the absence of either SprA or SprB. However, only the *sprB* mutant produced infectious SPβ c2 phage particles as verified by plaque assays using the prophage free strain TS01 (data not shown). We conclude that the heat-inducible SPβ excision of the c2 mutant also depends on the serine recombinase SprA while the heat-inducible induction of lysis is independent of SprA and SprB.

Identification of YosL, a novel component of the lysis-lysogeny management system of SPβ

When performing heat shock experiments with the strain KK001 carrying the SPβ c2 prophage, we observed that approximately 10% of the cells survived. Characterization of individual isolates of the surviving cells revealed that the lytic cycle of SPβ c2 was still inducible by heat, indicating the presence of intact prophages (data not shown). We speculated that among the surviving cells, there could be SPβ c2 mutant variants that had acquired intra- or extragenic mutations, which would prevent heat inducibility of the lysogens. To isolate SPβ c2 mutant variants that had lost the heat-sensitive phenotype, a small-scale adaptive laboratory evolution experiment was performed. For this purpose, the strain KK001 (SPβ c2) was grown at 37 °C until the culture reached an OD_{600} of about 0.8, heat shocked for 10 minutes at 50 °C and incubated for additional 6 hours at 37 °C. After 2 hours of incubation cell lysis took place, which could be recognized by the decrease in optical density. When the culture again reached an OD_{600} of 0.8, fresh medium was inoculated to an OD_{600} of 0.1 and incubated overnight at 37 °C. Next day, cells from the overnight culture were used to inoculate fresh medium to an OD_{600} of 0.1 and the heat shock cycle was repeated. After performing this cycle for 7 days, cell lysis could no longer be induced by heat, suggesting that genes of the SPβ lysis-lysogeny management system had probably acquired detrimental mutations. Next, 15 clones from the evolved culture were isolated, and the presence of the prophage was verified by a sublancin assay. The culture supernatants of five randomly selected clones were used to generate lysogens in the background of the prophage-free strain TS01. In two of the 19 isolated prophage-containing strains that were designated as KK026 and KK027, cell lysis could no longer be induced by heat (Figure 10A). Genome and Sanger sequencing revealed that the SPβ c2 prophage had acquired mutations in the *yosL* gene in both strains. In strain KK026, a single-nucleotide insertion (+A1) would lead to a frameshift that truncates the YosL protein after only four of the predicted 117 amino acids. The strain KK027 had a single-nucleotide exchange in *yosL* (T125A) that likewise would truncate YosL after 59 amino acids. We also observed that cell lysis of the strains KK026 (SPβ c2 [$yosL^{+A1}$]) and KK027 (SPβ c2 [$yosL^{T125A}$]) could not be induced by treatment with mitomycin C (Figure 10B). Thus, YosL is essential for the heat- and mitomycin C-dependent induction of the lytic cycle of SPβ c2.

Since the *yosL* gene is not expressed in the dormant state of the SPβ prophage [Kohm et al., 2022], *yosL* transcription must be activated when the phage enters the lytic cycle in a YopR-dependent manner. However, to assess whether YosL can trigger the lytic cycle

independent of YopR G136E, we constructed the plasmid pRH168 allowing the xylose-dependent expression of the *yosL* gene from the *ganA* locus. YosL is not toxic for the bacteria because the prophage-free control strains KK31 (P_{xylA}-*yosL*) and KK32 (P_{xylA}, control) grew in the presence of xylose (Figure 10C). Moreover, the expression of *yosL* in the strain KK033 (SPβ c2 P_{xylA}-*yosL*) carrying the prophage did not result in cell lysis (Figure 10C). Next, we tested whether the artificially expressed *yosL* gene complements the spontaneously inactivated *yosL*$^{+A1}$ allele and the deletion of *yosL* in the strains KK056 (SPβ c2 [*yosL*$^{+A1}$] P_{xylA}-*yosL*) and KK058 (SPβ c2 [*yosL::ermC*] P_{xylA}-*yosL*), respectively, upon heat shock. The parental strains KK028 (SPβ c2 [*yosL::ermC*]) and KK026 (SPβ c2 [*yosL*$^{+A1}$]) served as controls. As shown in Figure 10D, albeit to a lesser extent compared to the control strain KK034 (SPβ c2 P_{xylA}), the xylose-dependent expression of *yosL* in the strains KK056 (SPβ c2 [*yosL*$^{+A1}$] P_{xylA}-*yosL*) and KK058 (SPβ c2 [*yosL::ermC*] P_{xylA}-*yosL*) induced lysis after heat treatment. Thus, YosL depends on YopR^{G136E} to activate the lytic cycle of SPβ.

To assess whether the heat shock affects the synthesis of the YosL protein in the strain KK002 (SPβ c2), we performed a Western blot using polyclonal antibodies raised against YosL. The prophage free strain TS01 and the strain KK009 (SPβ) served as controls. Samples for the preparation of cell-free crude extracts were taken during cultivation at 37 °C before and 30 minutes after applying a heat shock at 50 °C. As expected, YosL was not synthesized in the strains TS01 (no prophage) and KK009 (SPβ) (Figure 10E). By contrast, immediately after the heat shock, the strain KK002 (SPβ c2) synthesized a protein corresponding to YosL (13 kDa). To conclude, we identified YosL as a novel component of the lysis-lysogeny management system that is required for the heat- and mitomycin C-dependent induction of the lytic cycle of the SPβ c2 mutant.

DISCUSSION

Previously, it has been shown that the *yopR* gene codes for the master repressor of the lytic cycle of the SPβ prophage, which is present in the *B. subtilis* laboratory strain 168 [Brady et al., 2021; Kohm et al., 2022]. Here, we confirmed that YopR is a key player in the lysis-lysogeny management system of SPβ. We show that a single mutation in the *yopR* gene enables induction of the SPβ c2 lytic cycle by transiently increasing the cultivation temperature. This finding suggested that either the stability or the folding of the encoded YopR^{G136E} protein is influenced by the ambient temperature of the bacterial culture. The first possibility could be excluded because the cellular levels of YopR^{G136E} were not affected by the ambient temperature (Figure 3A). By contrast, biochemical characterization of the YopR^{G139E} variant revealed that its unfolding temperature was decreased by about 10 °C and that this variant exhibited less higher order structure (Figure 3B and Figure 6). Thus, a single amino acid exchange in the YopR protein rather renders the folding of the protein sensitive to temperature. Our structural characterization of YopR revealed that the monomer shows a high similarity to bacterial and phage tyrosine recombinases and that the Y304 residue might be crucial for the DNA-binding activity of the protein (Figure 6 and S6). It is interesting to note that the replacement of tyrosine by phenylalanine or alanine at position 304 also makes the YopR^{Y304F} and YopR^{Y304A} variants temperature sensitive, albeit to a lesser extent than the G136E exchange in YopR^{G136E} (Figure 3B and 3C). However, the precise role of Y304 must be determined by structural characterization of YopR-DNA complexes. Like for many other systems, temperature-sensitive variants of DNA binding proteins, including the repressor of the lysogenic phage λ were shown to be helpful to study the underlying molecular mechanisms by which DNA-binding transcription factors exert their function [Lieb, 1996, 1981; Wissmann et al., 1991; Hurme et al., 1996]. Moreover, the entry into the host environment

and the accompanied temperature change serve as cues for thermosensing transcription factors to control virulence gene expression in pathogenic bacteria [Hurme et al., 1997]. Temperature-sensitive DNA binding transcription factors have also been employed for constructing expression systems that can be triggered by an ambient temperature [Jechlinger et al., 2005; Valdez-Cruz et al., 2010]. However, it is rather unlikely that the temperature serves as a signal for the SPβ wild-type prophage to enter the lytic cycle due inactivation of YopR because a heat shock does affect its repressor function. Recently, it has been suggested that the transcription factor AimR might be required to relieve YopR repression, thereby promoting the entry of SPβ into the lytic cycle [Brady et al., 2021]. It would be interesting to test whether the AimX nc RNA plays a role in this process. However, the environmental or host-derived signal that triggers the inactivation of YopR remains to be identified.

As described above, the overall structure of a YopR monomer shows a high similarity to bacterial and phage tyrosine recombinases (Table 3, Figure 5, Figure S6). However, our analysis indicates that YopR lacks recombinase activity, at least under the tested *in vitro* conditions (Figure S9). Furthermore, the exchange of Y304 to a phenylalanine or alanine residue, facilitated heat induction of the lytic cycle *in vivo* like the G136E variation (Figure 3C). As similar exchanges of the catalytic tyrosine residue in other tyrosine recombinases such as Cre, XerH or Lambda Int render the proteins inactive/incapable of DNA recombination [Grindley et al., 2006; Ennifar et al., 2003; Aihara et al., 2003; Bebel et al., 2016; Jayaram et al., 2015], this may be regarded as an indication that YopR does not act as a tyrosine recombinase despite the structural similarities. Instead, YopR might rather have evolved to a DNA-binding repressor protein. Along this line, YopR might be an evolutionary intermediate that is structurally related to a tyrosine recombinase as well as functionally to regulatory proteins. There are several examples for the evolution of an enzyme to a DNA-binding regulator [Commichau and Stülke, 2015]. For instance, the DNA-binding repressor protein Mlc from *Thermus thermophilus* responds to glucose that binds to a motif, which is conserved in glucose kinases [Titgemeyer et al., 1994; Chevance et al., 2006]. In fact, integrases have been described as acting as repressors to modulate their own synthesis [Piazolla et al., 2006; Chitto et al., 2020]. Probably, the recruitment of tyrosine recombinases as DNA-binding transcription factors is more widespread than previously anticipated.

Previously, it has been shown that SprA and SprB are key components required for the excision of the SPβ genome during sporulation (Figure 1) [Abe et al., 2014]. Here, we could show that lysis of a strain carrying the SPβ c2 allele was induced in when either *sprA* or *sprB* were absent (Figure 4G). The fact that only the strain lacking the *sprA* gene did not produce infective phage particles indicates that the heat-inducible SPβ excision of the c2 mutant also depends on the serine recombinase SprA but probably not on SprB. However, it is not unlikely that additional factors and regulatory circuits control prophage excision during sporulation or due to mitomycin C treatment. First, SprB overproduction was shown to trigger prophage excision but not the lytic cycle [Abe et al., 2014]. Second, a genome-reduced variant of SPβ containing only the *sprA* and *sprB* genes retained the ability to rearrange the *spsM* gene but did not undergo excision during mitomycin C treatment [Abe et al., 2014]. It will be interesting to elucidate whether the yet unknown prophage-derived or the host factors are involved excision of the SPβ.

As mentioned above, temperature-sensitive variants of DNA-binding proteins were helpful to study the functions of DNA-binding transcription factors. Here, we took advantage of the temperature-sensitive YopR^{G136E} variant to identify the YosL protein as a novel component of the lysis-lysogeny management system of SPβ. We showed that the YosL protein was synthesized when a *B. subtilis* lysogen carrying the SPβ c2 prophage was exposed

to heat (Figure 10). A bioinformatic analysis revealed that YosL is predicted to possess an Arc-type ribbon-helix-helix domain, which is also present in the structurally homologous repressors Mnt and Arc of the phage P22 that employs both repressors for maintaining the lysogenic state [Burgering et al., 1994; Anderson and Sauer, 2003]. There are two possibilities how the YosL protein might activate the SPβ c2 lytic cycle. First, elevated cellular amounts of YosL could inhibit the synthesis of another factor that prevents the synthesis of components activating the lytic cycle of SPβ c2. Second, YosL might directly activate yet unknown factors triggering the lytic cycle of SPβ c2. However, future structural and functional analysis is required to gain deeper insights into the regulatory role of YosL. Surprisingly, we found that the overexpression of YosL alone did not activate the lytic cycle of SPβ (Figure 10). A similar observation has been made when the transcription factor AimR that activates the expression of the nc RNA AimX, which in turn activates the lytic cycle of SPβ, was overexpressed [Brady et al., 2021]. These findings suggest that AimR and YosL act in concert with other yet unknown components to allow the switch from the lysogenic to the lytic cycle of SPβ.

The present study opens a wealth of interesting questions that need to be answered in the future. For instance, it remains to be resolved how the arbitrium system controls the activity of YopR. Moreover, it must be elucidated whether YopR serves as a transcription factor recognizing specific DNA elements or acts as a silencer to maintain the lysogenic state of SPβ. The latter possibility is not unlikely because the GC content of the SPβ genome is significantly lower than that of the *B. subtilis* genome [Lazarevic et al., 1999]. Furthermore, the function of YosL and other players of the lysis/lysogeny management system, such as YopN must be uncovered.

SUPPLEMENTARY DATA

Supplementary Data are available Online.

SOURCE DATA

Supplemental Dataset. The spreadsheet provides a summary of the conditions used for HDX-MS analyses and a full list of the peptides and residue-specific HDX obtained for YopR, $YopR^{G136E}$ and $YopR^{Y304F}$.

DATA AVAILABILITY

Coordinates and structure factors have been deposited within the protein data bank (PDB) under the accession code: 8a0a. The authors declare that all other data supporting the findings of this manuscript are available within the article and its supplementary data files.

ACKNOWLEDGEMENTS

We are grateful to Dr. Vladimir Lazarevic for providing the *B. subtilis* strain CU1147. We thank Pauline Plitzko for technical assistance. We also gratefully acknowledge the support of the Core Facility “Protein Spectroscopy” of the Medical School of the Philipps-University Marburg. We thank the European Synchrotron Radiation Facility (ESRF, Grenoble, France) and the Deutsche Elektronen Synchrotron (DESY, Hamburg, Germany) for excellent support.

FUNDING

This work was supported by the DFG grants CO 1139/3-1 (to F.M.C.), BA 5311/9-1 in the framework of the SPP2330 “New Concepts in Prokaryotic Virus-host Interactions – From Single Cells to Microbial Communities” (jointly to G.B. and L.C), the core facility for interactions,

dynamics and macromolecular assembly (project 324652314, to G.B.), and the Max Buchner Research Foundation (Re.3799 to R.H.).

Conflict of interest statement. None declared.

REFERENCES

Abe K, Kawano Y, Iwamoto K, Arai K, Maruyama Y, Eichenberger P, Sato T (2014) Developmentally-regulated excision of the SPβ prophage reconstitutes a gene required for spore maturation in *Bacillus subtilis*. PLoS Genet 10: e1004636.

Abe K, Takamatsu T, Sato T (2017) Mechanism of bacterial gene rearrangement: SprA-catalyzed precise DNA recombination and its directionality control by SprB ensure the gene rearrangement and stable expression of *spsM* during sporulation of *Bacillus subtilis*. Nucleic Acids Res 45: 6669-6683.

Abe K, Takahashi T, Sato T (2020) Extreme C-terminal element of SprA serine integrase is a potential component of the "molecular toggle switch" which controls the recombination and its directionality. Mol Microbiol 115: 1110-1121.

Aihara H, Kwon HJ, Nunes-Düby SE, Landy A, Ellenberger T (2003) A Conformational Switch Controls the DNA Cleavage Activity of λ Integrase. Mol Cell 12: 187–198.

Altenbuchner J (2016) Editing of the *Bacillus subtilis* genome by the CRISPR-Cas9 system. Appl Environ Microbiol 82: 5421-5427.

Anderson TA, Sauer RT (2003) Role of an N(cap) residue in determining the stability and operator-binding affinity of Arc repressor. Biophys Chem 100: 341-350.

Bebel A, Karaca E, Kumar B, Stark WM, Barabas O (2016) Structural snapshots of Xer recombination reveal activation by synaptic complex remodeling and DNA bending. Elife 5.

Biswas T, Aihara H, Radman-Livaja M, Filman D, Landy A, Ellenberger T (2005) A structural basis for allosteric control of DNA recombination by lambda integrase. Nature 435: 1059-1066.

Boltzmann L (1970) Weitere Studien über das Wärmegleichgewicht unter Gasmolekülen. In: Kinetische Theorie II. WTB Wissenschaftliche Taschenbücher, Vol. 67. Vieweg-Teubner Verlag, Wiesbaden.

Brady A, Quiles-Puchalt N, Gallego del Sol F, Zamora-Caballero S, Felipe-Ruiz A, Val-Calvo J, Meijer WJJ, Marina A, Penadés JR (2021) The arbitrium system controls prophage induction. Curr Biol 31: 5037-5045.

Burgering MJ, Boelens R, Gilbert DE, Breg JN Knight KL, Sauer RT Kaptein R (1994) Solution structure of dimeric Mnt repressor. Biochemistry 33: 15036-15045.

Chevance FF, Erhardt M, Lengsfeld C, Lee SJ, Boos W (2006) Mlc of *Thermus thermophilus*: a glucose-specific regulator for a glucose/mannose ABC transporter in the absence of the phosphotransferase system. J Bacteriol 188: 6561-6571.

Chittò M, Berger M, Berger P, Klotz L, Dröge P, Dobrindt U (2020) IHF stabilizes pathogenicity island I of uropathogenic *Escherichia coli* strain 536 by attenuating integrase I promoter activity. Sci Rep 10: 9397.

Commichau FM, Herzberg C, Tripal P, Valerius O, Stülke J (2007) A regulatory protein-protein interaction governs glutamate biosynthesis in *Bacillus subtilis*: the glutamate dehydrogenase RocG moonlights in controlling the transcription factor GltC. Mol Microbiol 65: 642-654.

Commichau FM, Stülke J (2015) Trigger enzymes: coordination of metabolism and virulence gene expression. Microbiol Spectr 3: doi: 10.1128/microbiolspec.MBP-0010-2014.

Deatherage DE, Barrick JE (2014) Identification of mutations in laboratory-evolved microbes from next-generation sequencing data using breseq. Methods Mol Biol 1151: 165-188.

Dion MB, Oechslin F, Moineau S (2020) Phage diversity, genomics and phylogeny. Nat Rev Microbiol 18: 125-138.

Diethmaier C, Pietack N, Gunka K, Wrede C, Lehnik-Habrink M, Herzberg C, Hübner S, Stülke J (2011) A novel factor controlling bistability in *Bacillus subtilis*: the YmdB protein affects flagellin expression and biofilm formation. J Bacteriol 193: 5997-6007.

Dou C, Xiong J, Gu Y, Yin K, Wang J, Hu Y, Zhou D, Fu X, Qi S, Zhu X, Yao S, Xu H, Nie C, Liang Z, Yang S, Wei Y, Cheng W (2018) Structural and functional insights into the regulation of the lysis-lysogeny decision in viral communities. Nat Microbiol 3: 1285-1294.

Emsley P, Cowtan K (2004) Coot: model-building tools for molecular graphics. Acta Crystallogr D Biol Crystallogr. 60: 2126-2132.

Ennifar E, Meyer JEW, Buchholz F, Stewart AF, Suck D (2003) Crystal structure of a wild-type Cre recombinase– lox P synapse reveals a novel spacer conformation suggesting an alternative mechanism for DNA cleavage activation. Nucleic Acids Res 31: 5449-5460.

Erez Z, Steinberger-Levy I, Shamir M, Doron S, Stokar-Avihail A, Peleg Y, Melamed S, Leavitt A, Savidor A, Albeck S, Amitai G, Sorek R (2017) Communication between viruses guides lysis-lysogeny decisions. Nature 541: 488-493.

Gallego Del Sol F, Penadés JR, Marina A (2019) Deciphering the molecular mechanism underpinning phage arbitrium communication systems. Mol Cell 74: 59-72.e3.

Gallego Del Sol F, Quiles-Puchalt N, Brady A, Penadés JR, Marina A (2022) Insights into the mechanism of action of the arbitrium communication system in SPbeta phages. Nat Commun 13: 3627.

Georgopoulos CP (1969) Suppressor system in *Bacillus subtilis* 168. J Bacteriol 97: 1397-1402.

Geromanos SJ, Vissers JP, Silva JC, Dorschel CA, Li GZ, Gorenstein MV, Bateman RH, Langridge JI (2009) The detection, correlation, and comparison of peptide precursor and product ions from data independent LC-MS with data dependant LC-MS/MS. Proteomics 9: 1683-1695.

Grant SG, Jessee J, Bloom FR, Hanahan D (1990) Differential plasmid rescue from transgenic mouse DNAs into *Escherichia coli* methylation-restriction mutants. Proc Natl Acad Sci USA 874645-874649.

Grindley NDF, Whiteson KL, Rice PA (2006) Mechanisms of site-specific recombination. Annu Rev Biochem 75: 567-605.

Guan Z, Pei K, Wang J, Cui Y, Zhu X, Su X, Zhou Y, Zhang D, Tang C, Yin P, Liu Z, Zou T (2019) Structural insights into DNA recognition by AimR of the arbitrium communication system in the SPbeta phage. Cell Discov 5:29.

Gundlach J, Herzberg C, Kaever V, Gunka K, Hoffmann T, Weiß M, Gibhardt J, Thürmer A, Hertel D, Daniel R, Bremer E, Commichau FM, Stülke J (2017) Control of potassium homeostasis is an essential function of the second messenger cyclic di-AMP in *Bacillus subtilis*. Sci Signal 10: eaal3011.

Hemphill HE, Gage I, Zahler SA, Korman RZ (1980) Prophage-mediated production of a bacteriocinlike substance by SP beta lysogens of *Bacillus subtilis*. Can J Microbiol 26: 1328-1333.

Hurme R, Berndt KD, Namork E, Rhen M (1996) DNA binding exerted by a bacterial gene regulator with an extensive coiled-coil domain. J Biol Chem 271: 12626-12631.

Hurme R, Berndt KD, Normark SJ, Rhen M (1997) A proteinaceous gene regulatory thermometer in *Salmonella*. Cell 90: 55-64.

Jayaram M, Ma CH, Kachroo AH, Rowley PA, Guga P, Fan HF, Voziyanov Y (2015) An overview of tyrosine site-specific recombination: From an flp perspective. Microbiol Spectr 3. doi: 10.1128/microbiolspec.MDNA3-0021-2014.

Jechlinger W, Glocker J, Haidinger W, Matis A, Szostak MP, Lubitz W (2005) Modulation of gene expression by promoter mutants of the λ cI857/pRM/pR system. J Biotechnol 116: 11-20.

Johnson CM, Grossman AD (2016) Complete genome sequence of *Bacillus subtilis* strain CU1050, which is sensitive to phage SPβ. Genome Announc 4: e00262-16.

Jumper J, Evans R, Pritzel A, Green T, Figurnov M, Ronneberger O, Tunyasuvunakool K, Bates R, Zidek A, Potapenko A, Bridgland A, Meyer C, Kohl SAA, Ballard AJ, Cowie A, Romera-Paredes B, Nikolov S, Jain R, Adler J, Back T, Petersen S, Reiman D, Clancy E, Zielinski M, Steinegger M, Pacholska M, Berghammer T, Bodenstein S, Silver D, Vinyals O, Senior AW,

Kavukcuoglu K, Kohli P, Hassabis D (2021) Highly accurate protein structure prediction with AlphaFold. Nature 596: 583–589

Kabsch W (2010) Integration, scaling, space-group assignment and post-refinement. Acta Crystallogr D Biol Crystallogr 66: 133-144.

Kohm K, Hertel R (2021) The life cycle of SPβ and related phages. Arch Virol 166: 2119-2130.

Kohm K, Floccari VA, Lutz VT, Nordmann B, Mittelstädt C, Poehlein A, Dragos A, Commichau FM, Hertel R (2022) The *Bacillus* phage SPβ and its relatives: a temperate phage model system reveals new strains, species, prophage integration loci, conserved proteins and lysogeny management components. Environ Microbiol. 24: 2098-2118.

Koo BM, Kritikos G, Farelli JD, Todor H, Tong K, Kimsey H, Wapinski I, Galardini M, Cabal A, Peters JM, Hachmann AB, Rudner DZ, Allen KN, Typas A, Gross CA (2017) Construction and analysis of two genome-scale deletion libraries for *Bacillus subtilis*. Cell Syst 4: 291-305.

Kunst F, Rapoport G (1995) Salt stress is an environmental signal affecting degradative enzyme synthesis in *Bacillus subtilis*. J Bacteriol 177: 2403-2407.

Kwon HJ, Tirumalai R, Landy A, Ellenberger T (1997) Flexibility in DNA recombination: structure of the lambda integrase catalytic core. Science 276: 126–131

Landy A (2015) The λ integrase site-specific recombination pathway. Microbiol Spectr 3: MDNA3-0051-2014.

Langmead B, Salzberg SL (2012) Fast gapped-read alignment with Bowtie 2. Nat Methods 9: 357-359.

Lazarevic V, Düsterhöft A, Soldo B, Hilbert H, Mauel C, Karamata D (1999) Nucleotide sequence of the *Bacillus subtilis* temperate bacteriophage SPβc2. Microbiology 145: 1055-1067.

Lazazzera BA, Solomon JM, Grossman AD (1997) An exported peptide functions intracellularly to contribute to cell density signaling in *B. subtilis*. Cell 89: 917-925.

Li GZ, Vissers JPC, Silva JC, Golick D, Gorenstein MV, Geromanos SJ (2009) Database searching and accounting of multiplexed precursor and product ion spectra from the data independent analysis of simple and complex peptide mixtures. Proteomics 9: 1696-16719.

Lieb M (1996) Studies of heat-inducible lambda bacteriophage, I. oder of genetic sites and properties of mutant prophages. J Mol Biol 16: 149-163.

Lieb M (1981) A fine structure map of spontaneous and induced mutations in the lambda repressor gene, including insertions of IS elements. Mol Gen Genet 184: 364-371.

Liebschner D, Afonine PV, Baker ML, Bunkóczi G, Chen VB, Croll TI, Hintze B, Hung LW, Jain S, McCoy AJ, Moriarty NW, Oeffner RD, Poon BK, Prisant MG, Read RJ, Richardson JS,

Sammito MD, Sobolev OV, Stockwell DH, Terwilliger TC, Urzhumtsev, AG, Videau LL, Williams CJ, Adams PD (2019) Macromolecular structure determination using X-rays, neutrons and electrons: Recent developments in Phenix. Acta Crystallogr Struct Biol. 75: 861-877.

Martin-Verstraete I, Débarboullié M, Klier A, Rapoport G (1992) Mutagenesis of the *Bacillus subtilis* "-12, -24" promoter of the levanase operon and evidence for the existence of an upstream activating sequence. J Mol Biol 226: 85-99.

Masson GR, Burke JE, Ahn NG, Anand GS, Borchers C, Bier S, Bou-Assaf GM, Engen JR, Englander SW, Faber J, Garlish R, Griffin PR, Gross ML, Guttman M, Hamuro Y, Heck AJR. Houde D, Iacob RE, Jorgensen TJD, Kaltashov IA, Klinman JP, Konermann L, Man P, Mayne L, Pascal BD, Reichmann D, Skehel M, Snijder J, Strutzenberg TS, Underbakke ES, Wagner C, Wales TE, Walters BT, Weis DD, Wilson DJ, Wintrode PL, Zhang Z, Zheng J, Schriemer DC, Rand KD. (2019) Recommendations for performing, interpreting and reporting hydrogen deuterium exchanges mass spectrometry (HDX-MS) experiments. Nat Methods 16: 595-602.

McCoy AJ (2006) Solving structures of protein complexes by molecular replacement with phaser. Acta Crystallogr Biol Crystallogr 63: 32-41.

McLaughlin JR, Wong HC, Ting YE, Van Arsdell JN, Chang S (1986) Control of lysogeny and immunity of *Bacillus subtilis* temperate bacteriophage SPβ by its d gene. J Bacteriol 167: 952-959.

Meinke G, Bohm A, Hauber J, Pisabarro MT, Buchholz F (2016) Cre Recombinase and Other Tyrosine Recombinases. Chem Rev 116: 12785–12820.

Niesen F, Berglund H, Vedadi M (2007) The use of differential scanning fluorimetry to detect ligand interactions that promote protein stability. Nat Protoc 2: 2212-2221.

Oman TJ, Boettcher JM, Wang H, Okalibe XN, van der Donk, WA (2011) Sublancin is not a lantibiotic but an *S*-linked glycopeptide. Nat Chem Biol 7: 78-80.

Osorio-Valeriano M, Altegoer F, Steinchen W, Urban S, Liu Y, Bange G, Thanbichler M (2019) ParB-type DNA segregation proteins are CTP-dependent molecular switches. Cell 179: 1512-1524.

Otte K, Kühne NM, Furrer AD, Baena-Lozanda LP, Lutz VT, Schilling T, Hertel R (2020) A CRISPR-Cas9 tool to explore the genetics of *Bacillus subtilis* phages. Lett Appl Microbiol 71: 588-595.

Pei K, Zhang J, Zou T, Liu Z (2021) AimR adopts preexisting dimer conformations for specific target recognition in lysis-lysogeny decisions of *Bacillus* phage phi3T. Biomolecules 11: 1321.

Piazolla D, Cali S, Spoldi E, Forti F, Sala C, Magnoni F, Dehò G, Ghisotti D (2006) Expression of phage P4 integrase is regulated negatively by both Int and Vis. J Gen Virol 87: 2423-2431.

Piraner DI, Abedi MH, Moser BA, Lee Gosselin A, Shapiro MG (2017) Tunable thermal bioswitches for *in vivo* control of microbial therapeutics. Nat Chem Biol 13: 75-80.

Reuss DR, Thürmer A, Daniel R, Quax WJ, Stülke J (2016) Complete genome sequence of *Bacillus subtilis* subsp. *subtilis* strain Δ6. Genome Announc 4: e00759-16.

Richts B, Hertel R, Potot S, Poehlein A, Daniel R, Schyns G, Prágai Z, Commichau FM (2020) Complete genome sequence of the prototrophic *Bacillus subtilis* subsp. *subtilis* strain SP1. Microbiol Resour Announc 9: e00825-20.

Rosenthal R, Toye PA, Korman RZ, Zahler SA (1979) The prophage of SP beta c2dcitK1, a defective specialized transducing phage of *Bacillus subtilis*. Genetics 92: 721-739.

Salmond GP, Fineran PC (2015) A century of the phage: past, present and future. Nat Rev Microbiol 13: 777-786.

Sambrook J, Fritsch EF, Maniatis T (1989) Molecular cloning: a laboratory manual, 2nd ed. Cold Spring Harbor Laboratory, Cold Spring Harbor, N.Y.

Schilling T, Dietrich S, Hoppert M, Hertel R (2018) A CRISPR-Cas9-based Toolkit for fast and precise *in vivo* genetic engineering of *Bacillus subtilis* phages. Viruses 10: 241.

Stülke J, Martin-Verstraete I, Zagorec M, Rose M, Klier A, Rapoport G (1997) Induction of the *Bacillus subtilis ptsGHI* operon by glucose is controlled by a novel antiterminator, GlcT. Mol Microbiol 25: 65-78.

Theveneau P, Baker R, Barrett R, Beteva A, Bowler MW, Carpentier P, Caserotto H, de Sanctis D, Dobias F, Flot D, Guijarro M, Giraud T, Lentini M, Leonard GA, Mattenet M, McCarthy AA, McSweeney SM, Morawe S, Nanao M, Nurizzo D, Ohlsson S, Pernot P, Popov AN, Round A, Royant A, Schmid W, Snigirev A, Surr J, Mueller-Dieckmann C (2013) The upgrade programme for the structural biology beamlines at the European synchrotronradiation facility-high throughput sample evaluation and automation. J Phys Confer Ser 425: 012001.

Titgemeyer F, Reizer J, Reizer A, Saier MH Jr (1994) Evolutionary relationships between sugar kinases and transcriptional repressors in bacteria. Microbiology 140: 2349-2354.

Trinh JT, Zeng L (2019) Structure regulates phage lysis-lysogeny decisions. Trends Microbiol 27: 3-4.

Valdez-Cruz NA, Caspeta L, Pérez NO, RamírezNO, Trujillo-Roldán MA (2020) Production of recombinant proteins in *E. coli* by the heat inducible expression system based on the phage lambda pL and/or pR promoters. Microb Cell Fact 9: 18.

Van Duyne GD (2001) A structural view of cre-loxp site-specific recombination. Annu Rev Biophys Biomol Struct 30: 87-104.

Van Duyne GD (2015) Cre recombinase. Microbiol Spectr 3: MDNA3-0014-2014.

Wales TE, Fadgen KE, Gerhardt GC, Engen JR (2008) High-speed and high-resolution UPLC separation at zero degrees celsius. Anal Chem 80: 6815-6820.

Wang Q, Guan Z, Pei K, Wang J, Liu J, Yin P, Peng D, Zou T (2018) Structural basis of the arbitrium peptide-AimR communication system in the phage lysis-lysogeny decision. Nat Microbiol 3: 1266-1273.

Warner FD, Kitos GA, Romano MP, Hemphill HE (1977) Characterization of SPβ: a temperate bacteriophage from *Bacillus subtilis* 168M. Can J Microbiol 23: 45-51.

Weinrauch Y, Msadek T, Kunst F, Dubnau D (1991) Sequence and properties of *comQ*, a new competence regulatory gene of *Bacillus subtilis*. J Bacteriol 173: 5685-5693.

Westers H, Dorenbos R, van Dijl JM, Kabel J, Flanagan T, Devine KM, Jude F, Seror SJ, Beekman AC, Darmon E, Eschevins C, de Jong A, Bron S, Kuipers OP, Albertini AM, Antelmann H, Hecker M, Zamboni N, Sauer U, Bruand C, Ehrlich DS, Alonso JC, Salas M, Quax WJ (2003) Genome engineering reveals large dispensible regions in *Bacillus subtilis*. Mol Biol Evol 20: 2076-2090.

Wissmann A, Wray LV Jr, Somaggio U, Baumeister R, Geissendörfer M, Hillen W (1991) Selestion for Tn10 *tet* repressor binding to *tet* operator in *Escherichia coli* isolation of temperature-sensitive mutants and combinatorial mutagenesis in the DNA binding motif. Genetics 128: 225-232.

Wu C, Biswas S, Garcia de Gonzalo CV, van der Donk WA (2019) Investigations into the mechanism of action of sublancin. ACS Infect Dis 5: 454-459.

Zahler SA, Korman RZ, Rosenthal R, Hemphill HE (1977) *Bacillus subtilis* bacteriophage SPbeta: localization of the prophage attachment site, and specialized transduction. J Bacteriol 129: 556-558.

Zeigler DR, Prágai Z, Rodriguez S, Chevreux B, Muffler A, Albert T, Wyss M, Perkins JB (2008) The origins of 168, W23, and other *Bacillus subtilis* legacy strains. J Bacteriol 190: 6983-6995.

Zhen X, Zhou H, Ding W, Zhou B, Xu X, Perculija V, Chen CJ, Chang MX, Choudhary MI, Ouyang S (2019) Structural basis of AimP signaling molecule recognition by AimR in Spbeta group bacteriophages. Protein Cell 10: 131-136.

FIGURE LEGENDS

Figure 1. Major steps of the lytic and lysogenic cycle of SPβ.
Gene and protein sizes are not drawn to scale. The target of the *aimX* sRNA is unknown and the potential RNase function of YokI remains to be elucidated. The signal that inhibits DNA-binding activity of YopR and the recombinase catalyzing the excision of the prophage are unknown.

Figure 2. The temperature sensitive SPβ c2 prophage produces sublancin and senses heat shocks due to a mutation in the *yopR* gene.

A. Heat shock experiment to assess the temperature sensitivity of the SPβ c2 prophage in the historical *B. subtilis* strain CU1147. Cultures of the strains 168 (SPβ [*yopR*], control) and CU1147 (SPβ c2 [*yopR*^{G407A}]) were grown for 2.5 h at 30 °C, heat shocked at 50 °C for 10 min and further cultivated at 30 °C. The gene marked with square brackets is present in the phage genome. The optical density at a wavelength of 600 nm (OD_{600}) was monitored over time. Further induction experiments revealed 37 °C as growing temperature and 10 min heat shock as best to induce SPβ c2. **B.** Plaque assay (upper panel) with SPβ and SPβ c2 lysates and sublancin assay with the strains KK009 and KK002 carrying SPβ and SPβ c2 prophages, respectively (see Materials and Methods). **C.** Heat shock experiment showing that the *yopR*^{G407A} allele causes the temperature-sensitive phenotype of the SPβ c2 prophage. The indicated strains were heat shocked as described in the Materials and Methods section. The gene marked with square brackets is present in the phage genome. The OD_{600} was monitored over time. The strains KK011, KK014 and KK015 express the *yopR/yopR*^{G407A} alleles from the *amyE* locus.

Figure 3. Cellular amounts of YopR ^{G136E} and characterization of YopR variants.
A. Cellular amounts of YopR^{G136E} were determined by Western blotting. Crude extracts of the indicated strains were isolated from overnight (ON) or exponentially growing LB cultures at timepoints t_1 and t_2, immediately and 30 min after the heat shock (10 min incubation at 50 °C), respectively. As a control served purified YopR-His_6 (100 ng). After electrophoresis in a 12.5% SDS-PAGE and transfer onto a PVDF membrane, YopR was detected by rabbit polyclonal antibodies raised against YopR-His_6. 20 mg of crude extracts were applied. **B.** Analysis of purified YopR wild type (blue), YopR^{G136E} (red), YopR^{Y304F} (green), YopR^{Y304A} (purple) and YopR^{K169A} (orange) stability by nanoDSF. Thermal unfolding curves of YopR and YopR variants were assessed in SEC buffer. Changes in the F350/F330 fluorescence ratio are shown and T_m values are indicated in the table. **C.** Heat shock experiment to assess the temperature sensitivities of the YopR wild type (blue), YopR^{G136E} (red), YopR^{Y304F} (green), YopR^{Y304A} (purple), and YopR^{K169A} (orange). The indicated strains were heat shocked as described in the Materials and Methods section. The OD_{600} was monitored over time.

Figure 4. In vitro and in vivo analysis of YopR DNA binding. A-F. Electrophoretic mobility shift assays (EMSAs) showing the DNA-binding activities of the YopR wild type protein and the YopR^{G136E} variant**. A, C, F.** Complex formation between the YopR wild-type protein and the P_{aimR}, P_{aimX} *and attR* DNA fragments. **B, D, F.** Complex formation between the YopR^{G136E} variant and the P_{aimR}, P_{aimX} *and attR* DNA fragments. See Materials and Methods for the experimental procedure. **G.** β-Galactosidase activity assays to assess the DNA-binding activity of wild type YopR and YopR^{G136E}. The indicated strains were grown in LB medium for 2.5 h at 37 °C, transferred to 50 °C and further cultivated for 2.5 h. The β-galactosidase activity is given as units per milligram protein. Experiments were carried out at least two times. Boxes indicate mean values.

Figure 5. Structural analysis of the YopR wild type protein. A. Overall fold of YopR and representation of the 15 alpha-helices and 4 β-strands. **B.** Structural rearrangements of the N- and C-terminal domains of YopR required for potential DNA binding and formation of a negatively charged groove. **C, D.** Electrostatic surface potential of YopR as present in the experimentally determined crystal structure (**C**) and after the proposed structural rearrangements required for DNA binding (**D**). YopR is colored by electrostatic surface potential, as calculated by APBS using the Pymol plug in. The color scale is the same for all

proteins, ranging from - 3 to + 3 kT/e, with negative charges in red and positive charges in blue. **E, F.** Schematic overview of YopR (**E**) topology compared to the topology of the well-studied tyrosine recombinase and close structural homolog Cre (**F**). Residues crucial for enzymatic function of tyrosine recombinases are labelled. Location of DNA in Cre is indicated in light blue. **G, H.** Comparison of the overall fold of YopR (**G**) to Cre in its DNA bound state (PDB 1q3u) [Ennifar et al., 2003].

Figure 6. YopR^{G136E} and YopR^{Y304F} exhibit perturbations in higher order structure compared to YopR. A. The difference in HDX-MS between YopR^{G136E} and YopR or YopR^{Y304F} and YopR is displayed on the amino acid sequence of YopR. Different tones of red indicate residues that incorporate more deuterium in the YopR^{G136E} and YopR^{Y304F} variants than in native YopR indicating perturbations in their higher order structure. The secondary structure of YopR is schematically illustrated above. **B.** Representative peptides of YopR exhibiting differences in HDX between YopR (blue trace), YopR^{G136E} (red trace) and YopR^{Y304F} (green trace). Data represent the mean ± s.d. of n=3 replicates. **C.** The difference in HDX-MS between YopR^{G136E} or YopR^{Y304F} and YopR (see panel A) was mapped onto the YopR crystal structure. Hereby, each residue was color-coded as per the highest difference in HDX observed at any time-point. Red colors represent higher HDX in YopR variants and grey color no HDX difference compared to native YopR. YopR residues for which no peptides could be identified in HDX-MS are colored black. The G136E and Y304F sites of variation are shown as sticks colored in magenta.

Figure 7. Detailed structural comparison of YopR and the core catalytic residues of tyrosine recombinases. A. Zoom into the potential DNA binding region and catalytic site of YopR. Residues that were compared to crucial catalytic residues of tyrosine recombinases in Table 3 are shown as light blue sticks and labelled. **B-D.** Comparison of the core catalytic residues in the tyrosine recombinases Cre (PDB 1q3u; Ennifar et al., 2003) (**B**), XerH (PDB 5jk0; Bebel et al., 2016) (**C**) and Lambda Int (PDB 1p7d; Aihara et al., 2003) (**D**). The catalytic residues are shown as red, blue and pink sticks, respectively. Detailed overlay of each residue with the corresponding amino acid residue found in the structure of YopR are shown in Supplementary Figure S7.

Figure 8. DNA binding of YopR, YopR^{G136E} and YopR^{Y304F} by HDX-MS. A. The difference in HDX-MS between the DNA-bound and apo states of YopR, YopR^{G136E} and YopR^{Y304F} is displayed on the amino acid sequence of YopR. Different tones of blue indicate reduced deuterium incorporation in presence of DNA. The secondary structure of YopR is schematically illustrated above. **B.** Representative peptides of YopR and variants thereof exhibiting differences in HDX with respect to DNA. Data represent the mean ± s.d. of n=3 replicates. **C.** The difference in HDX-MS between the DNA-bound and apo state of native YopR was projected onto a model of DNA-bound YopR. The model was generated by superimposing the CAT domains of YopR (residues 107-318) and DNA-bound Cre (PDB 1q3u [Ennifar et al.], 2003; residues 130-341) followed by superposition of the YopR CB domain (residues 1-106) onto that of DNA-bound Cre (residues 10-129). YopR residues were color-coded as per the highest difference in HDX observed at any time-point. The G136E and Y304F sites of variation are shown as sticks colored in magenta.

Figure 9. Heat-induced cell lysis of *B. subtilis* carrying SPβ c2 does not require SprA or SprB.

The indicated strains were grown for 2.5 h at 30 °C, heat shocked at 50 °C for 10 min and further cultivated at 30 °C. The square brackets indicate the *sprA* and *sprB* deletions in the phage genome. The OD_{600} was monitored over time.

Figure 10. YosL, a novel player in the lysis/lysogeny management system of SPβ.
A. Characterization of evolved SPβ c2 suppressor mutants. All strains were grown for 2.5 h at 37 °C, heat shocked at 50 °C for 10 min and further cultivated at 37 °C. The OD_{600} was monitored over time. **B.** Effect of mitomycin C on prophage induction in strains carrying SPβ c2 and its suppressors during growth in LB at 37 °C. Mitomycin was added to a final concentration of 0.5 µg ml^{-1} and OD_{600} was monitored over time. **C**. Effect of xylose (0.5% (w/v)) on prophage induction in the indicated strains that were grown in LB. **D.** Effect of xylose (0.5% (w/v)) and heat (10 min at 50 °C) on prophage induction in the indicated strains that were grown in LB. **E.** Cellular amounts of YosL were determined by Western blotting. Crude extracts of the indicated strains were isolated from exponentially growing LB cultures at timepoints t_0 (before the heat shock), t_1 (immediately after the heat shock) and t_2 (30 min after the heat shock). After electrophoresis in a 15% SDS-PAGE and transfer onto a PVDF membrane, YosL was detected by rabbit polyclonal antibodies raised against YosL-His_6. 20 mg of crude extracts were applied.

Table 1. Mutations identified in the SPβ c2 phage.

Region	Encoded function	Type of mutation	Coordinates[a]
yokI	Putative ribonuclease	G145A (G49S)	2.277.281
yopR	Repressor	G407A (G136E)	2.204.767
yoqA	Unknown	T68C (L23P)	2.201.412
yorN-yorM	Unknown	ΔAG, 25-24 bp upstream of *yorN*	2.174.763 - 2.174.762

[a]Coordinates refer to the position in the genome sequence CP058242 of the *B. subtilis* SP1 strain [Richts et al., 2020].

Table 2. Data collection and refinement statistics for YopR.

	YopR (PDB code: 8a0a)
Data collection	
Space group	$P2_12_12_1$
Cell dimensions	
a, b, c (Å)	49.55 98.87 162.24
α, β, γ (°)	90 90 90
Wavelength (Å)	0.976253
Resolution (Å)	47.45 - 2.902 (3.006 - 2.902)
R_{merge}	0.3707 (2.446)
I/σ(I)	8.89 (1.47)
Completeness (%)	99.88 (99.27)
Redundancy	12.4 (12.7)
CC1/2	0.991 (0.581)
Refinement	
Resolution (Å)	47.45 - 2.902
No. reflections	226928 (22388)
R_{work} / R_{free}	0.2149 / 0.2628
No. atoms	5182
protein	5182
Ligands/ion	0
water	0
B-factor	
protein	67.98
R.M.S. deviations	
Bond lengths (Å)	0.004
Bond angles (°)	0.75
Ramachandran	
favored (%)	97.33
allowed (%)	2.67
outliers (%)	0.00

*Statistics for the highest-resolution shell are shown in parentheses.

Data were collected on ID30B (ESRF).

Table 3. Comparison crucial residues for the activity of tyrosine recombinases to those found in YopR.

YopR PDB code: 8A0A	**Cre** PDB code: 1Q3U	**XerH** PDB code: 5JK0	**Lambda Int** PDB code: 1P7D
RMSD (Å) N- / C-terminus	4.61 / 4.53	6.04 / 5.14	4.03 / 4.06
V137/S138	R173	R213	R212
E144	E176	E216	D215
K169	K201	K239	K235
N254	H289	H309	H308
V257/R258	R292	R312	R311
V291	W315	H335	H333
Y304	Y324	Y344	Y342
References	[Ennifar et al., 2003; Van Duyne, 2015; Meinke et al., 2016]	[Bebel et al., 2016]	[Aihara et al., 2003; Biswas et al., 2005; Landy, 2015]

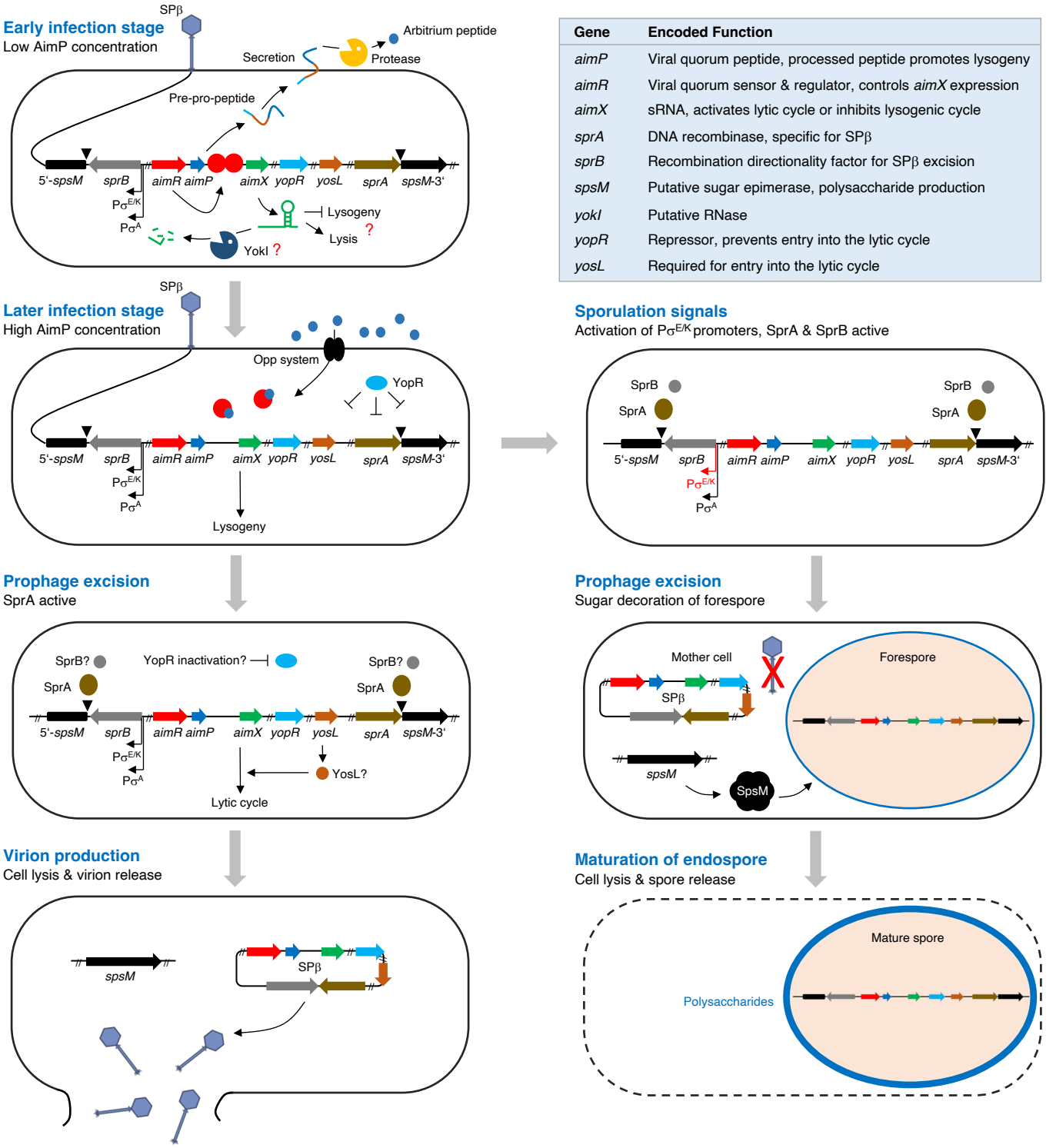

Gene	Encoded Function
aimP	Viral quorum peptide, processed peptide promotes lysogeny
aimR	Viral quorum sensor & regulator, controls *aimX* expression
aimX	sRNA, activates lytic cycle or inhibits lysogenic cycle
sprA	DNA recombinase, specific for SPβ
sprB	Recombination directionality factor for SPβ excision
spsM	Putative sugar epimerase, polysaccharide production
yokI	Putative RNase
yopR	Repressor, prevents entry into the lytic cycle
yosL	Required for entry into the lytic cycle

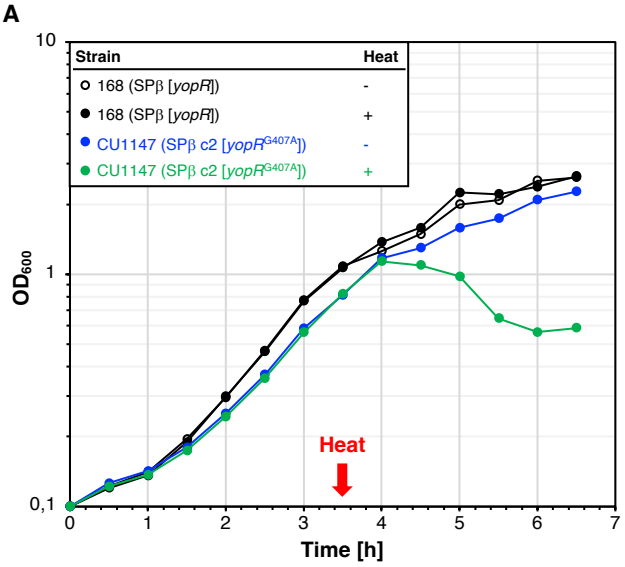
A
Strain
Heat
168 (SPβ [yopR])
-
168 (SPβ [yopR])
+
CU1147 (SPβ c2 [yopR^G407A])
-
CU1147 (SPβ c2 [yopR^G407A])
+
Heat
OD600
10
1
0,1
0
1
2
3
4
5
6
7
Time [h]

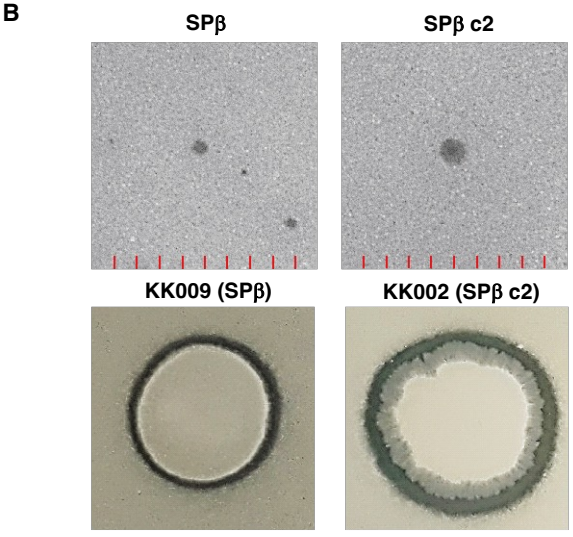
B
SPβ
SPβ c2
KK009 (SPβ)
KK002 (SPβ c2)

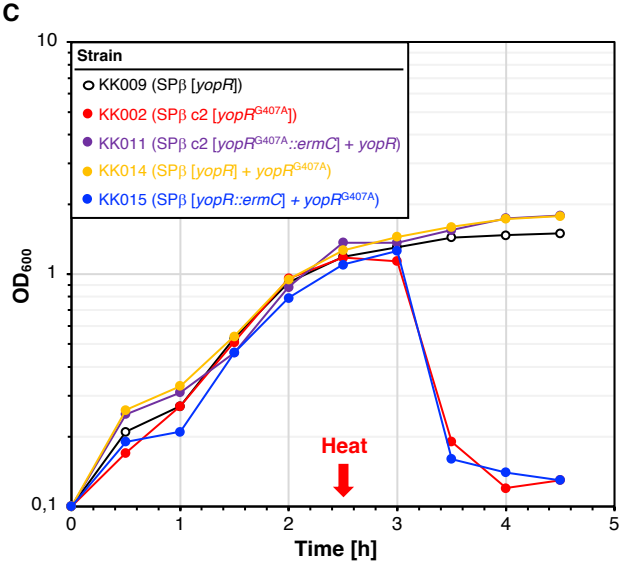
C
Strain
KK009 (SPβ [yopR])
KK002 (SPβ c2 [yopR^G407A])
KK011 (SPβ c2 [yopR^G407A::ermC] + yopR)
KK014 (SPβ [yopR] + yopR^G407A)
KK015 (SPβ [yopR::ermC] + yopR^G407A)
Heat
OD600
10
1
0,1
0
1
2
3
4
5
Time [h]

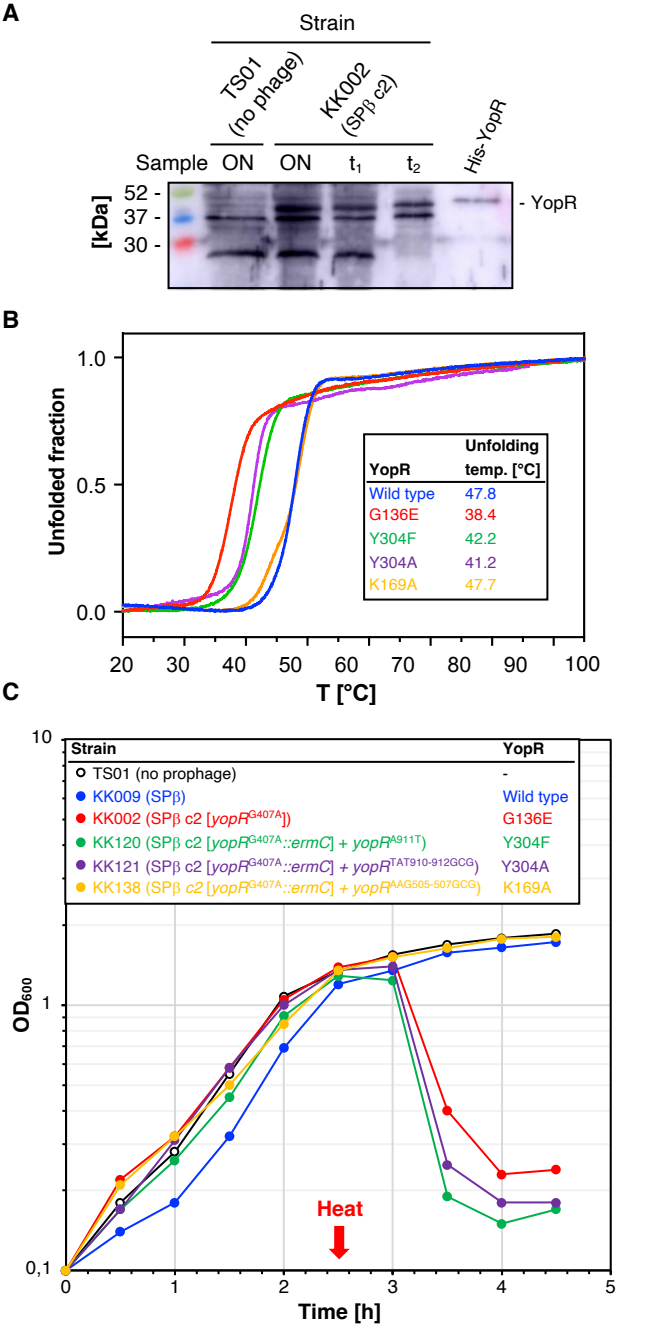
A
Strain
TS01 (no phage)
KK002 (SPβ c2)
His-YopR
Sample
ON
ON
t1
t2
[kDa]
52 -
37 -
30 -
- YopR
B
Unfolded fraction
1.0
0.5
0.0
20
30
40
50
60
70
80
90
100
T [°C]
YopR
Unfolding temp. [°C]
Wild type 47.8
G136E 38.4
Y304F 42.2
Y304A 41.2
K169A 47.7
C
Strain
YopR
TS01 (no prophage) -
KK009 (SPβ) Wild type
KK002 (SPβ c2 [yopR G407A]) G136E
KK120 (SPβ c2 [yopR G407A::ermC] + yopR A911T) Y304F
KK121 (SPβ c2 [yopR G407A::ermC] + yopR TAT910-912GCG) Y304A
KK138 (SPβ c2 [yopR G407A::ermC] + yopR AAG505-507GCG) K169A
OD600
10
1
0,1
Heat
0
1
2
3
4
5
Time [h]

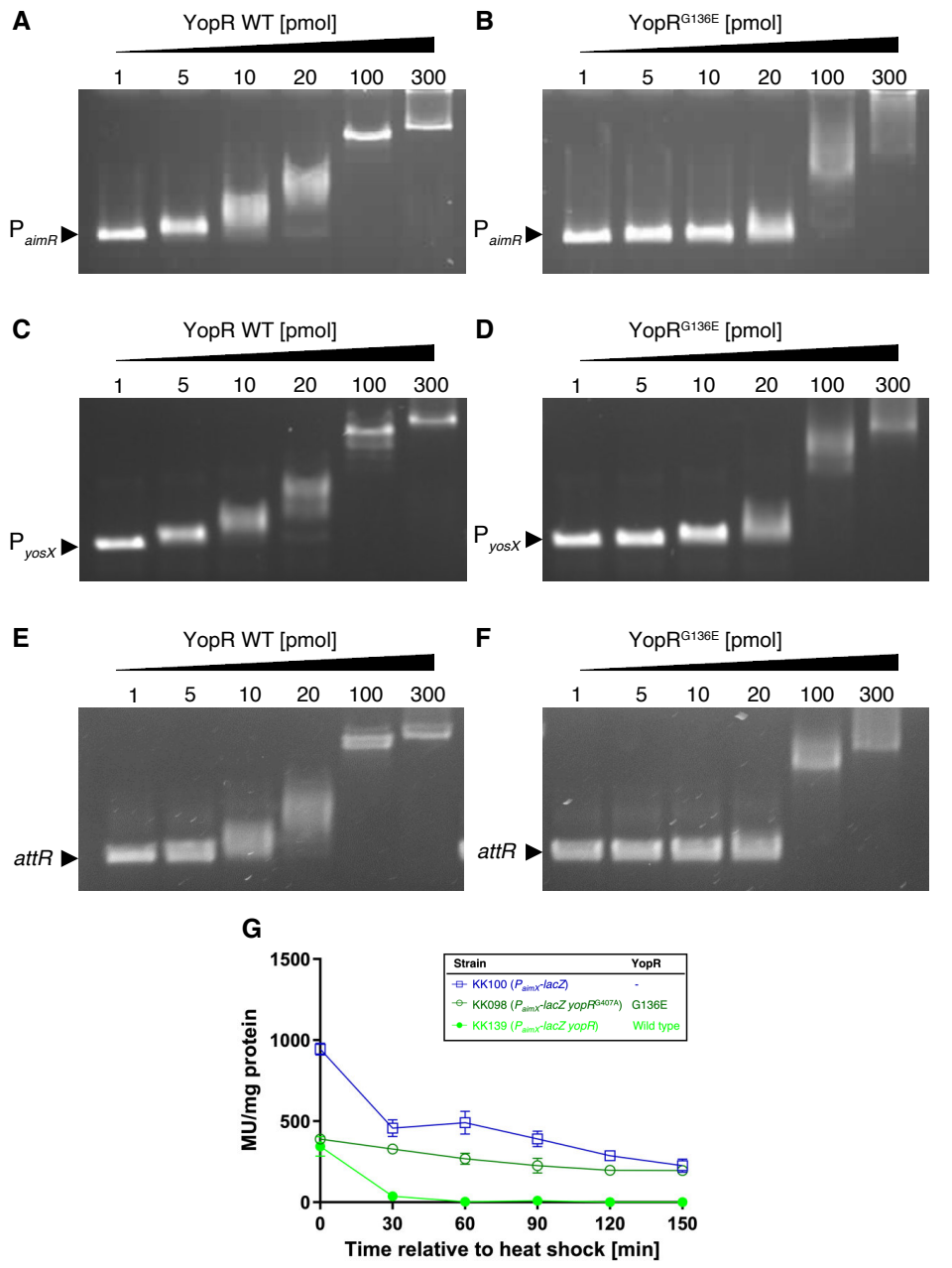
A
YopR WT [pmol]
1 5 10 20 100 300
P aimR
B
YopR G136E [pmol]
1 5 10 20 100 300
P aimR
C
YopR WT [pmol]
1 5 10 20 100 300
P yosX
D
YopR G136E [pmol]
1 5 10 20 100 300
P yosX
E
YopR WT [pmol]
1 5 10 20 100 300
attR
F
YopR G136E [pmol]
1 5 10 20 100 300
attR
G
Strain YopR
KK100 (P aimX-lacZ) -
KK098 (P aimX-lacZ yopR G407A) G136E
KK139 (P aimX-lacZ yopR) Wild type
MU/mg protein
1500
1000
500
0
0 30 60 90 120 150
Time relative to heat shock [min]

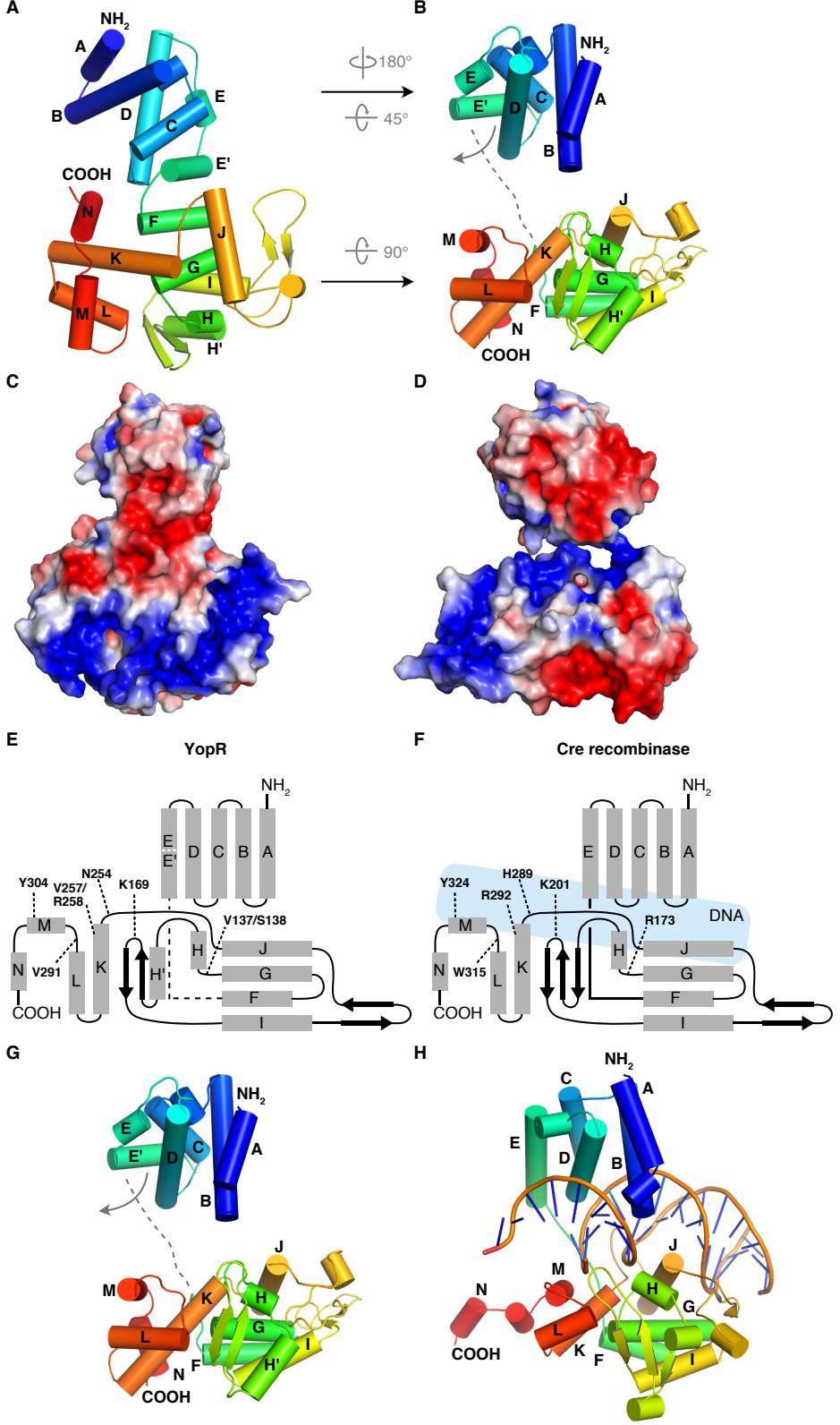
A
NH2
A
B
D
C
E
E'
COOH
N
F
J
K
G
I
M
L
H
H'
180°
45°
90°
B
NH2
E
E'
D
C
A
B
J
M
K
H
G
L
I
F
H'
N
COOH
C
D
E
YopR
NH2
E
E'
D
C
B
A
Y304
N254
V257/
R258
K169
V137/S138
M
N
V291
L
K
H'
H
J
G
F
I
COOH
F
Cre recombinase
NH2
E
D
C
B
A
Y324
H289
R292
K201
R173
DNA
M
N
W315
L
K
H
J
G
F
I
COOH
G
NH2
E
E'
D
C
A
B
J
M
K
H
G
L
I
F
H'
N
COOH
H
NH2
C
A
E
D
B
J
M
N
H
G
L
K
F
I
COOH

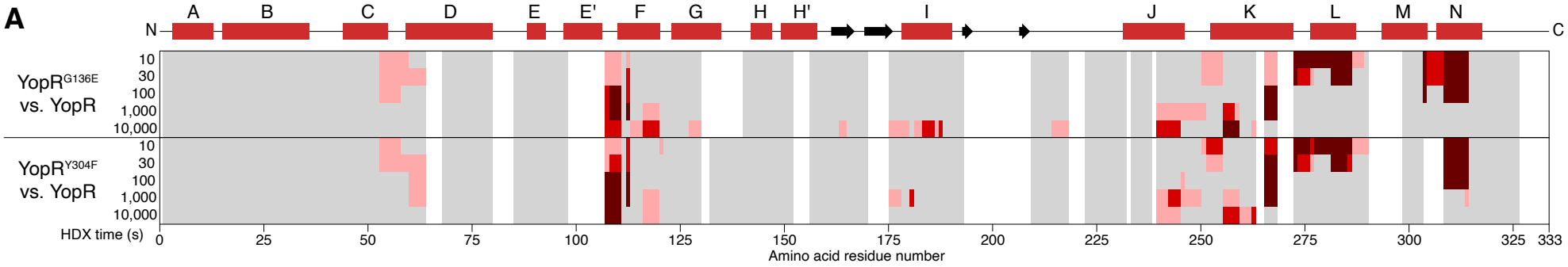
A
N
A
B
C
D
E
E'
F
G
H
H'
I
J
K
L
M
N
C
YopR^G136E vs. YopR
YopR^Y304F vs. YopR
10
30
100
1,000
10,000
HDX time (s)
0
25
50
75
100
125
150
175
200
225
250
275
300
325
333
Amino acid residue number

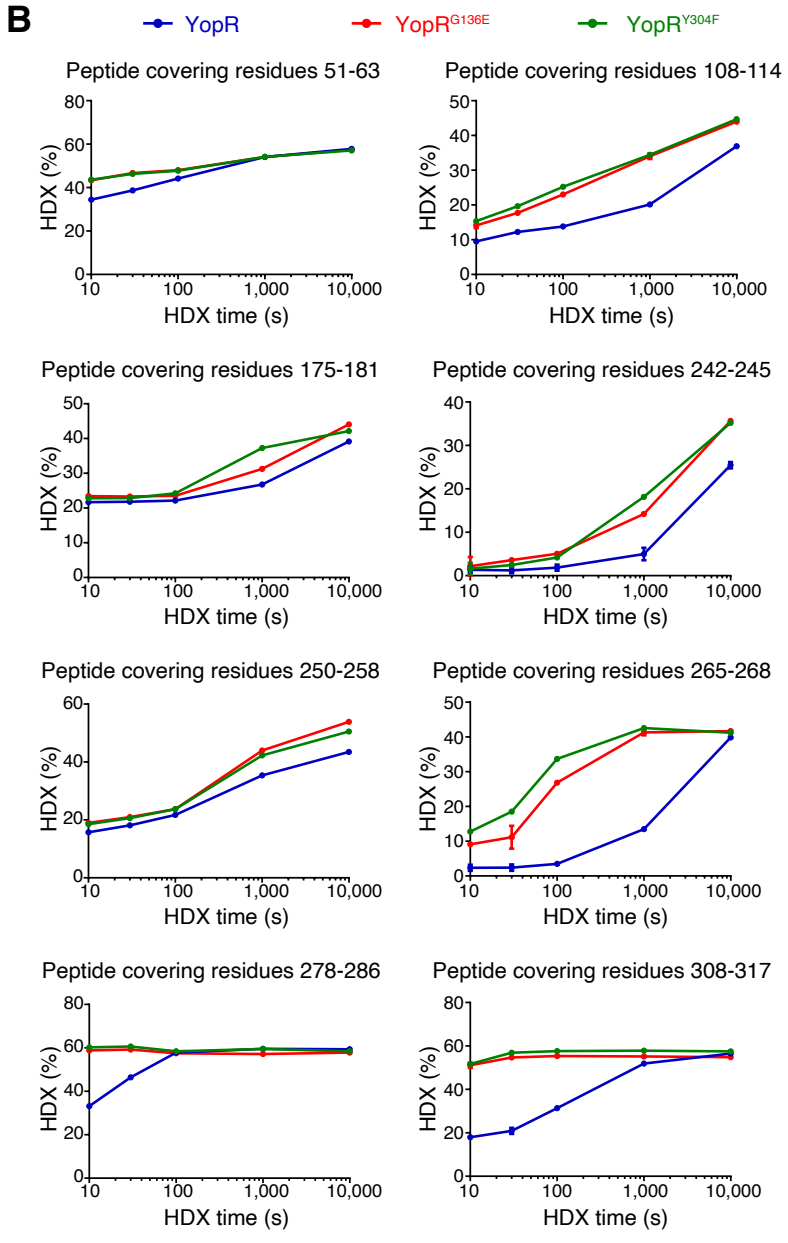
B
YopR
YopR^G136E
YopR^Y304F
Peptide covering residues 51-63
Peptide covering residues 108-114
Peptide covering residues 175-181
Peptide covering residues 242-245
Peptide covering residues 250-258
Peptide covering residues 265-268
Peptide covering residues 278-286
Peptide covering residues 308-317
HDX (%)
HDX time (s)
10
100
1,000
10,000

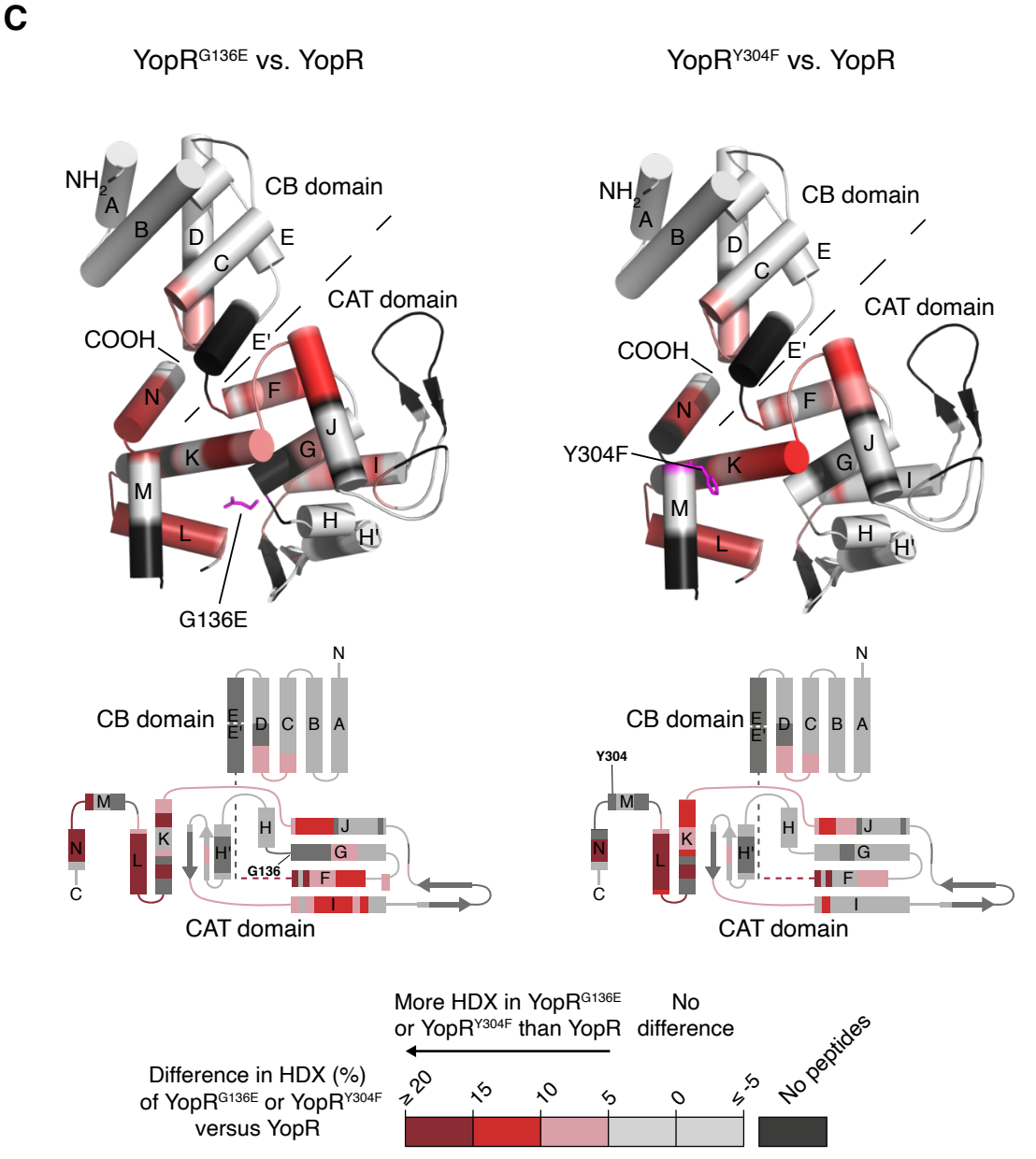
C
YopR^G136E vs. YopR
YopR^Y304F vs. YopR
NH2
CB domain
CAT domain
COOH
G136E
Y304F
Y304
G136
More HDX in YopR^G136E or YopR^Y304F than YopR
No difference
Difference in HDX (%) of YopR^G136E or YopR^Y304F versus YopR
≥ 20
15
10
5
0
≤ -5
No peptides

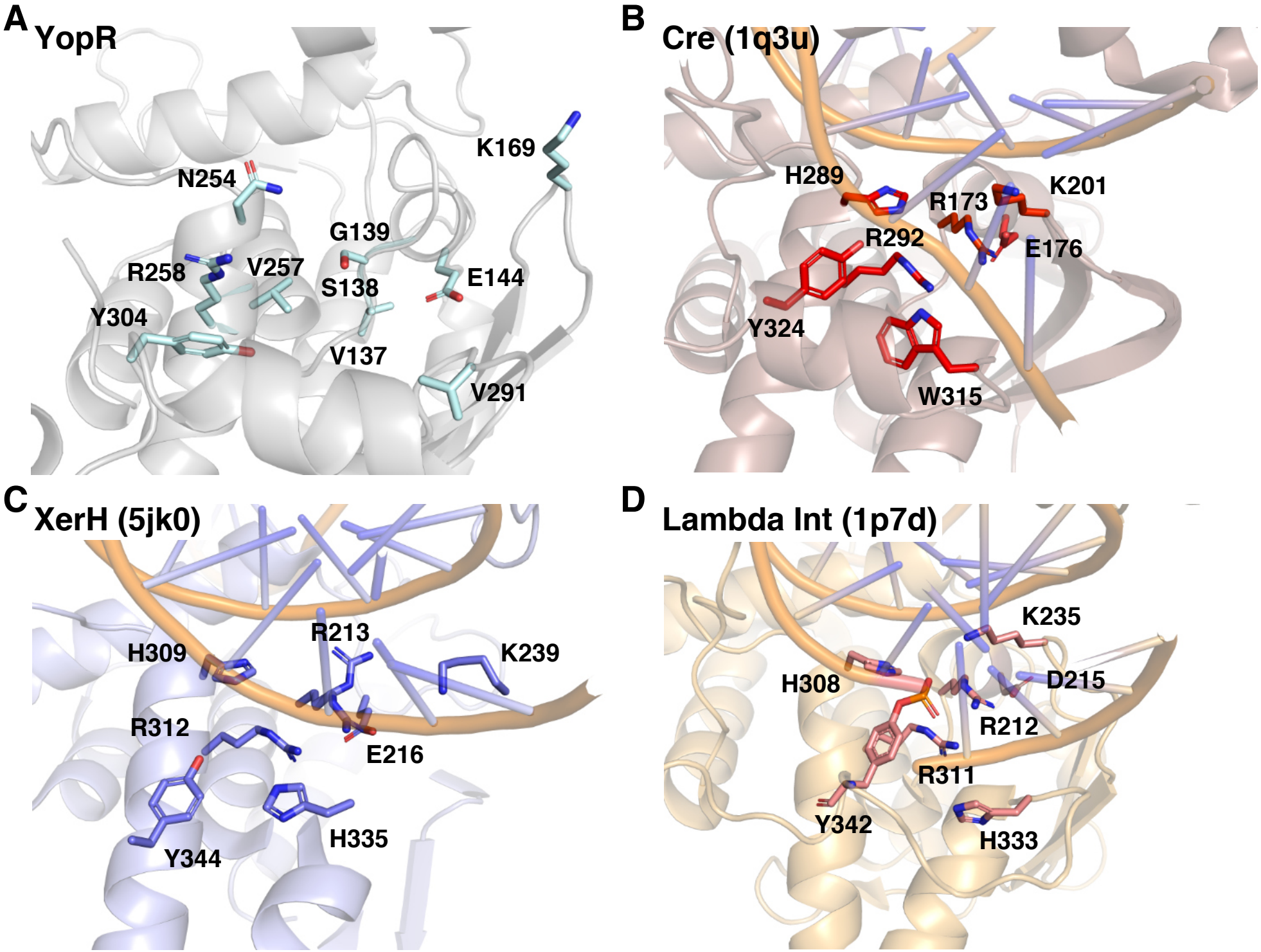
A
YopR
K169
N254
G139
R258
V257
S138
E144
Y304
V137
V291
B
Cre (1q3u)
H289
K201
R173
R292
E176
Y324
W315
C
XerH (5jk0)
R213
H309
K239
R312
E216
H335
Y344
D
Lambda Int (1p7d)
K235
H308
D215
R212
R311
Y342
H333

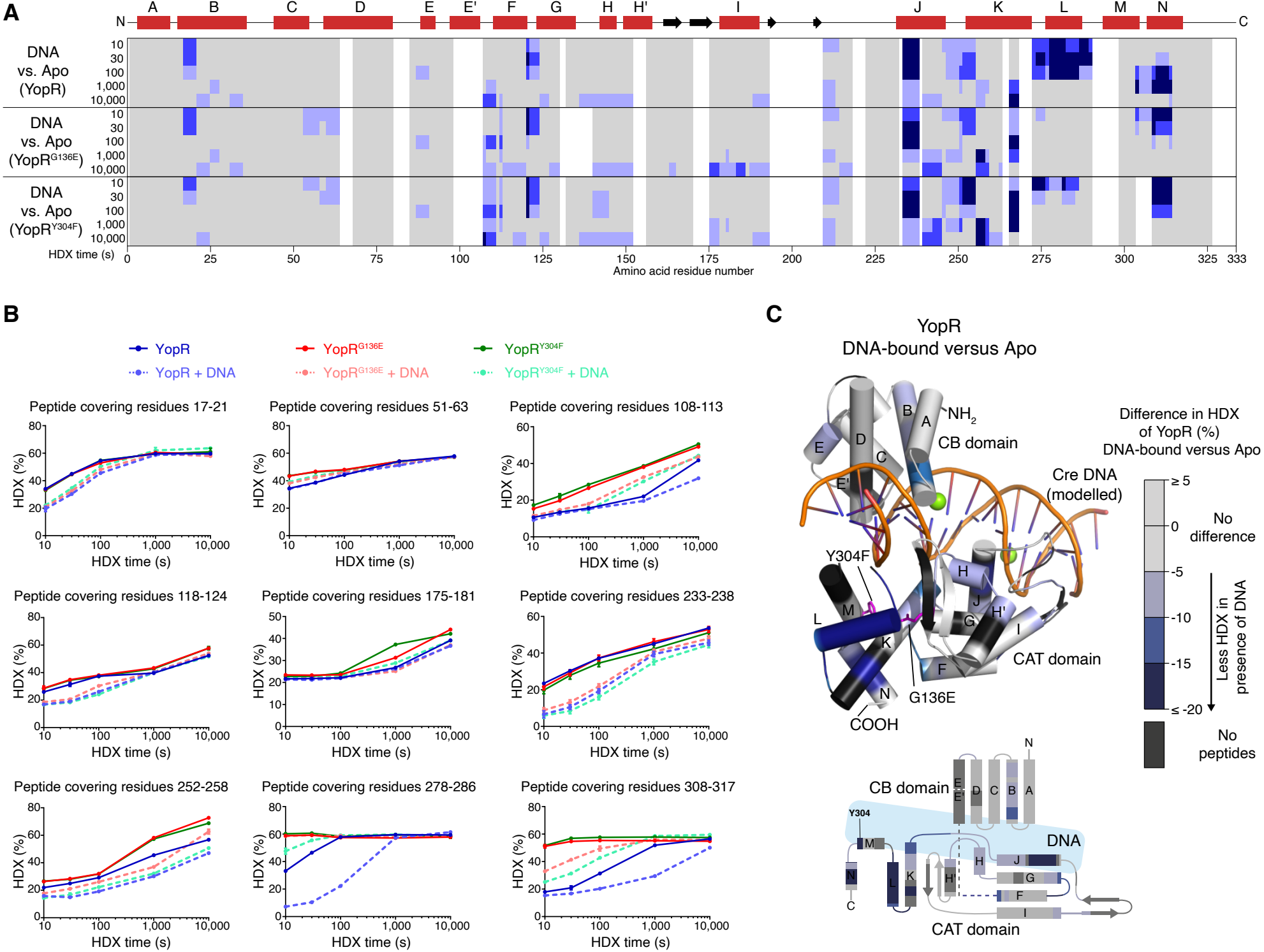
A
N
A B C D E E' F G H H' I J K L M N
C
DNA vs. Apo (YopR)
DNA vs. Apo (YopR^{G136E})
DNA vs. Apo (YopR^{Y304F})
10 30 100 1,000 10,000
HDX time (s)
0 25 50 75 100 125 150 175 200 225 250 275 300 325 333
Amino acid residue number
B
YopR
YopR + DNA
YopR^{G136E}
YopR^{G136E} + DNA
YopR^{Y304F}
YopR^{Y304F} + DNA
Peptide covering residues 17-21
Peptide covering residues 51-63
Peptide covering residues 108-113
Peptide covering residues 118-124
Peptide covering residues 175-181
Peptide covering residues 233-238
Peptide covering residues 252-258
Peptide covering residues 278-286
Peptide covering residues 308-317
HDX (%)
HDX time (s)
C
YopR
DNA-bound versus Apo
NH$_2$
CB domain
Cre DNA (modelled)
Y304F
G136E
CAT domain
COOH
Difference in HDX of YopR (%) DNA-bound versus Apo
≥ 5
0
-5
-10
-15
≤ -20
No difference
Less HDX in presence of DNA
No peptides
CB domain
DNA
CAT domain
Y304

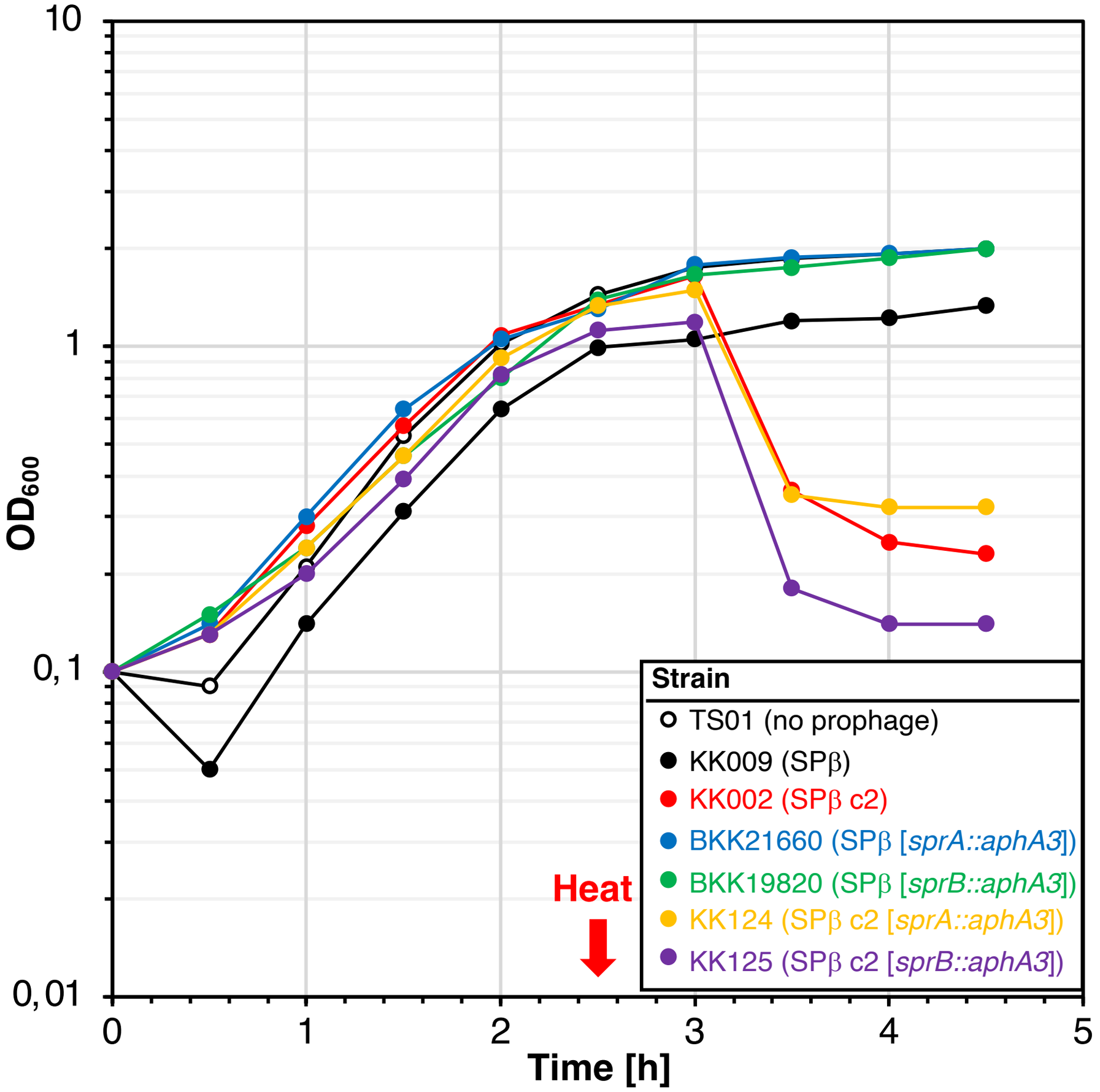
10
1
0,1
0,01
OD600
0
1
2
3
4
5
Time [h]
Heat
Strain
TS01 (no prophage)
KK009 (SPβ)
KK002 (SPβ c2)
BKK21660 (SPβ [sprA::aphA3])
BKK19820 (SPβ [sprB::aphA3])
KK124 (SPβ c2 [sprA::aphA3])
KK125 (SPβ c2 [sprB::aphA3])

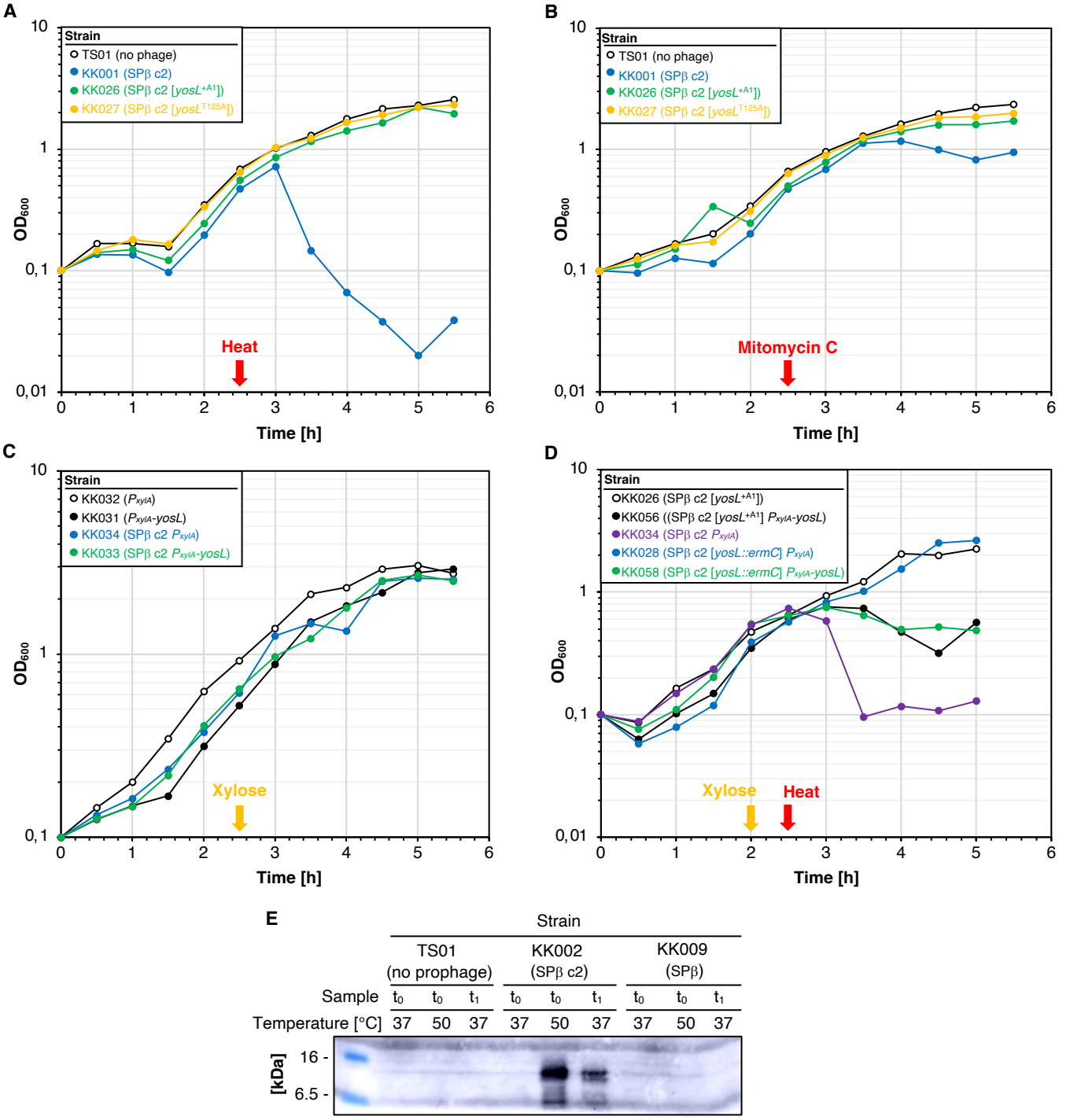
A
Strain
TS01 (no phage)
KK001 (SPβ c2)
KK026 (SPβ c2 [yosL+A1])
KK027 (SPβ c2 [yosLT125A])
Heat
OD600
Time [h]
B
Strain
TS01 (no phage)
KK001 (SPβ c2)
KK026 (SPβ c2 [yosL+A1])
KK027 (SPβ c2 [yosLT125A])
Mitomycin C
OD600
Time [h]
C
Strain
KK032 (PxylA)
KK031 (PxylA-yosL)
KK034 (SPβ c2 PxylA)
KK033 (SPβ c2 PxylA-yosL)
Xylose
OD600
Time [h]
D
Strain
KK026 (SPβ c2 [yosL+A1])
KK056 ((SPβ c2 [yosL+A1] PxylA-yosL)
KK034 (SPβ c2 PxylA)
KK028 (SPβ c2 [yosL::ermC] PxylA)
KK058 (SPβ c2 [yosL::ermC] PxylA-yosL)
Xylose
Heat
OD600
Time [h]
E
Strain
TS01 (no prophage)
KK002 (SPβ c2)
KK009 (SPβ)
Sample
Temperature [°C]
[kDa]
16 -
6.5 -

Supplementary Material for:

Structural and functional analysis of YopR and identification of an additional key component of the SPβ phage lysis-lysogeny management system

Katharina Kohm[1,2,6], Ekaterina Jalomo-Khayrova[3,6], Syamantak Basu[1], Wieland Steinchen[3], Gert Bange[3,4], Robert Hertel[1,5,*], Fabian M. Commichau[1,2,*], Laura Czech[3,*]

[1]FG Synthetic Microbiology, Institute for Biotechnology, BTU Cottbus-Senftenberg, Senftenberg, Germany
[2]FG Molecular Microbiology, Institute for Biology, University of Hohenheim, Stuttgart, Germany
[3]Center for Synthetic Microbiology (SYNMIKRO) and Department of Chemistry, Phillips-University Marburg, Marburg, Germany
[4]Max-Planck Institute for Terrestrial Microbiology, Marburg, Germany
[5]Department of Genomic and Applied Microbiology, Institute of Microbiology and Genetics, Georg-August-University of Göttingen, Göttingen, Germany
[6]Equally contributing

*Corresponding authors:
czechla@staff.uni-marburg.de; fabian.commichau@uni-hohenheim.de; rhertel@gwdg.de

Universität Göttingen
37077 Göttingen
Phone: +49-175-7916901
Mail: rhertel@gwdg.de

Universität Hohenheim
70699 Stuttgart
Phone: +49-711459-22222
Mail: fabian.commichau@uni-hohenheim.de

Phillips-Universität Marburg
35043 Marburg
Phone: +49-177-7555527
Mail: czechla@staff.uni-marburg.de

RUNNING TITLE: Control of the SPβ phage lysogeny management system

KEYWORDS: prophage, regulation, repressor, recombinase, suppressor mutant

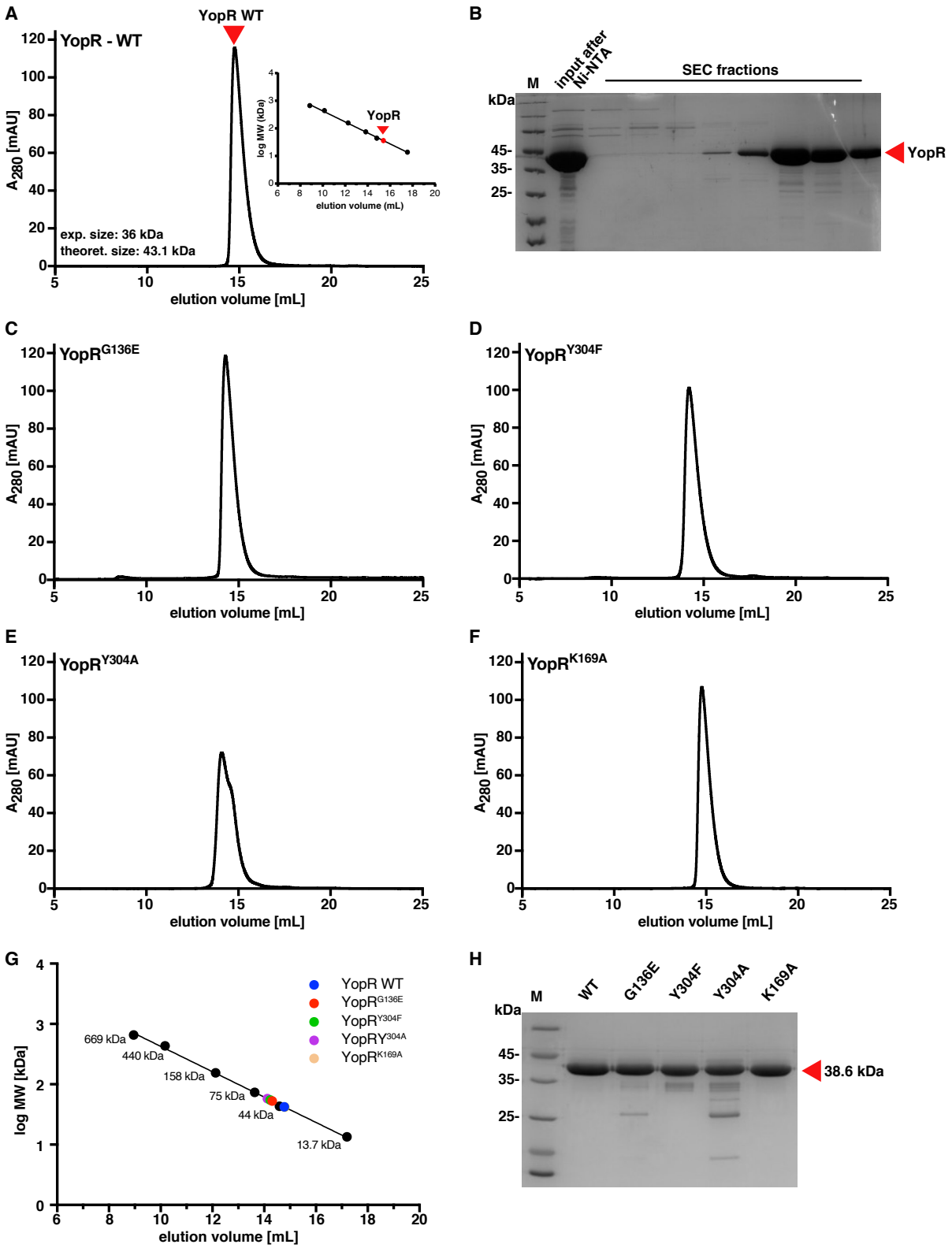

Figure S1. Analytical SEC and SDS PAGE analysis of YopR and YopR variants. A. Analytical SEC of YopR WT after additional heparin purification. Comparison to standard protein solutions is shown in the smaller graph. **B.** SDS-PAGE analysis of SEC fractions of YopR WT protein. **C-F.** Analytical SEC analysis of the variants YopR^{G136E} (**C**), YopR^{Y304F} (**D**), YopR^{Y304A} (**E**) and YopR^{K169A} (**F**). **G.** Comparison of YopR WT and variants to SEC of standard protein solutions (thyroglobulin [660 kDa], ferritin [474 kDa], aldolase [160 kDa], conalbumin [76 kDa], ovalbumin [43 kDa] and

ribonuclease A [13.7 kDa]). **H.** SDS-PAGE of purified YopR WT, and the variants YopR^{G136E}, YopR^{Y304F}, YopR^{Y304A}, and YopR^{K169A}.

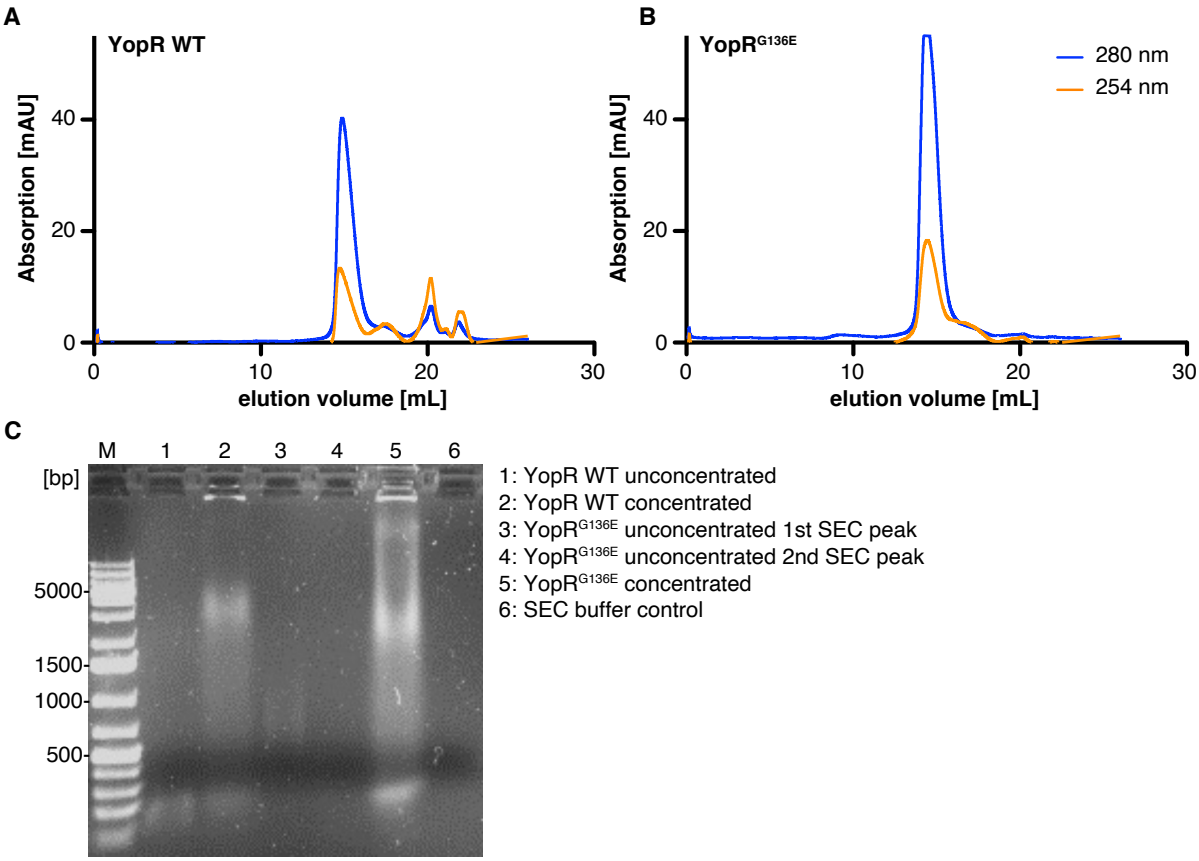

Figure S2. DNA contamination during purification of YopR and YopR^{G136E}. A, B. Size-exclusion chromatography (SEC) of YopR WT (**A**) and YopR^{G136E} (**B**). Absorption at 280 nm is shown in blue, and 254 nm in orange. **C.** Analysis of co-purified DNA present in affinity purified YopR WT and YopR^{G136E} using agarose gel electrophoresis. Lanes are labelled within the figure.

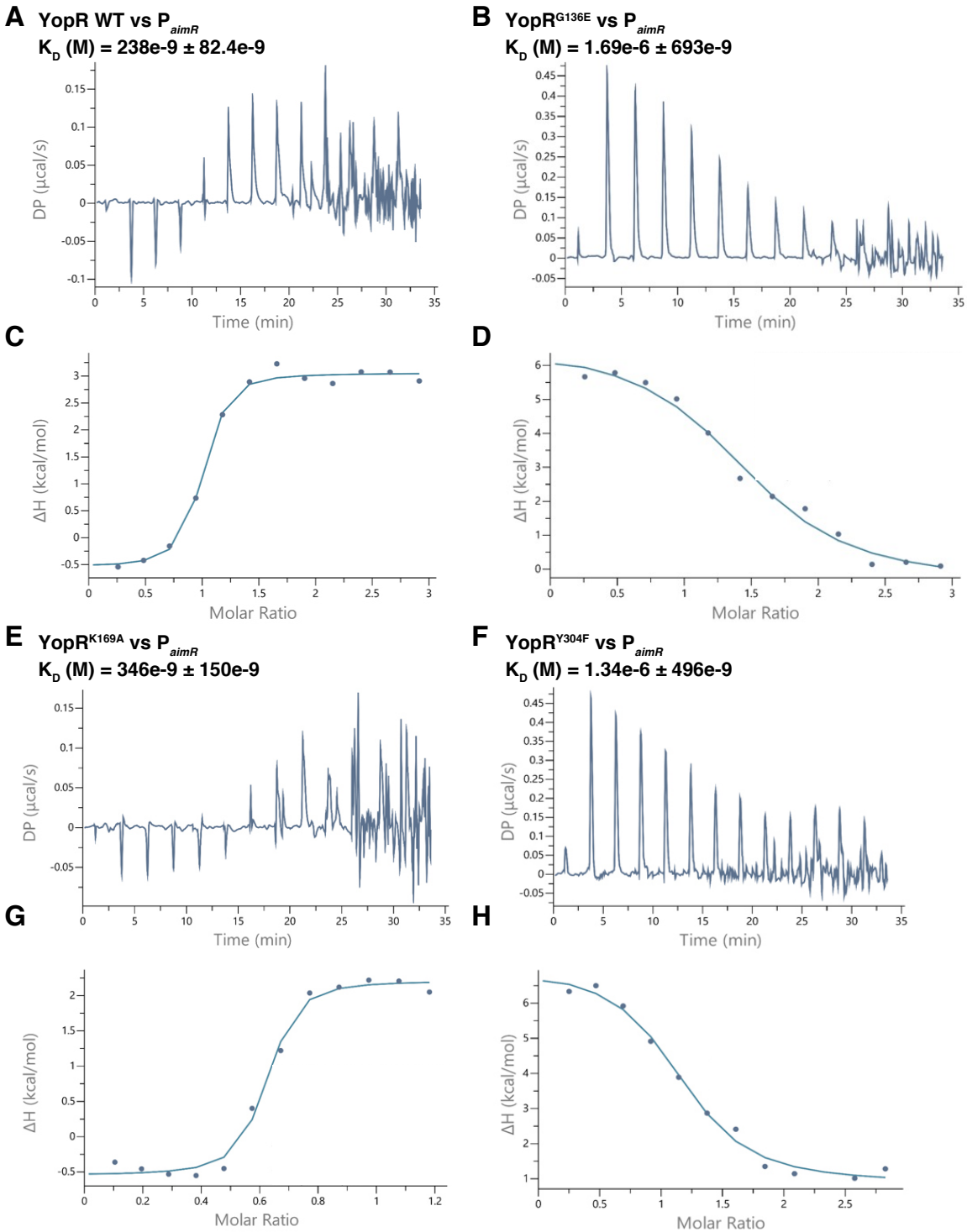

Figure S3. Binding of DNA to YopR and YopR variants determined by isothermal titration calorimetry (ITC). DNA of the *aimR* promoter region was added to the sample cell and titrated with purified YopR WT (**A**, **C**) and YopR variant proteins YopR^{G136E} (**B**, **D**), YopR^{K169A} (**E**, **G**) and YopR^{Y304F} (**F**, **H**). Panels A, B, E and F show the thermograms for each ITC run, and panels C, D, G and H are the resulting fitted plots; the blue dots represent the binding enthalpies (ΔH) per injection versus ligand concentration. DP stands for differential power.

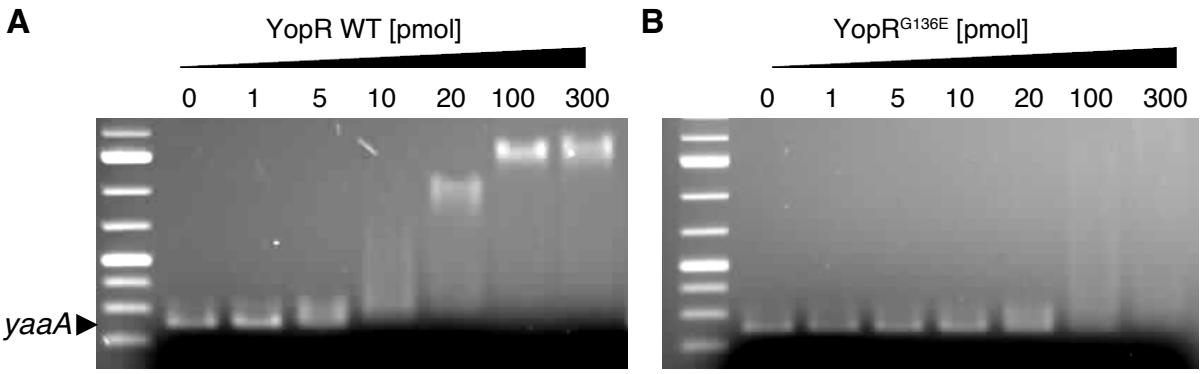

Figure S4. Electrophoretic mobility shift assays (EMSAs) showing the DNA-binding activities of the YopR wild type protein and the YopR^{G136E} variant. A, B. Complex formation between the YopR wild type protein (**A**) and the YopR^{G136E} variant (**B**) with the unrelated *B. subtilis* DNA fragment *yaaA*.

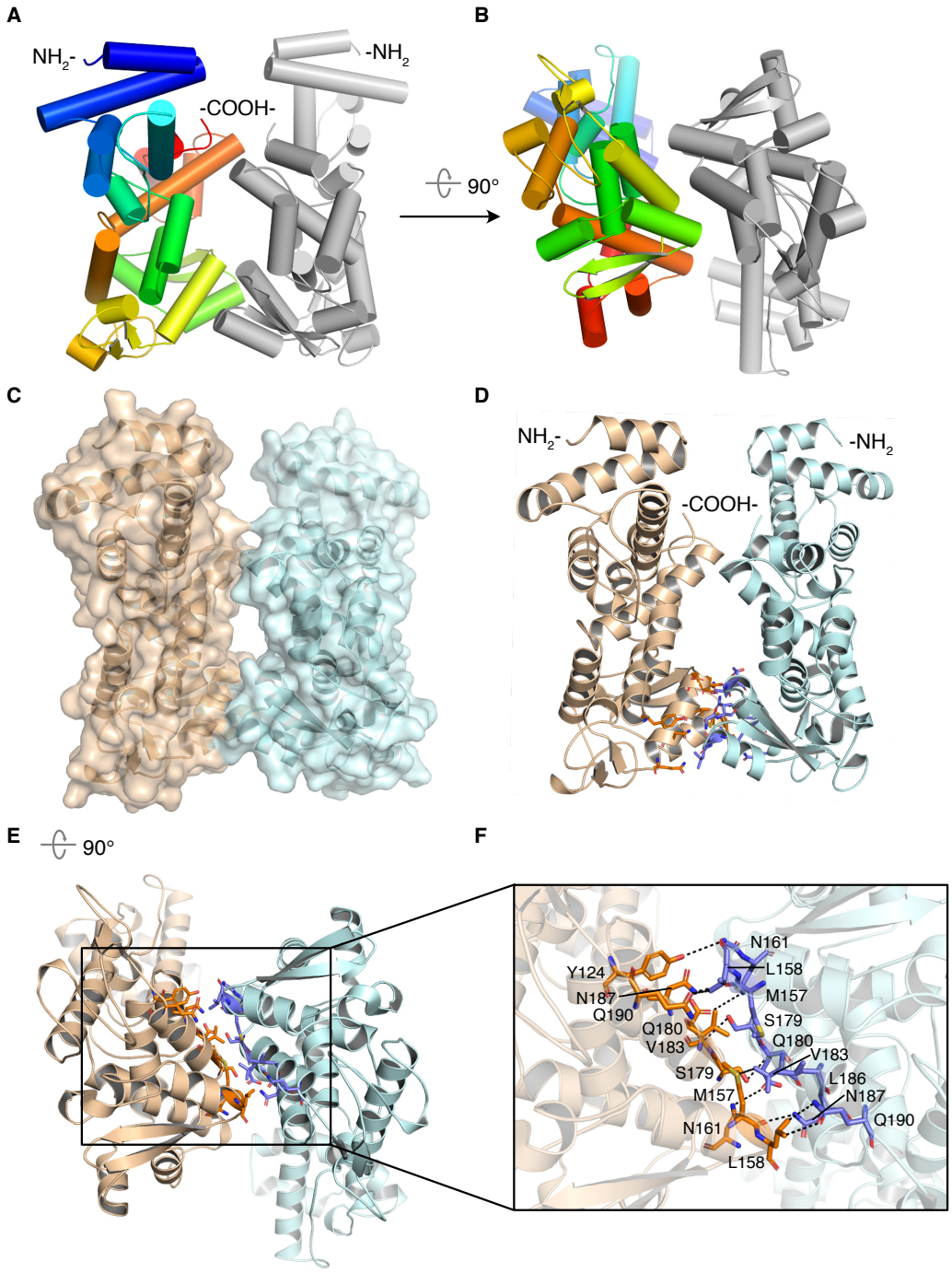

Figure S5. Analysis of the asymmetric unit (ASU) of the YopR crystal structure. A, B. Overall fold of the two YopR molecules found in the asymmetric unit (ASU) of the crystallographic analysis. One monomer is shown in rainbow color and one in grey. **C.** Surface representation of the two monomers present in the ASU shown in beige and light blue, respectively. **D.** Interacting residues in helices H' and I of the two YopR monomers are shown as orange and purple sticks. **E, F.** Zoom into the region of helices H' and I highlighting the interacting residues found in the ASU of the YopR crystal structure.

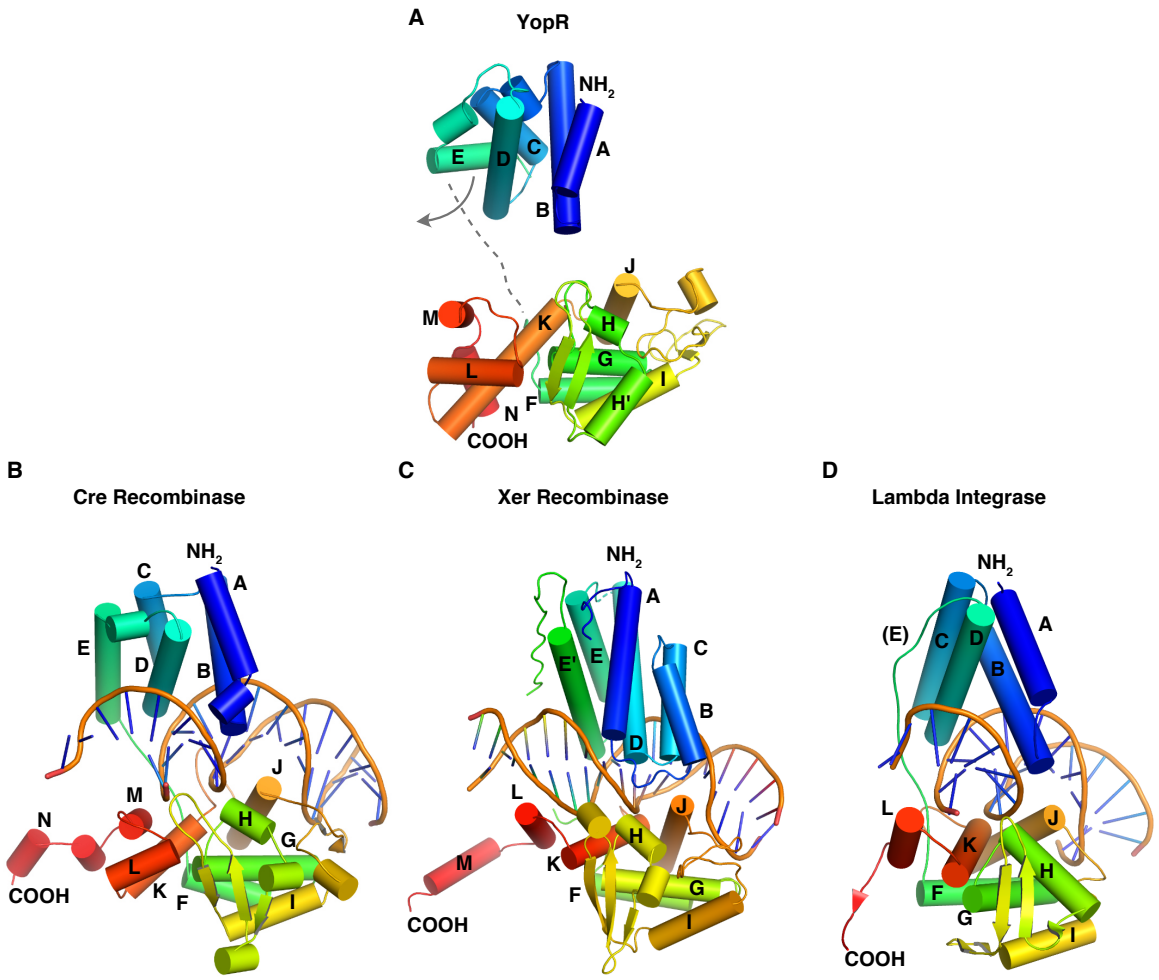

Figure S6. Structural comparison of YopR to known tyrosine recombinases. A. N- and C-terminal domains of the YopR crystal structure were individually overlayed with the structure of the Cre recombinase Cre (PDB-ID: 1q3u) [Ennifar et al., 2003] as described in the main text and figure 5. **B-D.** Crystal structures of the tyrosine recombinases (**B**) Cre (PDB-ID: 1q3u) [Ennifar et al., 2003]; (**C**) XerH (PDB-ID: 5jk0) [Bebel et al., 2016], and (**D**) Lambda Int (PDB-ID: 1p7d) [Aihara et al., 2003], all bound to DNA.

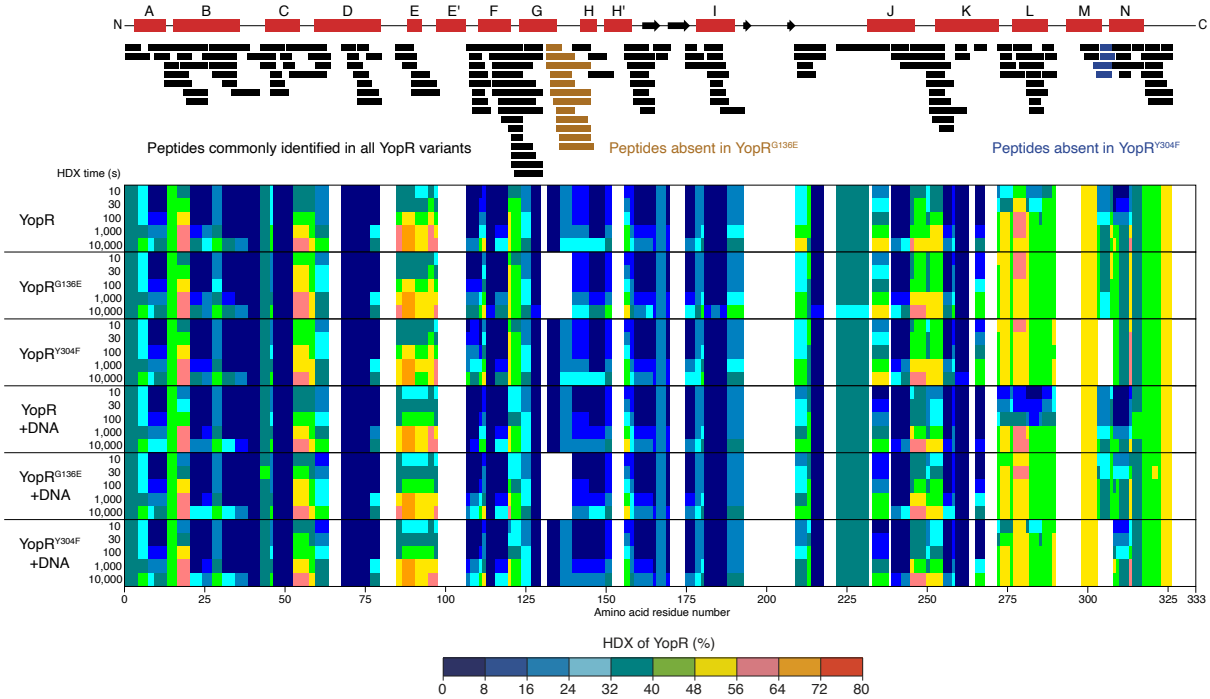

Figure S7. Hydrogen/deuterium exchange mass spectrometry of YopR. Each bar represents a peptide of YopR that was identified in HDX-MS experiments. Peptides that could not be identified for YopR^{G136E} or YopR^{Y304F} variants due to the variations are highlighted in ocre and blue, respectively. The secondary structure of YopR is depicted above (red boxes, α-helices; black arrows, β-strands). The residue-specific HDX of individual YopR, YopR^{G136E} and YopR^{Y304F} residues in apo and DNA-bound states was calculated with DynamX 3.0 from peptides as follows: When any residue was covered by only a single peptide, the residue-specific deuterium uptake equals that of the whole peptide. In the case of overlapping peptides for any given residue, residue-specific deuterium uptake was determined by the shortest peptide covering that residue. Where multiple peptides were of the shortest length, the peptide with the residue closest to the peptide C-terminus was utilized. Numerical values for deuterium uptake by peptides and residue-specific HDX are provided in Supplemental Dataset.

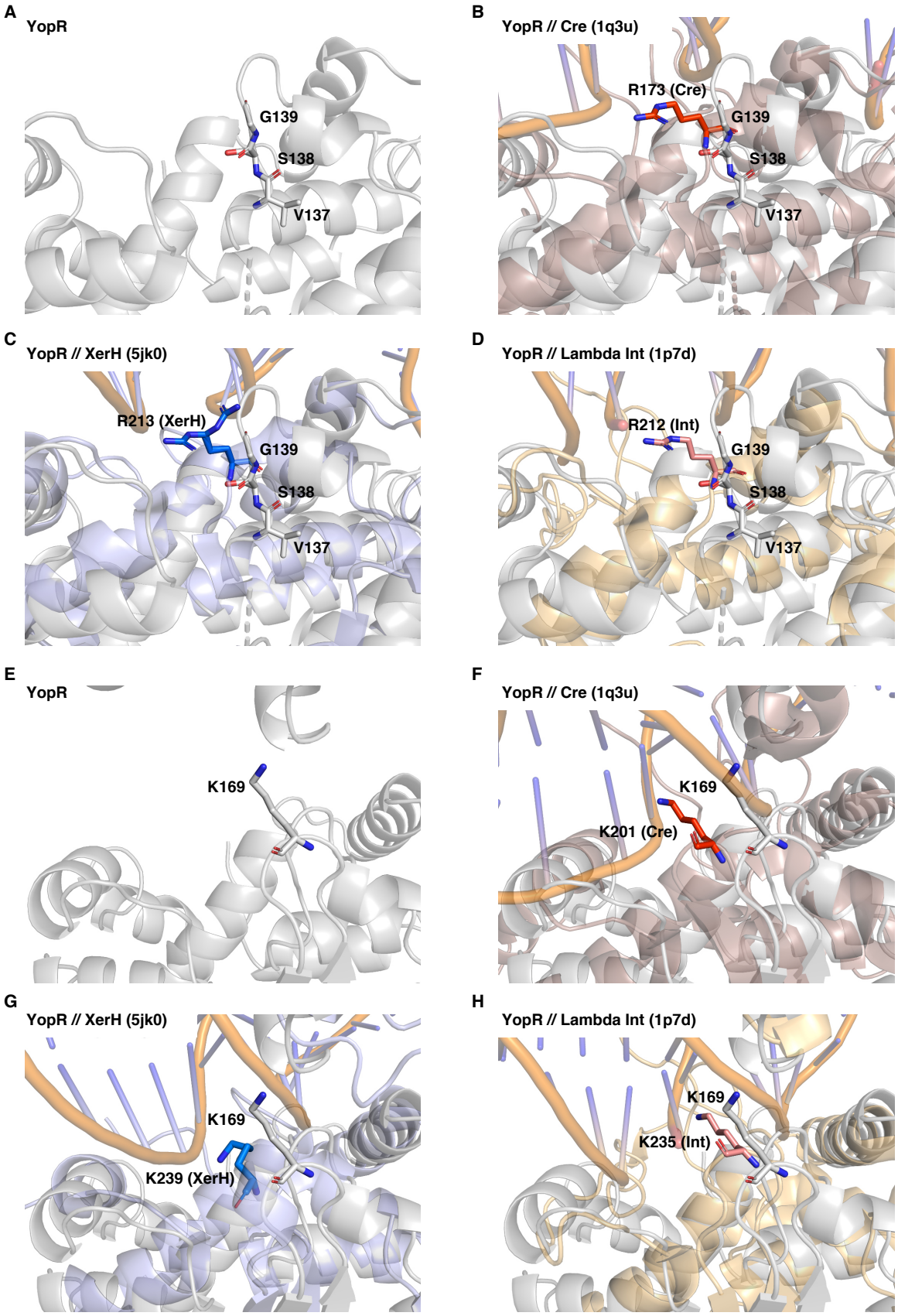
A
YopR
G139
S138
V137
B
YopR // Cre (1q3u)
R173 (Cre)
G139
S138
V137
C
YopR // XerH (5jk0)
R213 (XerH)
G139
S138
V137
D
YopR // Lambda Int (1p7d)
R212 (Int)
G139
S138
V137
E
YopR
K169
F
YopR // Cre (1q3u)
K169
K201 (Cre)
G
YopR // XerH (5jk0)
K169
K239 (XerH)
H
YopR // Lambda Int (1p7d)
K169
K235 (Int)

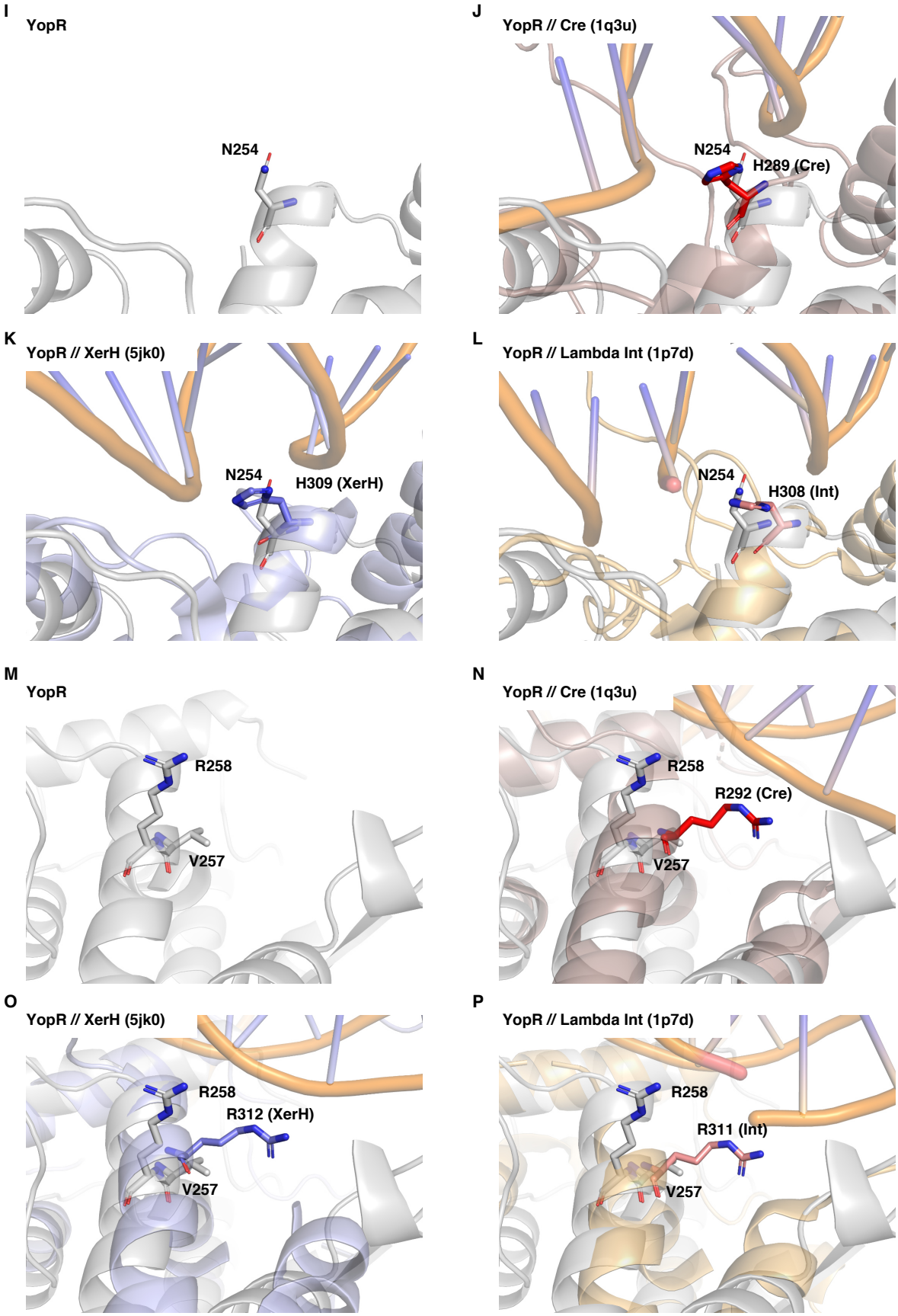
I
YopR
N254
J
YopR // Cre (1q3u)
N254
H289 (Cre)
K
YopR // XerH (5jk0)
N254
H309 (XerH)
L
YopR // Lambda Int (1p7d)
N254
H308 (Int)
M
YopR
R258
V257
N
YopR // Cre (1q3u)
R258
R292 (Cre)
V257
O
YopR // XerH (5jk0)
R258
R312 (XerH)
V257
P
YopR // Lambda Int (1p7d)
R258
R311 (Int)
V257

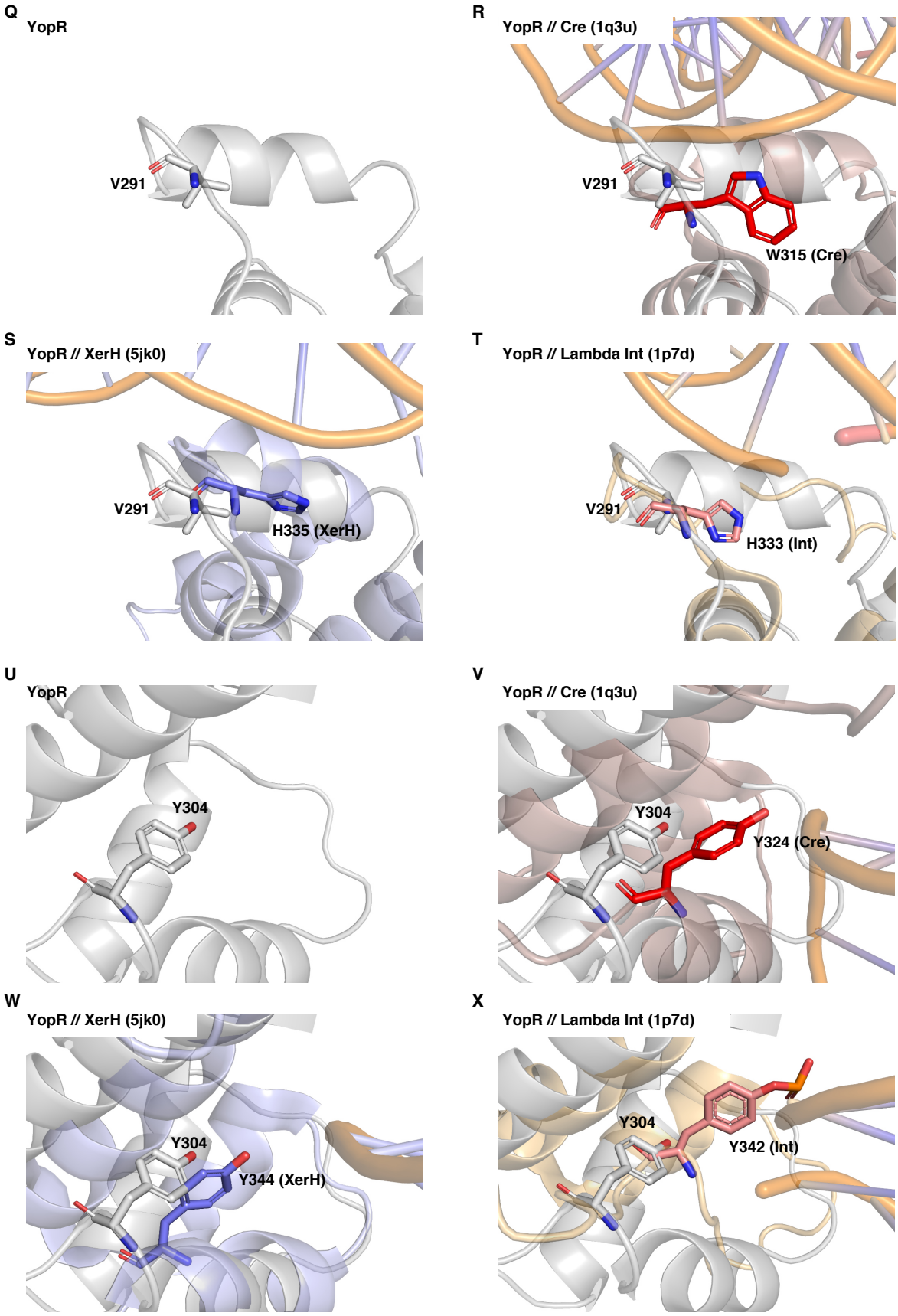

Figure S8. Structural comparison of catalytically important amino acid residues of tyrosine recombinases to those found in YopR. A-D. Comparison of V137/S138/G139 in YopR (**A**) to R173 in Cre (**B**), R213 in XerH (**C**) and R212 in Lambda Int (**D**). **E-H.** Comparison of K169 in YopR (**E**) to K201 in Cre (**F**), K239 in XerH (**G**) and K235 in Lambda Int (**H**). **I-L.** Comparison of N254 in

YopR (**I**) to H289 in Cre (**J**), H309 in XerH (**K**) and H308 in Lambda Int (**L**). **M-P.** Comparison of V257/R258 in YopR (**M**) to R292 in Cre (**N**), R312 in XerH (**O**) and R311 in Lambda Int (**P**). **Q-T.** Comparison of V291 in YopR (**Q**) to W315 in Cre (**R**), H335 in XerH (**S**) and H333 in Lambda Int (**T**). **U-X.** Comparison of Y304 in YopR (**U**) to Y324 in Cre (**V**), Y344 in XerH (**W**) and Y342 in Lambda Int (**X**).

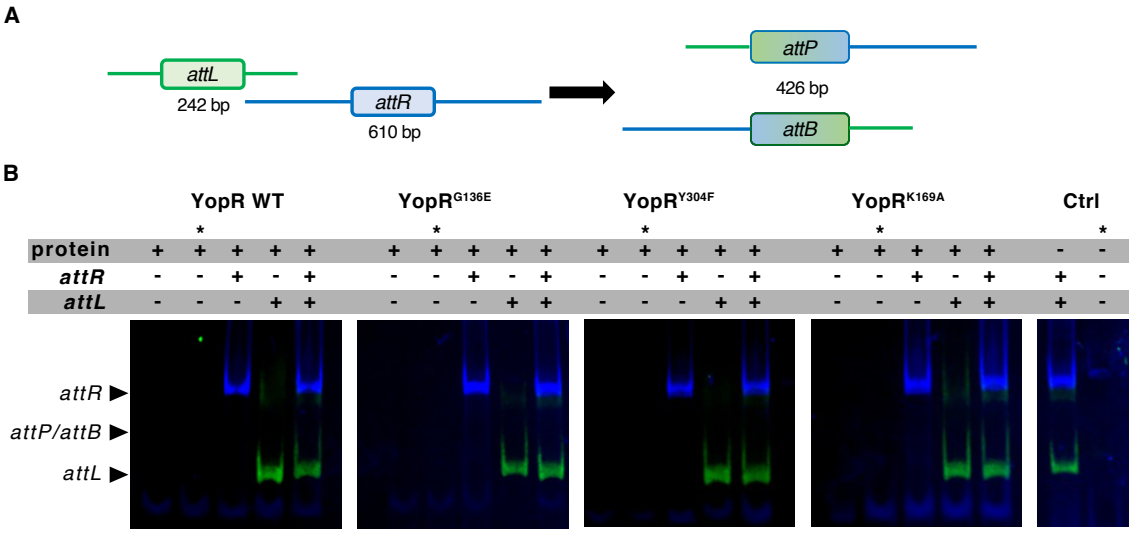

Figure S9. *In vitro* recombinase assay. A. Schematic overview of the *in vitro* recombination. The *attL* fragment (242 bp) is labeled with Cy5 (green) and the *attR* fragment (610 bp) is labeled with Cy3 (blue). The resulting hybrid *attP* and *attB* fragments indicative for DNA recombination have an expected size of 426 bp. **B.** Recombinase assay using the *attR* and *attL* regions of the SPβ phage [Abe et al., 2017] assessing the recombinase activity of the purified YopR WT protein and the YopR variants YopR^{G136E}, YopR^{Y304F}, and YopR^{K169A}. Lanes marked with an asterisk (*) are reactions in which the labeled DNA fragments were exchanged by an unlabeled DNA fragment carrying no fluorescent dye.

Table S1. Primers used in the study.

Name	Features*	Purpose
PP073	5'-TACGTGATGCCTTCATCAACTAGA	Sequencing of *yopR* deletion
PP312	5'-GGAACTAAGGTCGCAAATGG	Sequencing of *yokI*
PP318	5'-AGCCTAGACGAGTTGGAAAG	Sequencing of *yopR*
PP319	5'-GCAGCTGAGCGACTATAATC	Sequencing of *yopR*
PP326	5'-GTCCCATAAGCCGGTTACAG	Sequencing of *yokI*
PP342	5'-TTTCACCGGACAAAGCAACC	Sequencing of *yokI*
PP345	5'-CCGCATTGCACATCTTTAGC	Sequencing of *yokI*
PP359	5'-TGTTTACCGGTGGATCGATG	Sequencing of *yosL*
PP360	5'-CTATGTACGGCCTCCTTATC	Sequencing of *yosL*
PP366	5'-ATA**GGATCC**ATAAGGAGATGTAAAATGGGG	Cloning of *yosL* with *Bam*HI
PP367	5'-TAT**GAATTC**CTAATCGTTATAAGCCCCTG	Cloning of *yosL* with *Eco*RI
PP375	5'-AAA**GAATTCT**TGTCAAGTGAAGGCGCGCTATGCTACAATACAGCTTGGTTTAAAGGAGGAAACAATCATGTTCAATAGTGAGATTAAGGAA	Cloning of *yopR* with *Eco*RI
PP376	5'-TTT**GGATCC**ATTACATGATCCTCCTTATTAAATGGTCGTCTCTTTTAGAC	Cloning of *yopR* with *Bam*HI
PP390	5'-ATA**GAATTC**AGGATATTGCGGAAGAGGTG	Cloning of P_{aimR} with *Eco*RI
PP391	5'-TAT**GGATCC**ATTATTTCCCCTCATTTCTTTTTG	Cloning of P_{aimR} with *Bam*HI
PPKK001	5'-GACGAGCGGGATTTATCAGC	*sprA::aphA3* amplification from BKK21660
PPKK002	5'-CATATCACGAGGCAGTGTTG	*sprA::aphA3* amplification from BKK21660
PPKK003	5'-CATACACAACGAGCCCTGAC	*sprB::aphA3* amplification from BKK19820
PPKK004	5'-CAGTGAAGGAGGCCATTGAAG	*sprB::aphA3* amplification from BKK19820

TS037	5‘-TGAAATTTCACCTCTAATGGTGGTGGTGATGATG TTCGCCATTCAGGCTGCGCA	Sequencing of pAC5 and pAC7 based vectors
BR084	5‘-CCTGCTGTAATAATGGGTAGAAGGT	Sequencing of pAC5 and pAC7 based vectors
KG208	5‘-TTT**AGATCT**TCATTACTTGTACAGCTCGTCCATGC CGA	Sequencing of pGP888 based vectors
JD024	5‘-GTTGGAGTTCGGAGTGAAAACAATTTTTTGATCT	Sequencing of pGP888 based vectors
IS096	5‘-GCAACTGTTGGGAAGGGCG	Sequencing of pAC5, pAC7 based vectors
MD082	5‘-CGTCAGCCGTAAACGCTTTT	Sequencing of *ganA*
MD083	5‘-ATGGCTGACACACCGGATTT	Sequencing of *ganA*
RH070	5’-AGA**TCTAGA**TCAATGGGGAAGAGAACCGC	*ermD* deletion cassette flankA
RH075	5’-TACGTTCCACTGCCAATACCTTAC	sgRNA targeting *ermD*
RH076	5’-AAACGTAAGGTATTGGCAGTGGAA	sgRNA targeting *ermD*
RH080	5’-TACGTACAATAGCGACGGAGAGTT	sgRNA targeting *cat*
RH081	5’-AAACAACTCTCCGTCGCTATTGTA	sgRNA targeting *cat*
RH082	5’-TAGGATCCGGCCAACGAGGCCGGCAAGGAATAG CAGTCCTAATGTATGT	Deletion of *cat* gene
RH083	5’-AAAACCTTCTTCACATTTGATATGCCTCCTAAATTT TTATCTAAAGTGA	Deletion of *cat* gene
RH084	5’-GGCATATCAAATGTGAAGAAGGTTTTTATATTAC AGCTCCAGAT	Deletion of *cat* gene
RH085	5’-TAGGATCCGGCCTTATTGGCCGAGATTTCCTGATA TTGAACTTGCGGTT	Deletion of *cat* gene
RH112	5‘-CCATGTCGACCCGCTAGCTTTTTATTTTTAAAAAAT TGTCAC	*ermD* deletion cassette flank A
RH113	5‘-AGA**TCTAGA**GTTCAGAGAATGATGCTTCC	*ermD* deletion cassette flank B

RH114	5’-AGCTAGCGGGTCGACATGGATGAGCGATG	*ermD* deletion cassette flank B
LC193	5‘-TTAA**GGTCTCC**CATGGGCGGGGCAGCTAGACGTATTGATC	Forward for pEJK9
LC194	5´-TTAA**GGTCTCC**TCGAGATCGTTATAAGCCCCTGTAATTAATTTTGTAG	Reverse for pEJK9
LC195	5´-TTAA**GGTCTCC**CATGGGCTTCAATAGTGAGATTAAGGAAAAATATTTAG	Forward for pEJK11 and pEJK13
LC196	5´-TTAA**GGTCTCC**TCGAGAATGGTCGTCTCTTTTAGACC	Reverse for pEJK11 and pEJK13
LC226	5´-GCCGGAGATATGAACTACAAAGACATG	Forward for P_{aimR} promotor
LC230	5´-GAGTGTGCTTGATAATTCAACTCCAG	Forward for σ^A dependent P_{yosX} promoter
LC252	5´-CAGCATACTCCAATGCACTTCTTGC	Reverse for P_{aimR} promotor
LC254	5´-CAAGCTTAGCTTTGTTTTGCTGTGTTTC	Reverse for σ^A dependent P_{yosX} promoter
LC255*	5´-[Cy3] GCTGCATTAGATGAAGAATTTAAAGAGC	Forward for *attR* site. Cy3 label at 5’
LC255	5´-GCTGCATTAGATGAAGAATTTAAAGAGC	Forward for *attR* site
LC256	5´-CTTTTGTAATAGCAGCCGATTGTAATG	Reverse for *attR* site
LC257	5´-CTATGATTCAgcgCACGGTGAACG	Forward for pEJK25
LC258	5´- AGGGTTAAAACGTTACCG	Forward for pEJK25
LC259	5´- AATGCAAGATgcgATTAATGAGGAAGAAG	Forward for pEJK29
LC260	5´- GAATAAACTGCTCGATATTTG	Reverse for pEJK27 and pEJK29
LC266	5´- AATGCAAGATtttATTAATGAGGAAGAAG	Forward for pEJK27
LC292	5´-GAATTTTAAAGAGATTACAAATACAAAAAATATGTATAAAATAATTGACTCGTAATG	*aimR* promotor
LC293	5´-CATTACGAGTCAATTATTTTATACATATTTTTTGTATTTGTAATCTCTTTAAAATTC	*aimR* promotor

EJK54	5´-GGATGAAGCAAGTAATGACTTAGATGAG	Forward for *attL* site
EJK55*	5´-[Cy5] GACCATCCATTTGAAGCGATCC	Reverse for *attL* site. Cy5 label at 5'

***** Restriction sites are shown in bold letters, ribosome-binding sites and promoter elements are underlined; lower case letters indicate bases leading to a mutation/base exchange.

Table S2. Strains and plasmids

Strains

Name	**Genotype**	**Usage/ construction[a]**	**Reference/ source**
E. coli			
DH10B	F⁻*mcr*A Δ(*mrr-hsd*RMS-*mcr*BC) ϕ80*lac*ZΔM15 Δ*lac*X74 *rec*A1 *end*A1 *ara*D139 Δ(*ara-leu*)7697 *gal*U *gal*K λ⁻*rps*L(Str^R) *nup*G	Cloning	Grant et al., 1990
XL1-Blue	*recA1 endA1 gyrA96 thi-1 hsdR17 supE44 relA1 lac* [F' *proAB lacI*^{q} *ZΔM15* Tn*10* (*Tet*^{r})]	Cloning	Stratagene
BL21(DE3)	F⁻*omp*T *hsd*S$_B$ (r$_B$⁻, m$_B$⁻) *gal dcm* (DE3)	Protein expression	NEB
B. subtilis			
168	*trpC2*	Laboratory strain	Laboratory collection
SP1	Derivative of 168	Laboratory strain	Richts et al., 2020
Δ6	*trpC2* ΔSPβ (sublancin sensitive) Δ*skin* ΔPBSX Δprophage 1 *pks*::*cat* Δprophage 3 ΔICEBs1	Derivative of 168	Westers et al., 2003
CU1147	*trpC2* SPβ c2		Rosenthal et al., 1979
TS01	Δ6 *amyE*::(*P*$_{mtlA}$-*comKS ermD*)	Derivative of Δ6	Schilling et al., 2018
TS03	Δ6 Δ*cat amyE*::(*P*$_{mtlA}$-*comKS ermD*)	Derivative of TS01	This study
BKK19820	*sprB*::*aphA3*	Derivative of 168	Koo et al., 2017
BKE20080	*yosL*::*ermC*	Derivative of 168	Koo et al., 2017
BKE20700	*yoqA*::*ermC*	Derivative of 168	Koo et al., 2017

BKE20790	*yopR*::*ermC*	Derivative of 168	Koo et al., 2017
BKE20800	*yopQ*::*ermC*	Derivative of 168	Koo et al., 2017
BKE21570	*yokJ*::*ermC*	Derivative of 168	Koo et al., 2017
BKE21580	*yokI*::*ermC*	Derivative of 168	Koo et al., 2017
BKK21660	*sprA*::*aphA3*	Derivative of 168	Koo et al., 2017
KK001	Δ6 *amyE*::(P_{mtlA}-*comKS ermD*) SPβ c2	SPβ c2 → TS01	Kohm et al., 2022
KK002	Δ6 *amyE*::(P_{mtlA}-*comKS*) SPβ c2	Derivative of KK001	Kohm et al., 2022
KK004	Δ6 *amyE*::(P_{mtlA}-*comKS ermD*) *amyE*::(P_{alf4}-*yopR aphA3*)	Derivative of TS01	Kohm et al., 2022
KK137	Δ6 *amyE*::(P_{mtlA}-*comKS ermD*) SPβ	SPβ → TS01	This study
KK009	Δ6 *amyE*::(P_{mtlA}-*comKS*) SPβ	Derivative of KK137	This study
KK010	Δ6 *amyE*::(P_{mtlA}-*comKS ermD*) *amyE*::(P_{alf4}-*yopR*^{G407A} *aphA3*)	pRH166 → TS01	This study
KK011	Δ6 *amyE*::(P_{mtlA}-*comKS*) SPβ c2 *amyE*::(P_{alf4}-*yopR aphA3*)	pRH167 → KK002	This study
KK014	Δ6 *amyE*::(P_{mtlA}-*comKS*) SPβ *amyE*::(P_{alf4}-*yopR*^{G407A} *aphA3*)	pRH166 → KK009	This study
KK015	Δ6 *amyE*::(P_{mtlA}-*comKS*) SPβ *yopR*::*ermC amyE*::(P_{alf4}-*yopR*^{G407A} *aphA3*)	BKE20790 → KK014	This study
KK026	Δ6 *amyE*::(P_{mtlA}-*comKS ermD*) SPβ c2 *yosL*$^{+A1}$	Derivative of KK001	This study
KK027	Δ6 *amyE*::(P_{mtlA}-*comKS ermD*) SPβ c2 *yosL*^{T125A}	Derivative of KK001	This study
KK028	Δ6 *amyE*::(P_{mtlA}-*comKS*) SPβ c2 *yosL*::*ermC*	BKE20080 → KK002	This study
KK031	Δ6 *amyE*::(P_{mtlA}-*comKS ermD*) *ganA*::(*xylR* P_{xylA}-*yosL aphA3*)	pRH168 → TS01	This study
KK032	Δ6 *amyE*::(P_{mtlA}-*comKS ermD*) *ganA*::(*xylR* P_{xylA} *aphA3*)	pGP888→ TS01	This study
KK033	Δ6 *amyE*::(P_{mtlA}-*comKS*) SPβ c2 *ganA*::(*xylR* P_{xylA}-*yosL aphA3*)	pRH168→ KK002	This study
KK034	Δ6 *amyE*::(P_{mtlA}-*comKS*) SPβ c2 *ganA*::(*xylR* P_{xylA} *aphA3*)	pGP888 → KK002	This study
KK056	Δ6 *amyE*::(P_{mtlA}-*comKS ermD*) SPβ c2 *yosL*$^{+A1}$ *ganA*::(*xylR* P_{xylA}-*yosL aphA3*)	pRH168 → KK026	This study
KK058	Δ6 *amyE*::(P_{mtlA}-*comKS*) SPβ c2 *yosL*::*ermC ganA*::(*xylR* P_{xylA}-*yosL aphA3*)	pRH168 → KK028	This study

KK097	Δ6 Δ*cat amyE*::(P_{yosX}-*lacZ cat*) *ganA*::(*xylR* P_{alf4}-*yopR*^{G407A} *aphA3*)	pRH172 and pRH174 → TS03	This study
KK098	Δ6 Δ*cat amyE*::(P_{aimR}-*lacZ cat*) *ganA*::(*xylR* P_{alf4}-*yopR*^{G407A} *aphA3*)	pRH173 and pRH174 → TS03	This study
KK100	Δ6 Δ*cat amyE*::(P_{aimR}-*lacZ cat*)	pRH173 → TS03	This study
KK101	Δ6 Δ*cat ganA*::(*xylR* P_{alf4}-*yopR*^{G407A} *aphA3*)	pRH174 → TS03	This study
KK108	Δ6 SPβ c2 *amyE*::(P_{alf4}-*yopR*$^{AAG505-507GCG}$ *aphA3*)	pBP182 → KK002	This study
KK118	Δ6 SPβ c2 *amyE*::(P_{alf4}-*yopR*$^{TAT910-912TTT}$)	pRH180 → KK002	This study
KK119	Δ6 SPβ c2 *amyE*::(P_{alf4}-*yopR*$^{TAT910-912GCG}$ *aphA3*)	pRH181 → KK002	This study
KK120	Δ6 SPβ c2 *yopR::ermC amyE*::(P_{alf4}-*yopR*$^{TAT910-912TTT}$)	BKE20790 → KK118	This study
KK121	Δ6 SPβ c2 *yopR*::*ermC amyE*::(P_{alf4}-*yopR*$^{TAT910-912GCG}$ *aphA3*)	BKE20790 → KK119	This study
KK124	Δ6 *amyE*::(P_{mtlA}-*comKS*) SPβ c2 *sprA*::*aphA3*	BKE21660 → KK002	This study
KK125	Δ6 *amyE*::(P_{mtlA}-*comKS*) SPβ c2 *sprB::aphA3*	BKE19820 → KK002	This study
KK138	Δ6 SPβ c2 *yopR*::*ermC amyE*::(P_{alf4}-*yopR*$^{AAG505-507GCG}$ *aphA3*)	BKE20790 → KK108	This study
KK139	Δ6 Δ*cat amyE*::(P_{aimR}-*lacZ cat*) *ganA*::(*xylR* P_{alf4}-*yopR aphA3*)	pRH173 → KK101	This study

[a]Arrows indicate construction by transformation or phage infection.

Plasmids

Name	**Insert/purpose**	**Reference**
pAC5	No/translational promoter-*lacZ* fusions, complementation	Martin-Verstraete et al., 1992
pAC6	No/transcriptional promoter-*lacZ* fusions, complementation	Stülke et al., 1997
pAC7	No/translational promoter-*lacZ* fusions, complementation	Weinrauch et al., 1991
pBP164	P_{alf4}-*lacZ cat/* transcriptional promoter-*lacZ* fusion	Gundlach et al., 2017
pET24d	For heterologous protein overproduction	Novagen
pGP888	No/complementation	Diethmaier et al., 2011

pJOE8999	CRISPR-Cas9 engineering of *B. subtilis*	Altenbuchner et al., 2016
pKK005	*aphA3* P_{alf4}-*yopR* P_{xylA} *xylR*/expression of *yopR*	This study
pRH001	Deletion of *ermD* gene from TS01 derivatives/ gRNA targeting *ermD* gene	This study
pRH004	Deletion of the *cat* gene in TS001/gRNA targeting *cat* gene	This study
pRH005	Deletion of the *cat* gene in TS001/gRNA targeting *cat* gene and recombination cassette	This study
pRH029	Deletion of *ermD* gene from KK001 and KK137/gRNA targeting *ermD* gene and recombination cassette	This study
pRH166	P_{alf4}-*yopR*^{G407A}/expression of *yopR*^{G407A} and complementation	This study
pRH167	P_{alf4}-*yopR*/expression of *yopR* and complementation	Kohm et al., 2022
pRH168	*xylR* P_{xylA}-*yosL aphA3*/expression of *yosL*	This study
pRH173	P_{aimR}-*lacZ cat*/translational promoter-*lacZ* fusion	This study
pRH174	P_{alf4}-*yopR*^{G407A} *xylR* P_{xylA} *aphA3*/expression of *yopR*^{G407A}	This study
pRH180	P_{alf4}-*yopR*^{A911T}/expression of *yopR*^{A911T} and complementation	This study
pRH181	P_{alf4}-*yopR*$^{TAT910-912GCG}$/expression of *yopR*$^{TAT910-912GCG}$ and complementation	This study
pRH182	P_{alf4}-*yopR*$^{AAG505-507GCG}$/expression of *yopR*$^{AAG505-507GCG}$ and complementation	This study
AL324	pET24d derivative/Overproduction of C-terminal His_6-tagged proteins	Laboratory collection Bange
pEJK9	Heterologous overproduction of YosL-His_6	This study
pEJK11	Heterologous overproduction of YopR-His_6	This study
pEJK13	Heterologous overproduction of YopR^{G136E}-His_6	This study
pEJK25	Heterologous overproduction of YopR^{K169A}-His_6	This study
pEJK27	Heterologous overproduction of YopR^{Y304F}-His_6	This study
pEJK29	Heterologous overproduction of YopR^{Y304A}-His_6	This study

REFERENCES

Abe K, Takamatsu T, Sato T (2017) Mechanism of bacterial gene rearrangement: SprA-catalyzed precise DNA recombination and its directionality control by SprB ensure the gene rearrangement and stable expression of *spsM* during sporulation of *Bacillus subtilis*. Nucleic Acids Res 45: 6669-6683.

Aihara H, Kwon HJ, Nunes-Düby SE, Landy A, Ellenberger T (2003) A Conformational Switch Controls the DNA Cleavage Activity of λ Integrase. Mol Cell 12: 187–198.

Altenbuchner J (2016) Editing of the *Bacillus subtilis* genome by the CRISPR-Cas9 system. Appl Environ Microbiol 82: 5421-5427.

Bebel A, Karaca E, Kumar B, Stark WM, Barabas O (2016) Structural snapshots of Xer recombination reveal activation by synaptic complex remodeling and DNA bending. Elife 5.

Diethmaier C, Pietack N, Gunka K, Wrede C, Lehnik-Habrink M, Herzberg C, Hübner S, Stülke J (2011) A novel factor controlling bistability in *Bacillus subtilis*: the YmdB protein affects flagellin expression and biofilm formation. J Bacteriol 193: 5997-6007.

Ennifar E, Meyer JEW, Buchholz F, Stewart AF, Suck D (2003) Crystal structure of a wild-type Cre recombinase– lox P synapse reveals a novel spacer conformation suggesting an alternative mechanism for DNA cleavage activation. Nucleic Acids Res 31: 5449-5460.

Grant SG, Jessee J, Bloom FR, Hanahan D (1990) Differential plasmid rescue from transgenic mouse DNAs into *Escherichia coli* methylation-restriction mutants. Proc Natl Acad Sci USA 874645-874649.

Gundlach J, Herzberg C, Kaever V, Gunka K, Hoffmann T, Weiß M, Gibhardt J, Thürmer A, Hertel D, Daniel R, Bremer E, Commichau FM, Stülke J (2017) Control of potassium homeostasis is an essential function of the second messenger cyclic di-AMP in *Bacillus subtilis*. Sci Signal 10: eaal3011.

Kohm K, Floccari VA, Lutz VT, Nordmann B, Mittelstädt C, Poehlein A, Dragos A, Commichau FM, Hertel R (2022) The *Bacillus* phage SPβ and its relatives: a temperate phage model system reveals new strains, species, prophage integration loci, conserved proteins and lysogeny management components. Environ Microbiol. 24: 2098-2118.

Koo BM, Kritikos G, Farelli JD, Todor H, Tong K, Kimsey H, Wapinski I, Galardini M, Cabal A, Peters JM, Hachmann AB, Rudner DZ, Allen KN, Typas A, Gross CA (2017) Construction and analysis of two genome-scale deletion libraries for *Bacillus subtilis*. Cell Syst 4: 291-305.

Martin-Verstraete I, Débarboullié M, Klier A, Rapoport G (1992) Mutagenesis of the *Bacillus subtilis* "-12, -24" promoter of the levanase operon and evidence for the existence of an upstream activating sequence. J Mol Biol 226: 85-99.

Richts B, Hertel R, Potot S, Poehlein A, Daniel R, Schyns G, Prágai Z, Commichau FM (2020) Complete genome sequence of the prototrophic *Bacillus subtilis* subsp. *subtilis* strain SP1. Microbiol Resour Announc 9: e00825-20.

Rosenthal R, Toye PA, Korman RZ, Zahler SA (1979) The prophage of SP beta c2dcitK1, a defective specialized transducing phage of *Bacillus subtilis*. Genetics 92: 721-739.
Schilling T, Dietrich S, Hoppert M, Hertel R (2018) A CRISPR-Cas9-based Toolkit for fast and precise *in vivo* genetic engineering of *Bacillus subtilis* phages. Viruses 10: 241.

Stülke J, Martin-Verstraete I, Zagorec M, Rose M, Klier A, Rapoport G (1997) Induction of the *Bacillus subtilis ptsGHI* operon by glucose is controlled by a novel antiterminator, GlcT. Mol Microbiol 25: 65-78.

Weinrauch Y, Msadek T, Kunst F, Dubnau D (1991) Sequence and properties of *comQ*, a new competence regulatory gene of *Bacillus subtilis*. J Bacteriol 173: 5685-5693.

Westers H, Dorenbos R, van Dijl JM, Kabel J, Flanagan T, Devine KM, Jude F, Seror SJ, Beekman AC, Darmon E, Eschevins C, de Jong A, Bron S, Kuipers OP, Albertini AM, Antelmann H, Hecker M, Zamboni N, Sauer U, Bruand C, Ehrlich DS, Alonso JC, Salas M, Quax WJ (2003) Genome engineering reveals large dispensible regions in *Bacillus subtilis*. Mol Biol Evol 20: 2076-2090.